

行政院國家科學委員會專題研究計畫 成果報告

雙體鑰系稀土離子之大環多氨基酸配位化學及 DNA/RNA 切割劑之應用(3/3)

計畫類別：個別型計畫

計畫編號：NSC93-2113-M-009-004-

執行期間：93 年 08 月 01 日至 94 年 07 月 31 日

執行單位：國立交通大學生物科技研究所

計畫主持人：張正

報告類型：完整報告

報告附件：出席國際會議研究心得報告及發表論文

處理方式：本計畫可公開查詢

中 華 民 國 94 年 11 月 28 日

行政院國家科學委員會專題研究計畫進度報告

雙體鑰系稀土離子之大環多氨基酸配位化學 及 DNA/RNA 切割劑之應用(3/3)

計畫類別： 個別計畫 整合計畫

計畫編號： NSC 93-2113-M-009-004 (3rd Year)

執行期間： 93年 08 月 01 日 至 94年 07 月 31 日

個別型計畫： 計畫主持人： 張 正
 共同主持人： N/A

整合型計畫： 總計畫主持人： N/A
 子計畫主持人： N/A

註： 整合型計畫總報告與子計畫報告請分開編印各成一冊，彙整一起繳送國科會。

處理方式： 可立即對外提供參考
 一年候可對外提供參考
 兩年候可對外提供參考
 (必要時，本會得展延發表時限)

執行單位：交通大學生物科技研究所

中華民國 94 年 10 月 30 日

雙體鑷系稀土離子之大環多氨基酸配位化學及 DNA/RNA 切割劑之應用

關鍵詞：雙體及單體大環多氨基酸分子配位基、鑷系稀土離子大環錯化物、穩定常數、選擇性、形成動力學、解離動力學、螢光光譜、結構、DNA/RNA 切割劑。

本研究計畫為一多年期基礎研究計畫，其主要目的是對鑷系金屬離子與大環多氨基酸配位子所形成錯合物之配位化學（熱力學、動力學、光譜學及結構學）作進一步的探討，進而找出影響鑷系稀土離子多氨基酸錯合物之物理化學性質（如穩定性、選擇性、反應速率、及螢光性質等）之重要因素，以便能在磁振造影劑、稀土離子之萃取分離、photodynamic 療法、生物分子之螢光附著劑及切斷 RNA 及 DNA 反應之催化劑等有所應用。最近之研究結果顯示 $\text{Eu}(\text{DO2A})^+$ 切割 *phosphate diester bond* 之速率與 *pH* 有類似滴定曲線之關係，初步判定可能是在高 *pH* 時， $\text{Eu}(\text{DO2A})^+$ 會形成更具活性之 *hydroxo-bridged* $[\text{EuL}(\text{OH})]_2$ 雙體之故。為進一步證實此假設，本期之研究以雙體鑷系稀土離子之大環多氨基酸配位錯化物為主要目標。研究要點包括：

- (1) 大環多氨基酸配位子單體及雙體(如 DO2A、NO2A 及 dimers)的合成及特性研究 (NMR, IR, X 光單晶結構)。
- (2) 測量鑷系金屬離子多氨基酸配位子錯化物的穩定常數(stability constant)及選擇性(selectivity)。
- (3) 測量鑷系金屬離子大環多氨基酸配位子錯化物形成(formation)、解離(dissociation)及金屬離子或配位基置換(metal or ligand exchange)反應之速率及反應機理。
- (4) 探討鑷系金屬離子大環多氨基酸配位子錯化物之熱力學與動力學因素是否與多氨基酸配位子之 preorganization 或 ring strain 之能量有直接關係。
- (5) 合成鑷系稀土離子與大環多氨基酸配位子之錯化物，並作 NMR、螢光光譜及 X 光單晶結構的特性研究，並試圖建立物性-化性-結構之間的關係。
- (6) 試用鑷系稀土離子與多氨基酸配位子形成之陽離子錯化物如 $\text{Ln}(\text{DO2A})^+$ 、 $\text{Ln}(\text{NO2A})^+$ 與 dimers 切割磷酸酯類(如 BNPP)及 DNA 和 RNA 之 *phosphate diester bond*，並研究其反應速率與結構之關係。

Dimeric Macrocyclic Polyaminocarboxylate Lanthanide Coordination Chemistry and DNA/RNA Artificial Nucleases

Keywords: Dimeric and Monomeric Macrocyclic Polyaminocarboxylate Ligands, Lanthanides Complexes, Stability Constants, Selectivity, Formation and Dissociation Kinetics, Structure, Luminescence, NMR, Molecular Mechanics, DNA/RNA Cleavage.

Abstract:

The primary objective of this multi-year proposed research is to develop fundamental understanding of the major thermodynamic, kinetic, and structural factors that influence the desired physico-chemical properties of lanthanide complexes of macrocyclic polyaminocarboxylate ligands (e.g. complex formation stability and selectivity, reaction

kinetics, NMR relaxation, luminescence, and structure) for applications in magnetic resonance imaging (MRI), solvent extraction, photodynamic therapy, luminescence labeling for biomolecules and catalysis for DNA and RNA phosphate diester bond cleavage. Recently, we have found that the rate constants measured for the $\text{Eu}(\text{DO2A})^+$ reaction with BNPP (a model compound with phosphate diester bond) had a titration-curve-like dependence with pH. Our initial hypothesis was that at high pH, $\text{Eu}(\text{DO2A})^+$ could form the more reactive hydroxo-bridged $[\text{EuL}(\text{OH})]_2$ dimer. To verify this point, the research targets of this present project are primarily on the dimeric lanthanide macrocyclic complexes. The specific aims include the following: (1) Synthesize and characterize (NMR, IR, X-ray structural determination and potentiometry) new monomeric and dimeric macrocyclic polyaminocarboxylate ligands (e.g. DO2A and NO2A) with variable cumulative ring strains and pendent arms (e.g. carboxymethyl, amidemethyl and hydroxyethyl groups). (2) Determine the thermodynamic and conditional complex formation constants of these macrocyclic ligands with various metal ions including all trivalent lanthanide ions, alkaline earth metal ions, selected first and second row divalent transition metal ions (e.g. Ni^{2+} , Cu^{2+} , Zn^{2+} and Cd^{2+}) and post transition metal ions (e.g. Pb^{2+}) in aqueous solution. Evaluate ligand selectivity toward lanthanide complex formation. (3) Determine the macrocyclic lanthanide complex formation, dissociation, and metal/ligand exchange reaction rates in aqueous solution at various conditions (i.e. changing pH, metal ion/ligand concentration, temperature and ionic strength) and evaluate possible reaction mechanisms. (4) Determine if the thermodynamic and kinetic parameters, i.e. stability and selectivity constants, formation and dissociation reaction rates, activation enthalpy and entropy, of lanthanide DO2A/NO2A and dimeric complexes correlate with the ligand conformation, whether preorganized or not. (5) Synthesize and characterize (while possible, by single-crystal X-ray analyses, solution NMR, laser-excitation luminescence spectroscopy, NMR relaxation and molecular mechanics calculations) the macrocyclic complexes of La^{3+} , Eu^{3+} , Gd^{3+} , and Yb^{3+} . Correlate structural features (e.g. number of inner-sphere coordinated water molecules, number of ligand coordinated donor atoms, NMR chemical shifts, ligand cavity size, ligand cumulative ring strain, and metal ionic radii) with previously found thermodynamic and kinetic properties. (6) Use cationic lanthanide complexes such as $\text{Ce}(\text{DO2A})^+$, $\text{Eu}(\text{NO2A})^+$ and dimeric structural analogues to promote the cleavage of phosphate ester bonds of model compounds (e.g. disodium 4-nitrophenyl phosphate and diphenyl 4-nitrophenyl phosphate) and DNA and RNA. Determine reaction rates and possible mechanisms. Examine the effects of lanthanide ionic radius and charge of the complexes.

Progress Report

This is a research program originally started nine years ago (since 1995). Many postdoctoral research fellows (Dr. Liu, Yuh-Liang, 劉育良-目前任職永光化學公司; Dr. Chen, Chang-Yuh, 陳成裕-目前任職永勞工委員會勞工安全衛生研究所), research assistants and graduate students (陳煥源, 陳玉衡, 陳桂添(博士班), 謝發坤, 萬磊, 潘美蓉, 李亮緯, 許呈安, 林孟嘉, 管佈雲, 鄭昇沛, 謝明宏, 許地利, 張志杰, 陳家翎, 宋婉貞, 謝瑞偉, 曾繼鋒, 吳柏宏, 林志誠, 王文宏, 管燕芸, 林穎男, 林俊傑, 戴金華, 康名

慰，黃淑敏，李盈慧，張雅珍，羅千婷(博士班)，藍佩菁(博士班)，林志誠(博士班)，張順福(博士班)，林岳暉(博士班)，郭永斌(博士班)，蕭志祥(博士班)，蔡政憲，林玉淳，邱明慧，陳郁頻，李嫩如)， and undergraduate students (陳彥璋，黃崇道，陳伯翰，王文卿，李智凱，楊萬利) have been trained (紅字相關人員為現任學生). Recent research progresses are summarized in the following papers published or submitted for publication (see appendix for details), as well as patents applications:

A. Papers (2005-).

1. Hsuan-Chao Chiu, **C.A. Chang**, and Yuh-Jyh Hu. "Prediction of Orthologous Relationship by Functionally Important Sites". *Computer Methods and Programs in Biomedicine*, 2005, **78**, 209-222.
2. **C.A. Chang***, Bo-Hong Wu, Pu-Yun Kuan. "Macrocyclic Lanthanide Complexes as Artificial Nucleases and Ribonucleases. Effects of pH, Metal Ionic Radii, Number of Coordinated Water Molecules, Charge and Concentrations of the Metal Complexes." *Inorg. Chem.* 2005, **44**, 6646-6654.
3. S.-H. Lee, H.-Y. Fang, W.-C. Chen, H.-M. Lin, **C.A. Chang**, "Electrochemical Study on the Screen-printed Carbon Electrodes with Modification by Iron Nanoparticles in Fe(CN)₆^{4-/3-} Redox System." *Anal. Bioanal. Chem.*, 2005, 383:532-538.
4. P.C. Lan, C.F. Tseng, M.C. Lin, and **C.A. Chang**, "Expression and Purification of Human Placental Lactogen in *E. coli*." 2005, *Protein Expression & Purification*, in press (Online express publication).
5. K.-T. Chen, J.-D. Lin, H.-F. Weng, **C.A. Chang**, and E.-C. Chan. "An Aberrant Autocrine Activation of the Platelet-derived Growth Factor α -Receptor in Follicular Thyroid Carcinoma Cell Line and Papillary Thyroid Carcinoma Cell Line." *Cancer Letters*, 2005, in press (Online express publication).
6. **C.A. Chang*** and Bo Hong Wu, "Macrocyclic Lanthanide Complexes as Artificial Nucleases and Ribonucleases. Further Studies of Effects of Concentrations of the Europium(III) Complex of 1,7-Bis(carboxymethyl)-1,4,7,10-tetracyclododecane (EuDO2A)", Submitted to *J.C.S. Dalton Trans.*, 2005.
7. Ying-Hui Lee and **C.A. Chang**. "The Effects of Porcine Placental Extracts on Wound Healing", Submitted, 2005.
8. Chien -Ting Lo, Bor-Cheh Wang, **C.A. Chang**, "Polysaccharide Composition, *In Vitro* Immuno-Modulating and Anti-tumor Activities of Some Regional Different Strains of *Lentinula edodes*", submitted, 2005.
9. Chein Ting Lo, Hong Chang Wang, Usha Sree, Bor Cheh Wang, **C.A. Chang**, "Bioinformatic Studies of the relationship between polysaccharide composition and

macrophage activity of regionally different strains of *Lentinula edodes*", 2005, to be submitted

10. Ying-Nan Lin and **C.A. Chang**. "The Effects of Metal Complexes on Glucose Uptake in Muscle Cells", 2005, to be submitted.
11. **C.A. Chang**, Chia-Ling Chen, Yun-Ming Wang. "Dissociation Kinetics of Macrocyclic Lanthanide(III) Complexes of 1,4,7,10-tetraazacyclododecane-1,7-diacetic acid (DO2A)", 2005, to be submitted.

B. Patents.

1. 李世煌、林岳暉、顏嘉好、黃英哲、陳文章、林鴻明、張正、沈燕士，"電極試片及包含其之生物感測器"，中華民國、美國、歐盟專利申請，2005/07.
2. 李鴻文、林岳暉、張正、沈燕元、沈燕士，"一種便捷檢察測酵素抑制劑含量方法"，中華民國、美國、歐盟專利申請，2005/07.
3. 張正、林穎男，"促進血糖代謝之金屬複合物"，中華民國、美國專利申請，2005/10.

C. Other Articles

1. 張正，"台灣生技未來契機"、生技創業管理教戰首冊，國家生技醫療產業策進會，2004年6月出刊。

D. Recent Abstracts and Papers Presented at Scientific Meetings (Nov., 2003 - Oct., 2005)

1. B.H. Wu and C.A. Chang, "Kinetics of Phosphodiester Hydrolysis by Lanthanide DO2A Complexes", *2003 Annual Meeting of the Chinese Chemical Society (Taipei)*, Chungli, Taiwan, November 29-30.
2. C.C. Lin and C.A. Chang, "Synthesis of Ln(NO2A) Complexes and the Study of Their catalytic Activities toward Phosphodiester Bond", *2003 Annual Meeting of the Chinese Chemical Society (Taipei)*, Chungli, Taiwan, November 29-30.
3. Y.-C. Lin and C.A. Chang, "The Synthesis of Macrocyclic Ligand NO2A Dimer and The Study of Phosphodiester Bonds Hydrolysis Using Lanthanide NO2A Dimer Complexes", *2003 Annual Meeting of the Chinese Chemical Society (Taipei)*, Chungli, Taiwan, November 29-30.
4. P.C. Lan, Y.J. Chang, and C.A. Chang, "Construction of Porcine Placental cDNA

Yeast Two Hybrid System and Comparison of Physiological Activities of Various PLGF/VEGF Heterodimers for Researching the Relation of Growth Factors”. *The Nineteenth Joint Annual Conference of Biomedical Sciences*, Taipei, Taiwan, April 10-11, 2004.

5. Y.H. Lee, S.M. Huang, and C.A. Chang, “Effects of Porcine Placental Extract on Wound Healing, Anti-Aging and Whitening, and its Mechanism”, *The Nineteenth Joint Annual Conference of Biomedical Sciences*, Taipei, Taiwan, April 10-11, 2004.
6. Chien-Ting Lo, B-C. Wang, and C.A. Chang, “Phylogentic Groups and Immunological Bioactivity of *Lentinula Edodes*”, *The Nineteenth Joint Annual Conference of Biomedical Sciences*, Taipei, Taiwan, April 10-11, 2004.
7. C.T. Lo and C.A. Chang, “Structural Investigation of Immunologically Active Water-soluble Glucan from *Lentinula edodes* by Submerged Fermentation”, International Symposium for Chinese Medicinal Chemists Conference, Taiwan, Nov., 2004.
8. Ying-Nan Lin and C.A. Chang, “The Effect of Metal Ions on Glucose Uptake in Muscle Cell”, *2004 Annual Meeting of the Chinese Chemical Society (Taipei)*, Chungli, Taiwan, November 29-30.
9. Yu-Chuen Lin, Chih Cheng Lin, C.H. Hsiao, C.H. Tsai, and C.A. Chang, “The Synthesis of Macrocyclic Ligand Monomer and Dimer and the Results of Molecular Simulation of Metal Macrocyclic Ligand Complexes”, *2004 Annual Meeting of the Chinese Chemical Society (Taipei)*, Chungli, Taiwan, November 29-30.
10. P. C. Lan and C. A. Chang, “Construction of Porcine Placental cDNA Yeast Two Hybrid System and Clon the Gene Interaction with P53 Oncogen”. *The twentieth Joint Annual Conference of Biomedical Sciences*, Taipei, Taiwan, March 26-27, 2005.
11. T.S. Huang and C. A. Chang, “The Effect of Glycosylation of Human Follicle-stimulating Hormone (hFSH) on Ovarian Cancer Cell Proliferation”. *The twentieth Joint Annual Conference of Biomedical Sciences*, Taipei, Taiwan, March 26-27, 2005.
12. C.T. Lo and C.A. Chang, “Analysis of Water-soluble Extracellular Polysaccharides from *Lentinula edodes*”, *The 8th Asian Conference on Analytical Sciences*, Taipei, Taiwan, Oct. 16-20, 2005.

Thesis Supervised (Jul. 2003 – Oct. 2005)

	學生姓名	論文題目
1. M.S.	吳柏宏	銅系金屬離子錯合物水解磷酸酯之動力學研究

Jul., 2003	B.H. Wu	Kinetics of Phosphodiester Hydrolysis by Lanthanide Complexes
2. M.S. Jul. 2003	林俊傑 Chun Chieh Lin	銻系金屬與大環多氮多酸基配位錯合物的合成及其水解磷酸雙酯之效力的研究 Synthesis of Ln(NO ₂ A) and the Study of Their Hydrolytic Activity toward Phosphodiester Bond
3. M.S. Jul. 2004	李盈慧 Ying-Hui Lee	豬隻胎盤萃取液對傷口癒合之功效 The Effects of Porcine Placental Extracts on Wound Healing
4. M.S. Jul. 2004	黃淑旻 Shung Ming Huang	評估豬隻胎盤萃取液在抗皮膚老化及美白之功效 Evaluation of Porcine Placenta Extracts on the Efficacy of Anti-skin Aging and Whitening
5. M.S. Jul., 2004	張雅珍 Ya-Jen Chang	合成並比較不同接合型組合的血管內皮生長因子同質雙體及異質雙體之生理活性 Synthesis and Comparison of Physiological Activities of Homodimers and Heterodimers Comprising Different Splice Forms of Vascular Endothelial Growth Factor
6. M.S. Sep.,200 4	林穎男 Ying-Nan Lin	探討不同金屬錯合物在肌肉細胞中對葡萄糖吸收之影響 The Effect of Metal Complexes on Glucose Uptake in Muscle Cell
7. Ph.D. May., 2005	陳桂添 Kuei-Tien Chen	異常的 PDGFR- α 基因表現對誘發甲狀腺濾泡癌癌化之探討 The significance of aberrant gene expression of PDGFR- α in the carcinogenesis of follicular thyroid carcinoma
8. M.S. Oct., 2005	黃琮道 Tsung-Tao Huang	去醣基人類濾泡刺激素之菌體表現及其對於卵巢癌細胞增生影響之研究 Bacterial Expression of Non-glycosylated Human Follicle-stimulating Hormone (NG-hFSH) and Study on the Effect of NG-hFSH on Ovarian Cancer Cell Proliferation

Appendix 1

Macrocyclic Lanthanide Complexes as Artificial Nucleases and Ribonucleases¹.

Further Studies of Effects of Concentration and Equilibration Time of the Europium(III) Complex of 1,7-Bis(carboxymethyl)-1,4,7,10-tetraazacyclododecane (EuDO₂A) on BNPP Hydrolysis

C. Allen Chang* and Bo Hong Wu

Department of Biological Science and Technology
National Chiao Tung University
75 Po-Ai Street, Hsinchu, Taiwan 30039, R.O C.

RECEIVED DATE (to be automatically inserted after your manuscript is accepted if required according to the journal that you are submitting your paper to)

*Author to whom correspondence should be addressed: Tel: +886-3-5712121 ext. 56903.
Fax: +886-3-5729288. E-mail: changca@cc.nctu.edu.tw.

TITLE RUNNING HEAD : Artificial Macrocyclic EuDO₂A⁺ (Ribo)Nucleases

Abstract

We report here a more detailed study of the effects of concentration of the europium(III) complexes, EuDO₂A⁺ (DO₂A is 1,7-dicarboxymethyl-1,4,7,10-tetraazacyclododecane) and EuHEDTA (HEDTA is N-hydroxyethyl-ethylenediamine-N,N',N'-triacetic acid), as potential catalysts for the hydrolysis of the phosphodiester bond of a compound BNPP (sodium bis(4-nitrophenyl)-phosphate), at 25°C, pH 7.90, 9.35, and 11, respectively. Initial rate studies indicated that the order of the reaction was first order with respect to [BNPP] at both pH 7.90 and 9.35. However, the order of the reaction was greater than one with respect to [EuDO₂A], and it increased from 1.31 to 1.80 as the pH of reaction buffer solution was increased from 7.90 to 9.35. At pH 7.90, the BNPP hydrolysis rates increase with increasing [EuDO₂A⁺] (1.0 – 7.0 mM) in a second order fashion. The active species is assumed to be the deprotonated form, EuDO₂A(OH). The data could be fitted to a

monomer-dimer reaction model and the respective monomer and dimer rate constants are $k_1 = 7.4 \times 10^{-3} \text{ M}^{-1} \text{ s}^{-1}$ and $k_2 = 0.41 \text{ M}^{-1} \text{ s}^{-1}$. The dimer is 55 times more reactive than the monomer. At pH 9.35, the rates are faster than those at pH 7.90, and a second order dependence on $[\text{EuDO2A}^+]$ (1.0 – 20.0 mM) followed by a possible saturation behavior at higher concentration suggest that the reactive species is dinuclear. The data could be fitted to three reaction models, but a monomer-dimer saturation model is preferred. The $\text{EuDO2A}(\text{OH})$ monomer-BNPP binding constant $K_{m1} = 2.9 \text{ M}^{-1}$ and corresponding first order rate constant $k_p = 3.1 \times 10^{-3} \text{ s}^{-1}$ together with the $\{\text{EuDO2A}(\mu\text{-OH})\}_2$ dimer-BNPP binding constant $K_{m2} = 120 \text{ M}^{-1}$ and corresponding first order rate constant $k_q = 2.3 \times 10^{-2} \text{ s}^{-1}$ were determined. The $\{\text{EuDO2A}(\mu\text{-OH})\}_2$ dimer-BNPP binding constant is 40 times of that of the monomer and its BNPP hydrolysis rate constant is 8 times of that of the monomer, consistent with the fact that dimer has two substrate binding sites, each one of which is more reactive than an isolated monomer. The dimer formation ($2\text{EuDO2A}(\text{OH}) \leftrightarrow \{\text{EuDO2A}(\mu\text{-OH})\}_2$) constant is determined to be 11.8 M^{-1} . A simple monomer saturation kinetic behavior was observed for $[\text{EuHEDTA}] = 10\text{-}70 \text{ mM}$. A EuHEDTA -BNPP binding constant $K = 8.6 \text{ M}^{-1}$ and a first order rate constant $k = 7.3 \times 10^{-4} \text{ s}^{-1}$ were obtained. These results indicate that the EuDO2A^+ promoted BNPP hydrolysis is similar to or at least 10 times greater than those reported by other complexes. For the equilibration time studies, it was found that freshly prepared EuDO2A^+ solutions showed the fastest BNPP hydrolysis rates. As the EuDO2A^+ equilibration time was increased, the BNPP hydrolysis rates were found to be slower, particularly at high pH. This observed kinetic effect was very likely due to the slow formation of less active or inactive polynuclear species. Using a proposed dimerization, and deprotonation scheme of the EuDO2A^+ complex and by fitting of k_{obs} vs. pH data as functions of equilibration time reveals that the reactivity is in the decreasing order ($L = \text{DO2A}$): $L_2\text{Eu}_2(\text{H}_2\text{O})_2(\mu\text{-OH})_2 > L_2\text{Eu}_2(\text{H}_2\text{O})(\text{OH})(\mu\text{-OH})_2 > L_2\text{Eu}_2(\text{OH})_2(\mu\text{-OH})_2 > L\text{Eu}(\text{H}_2\text{O})_2(\text{OH})$ and that the possible conversions of $L_2\text{Eu}_2(\text{H}_2\text{O})_2(\mu\text{-OH})_2$, $L_2\text{Eu}_2(\text{H}_2\text{O})(\text{OH})(\mu\text{-OH})_2$, $L_2\text{Eu}_2(\text{OH})_2(\mu\text{-OH})_2$, and $L\text{Eu}(\text{H}_2\text{O})_2(\text{OH})$ to inactive species (e.g. $L_4\text{Eu}_4(\mu\text{-OH})_4$) are relatively faster initially and gradually slow down but continue even after 1-3 weeks.

KEYWORDS: lanthanides, macrocyclic ligands, artificial nucleases and ribonucleases, dinuclear and polynuclear lanthanide complexes

BRIEFS: More detailed analysis of the BNPP phosphodiester bond hydrolysis rate constants data vs. $[\text{EuDO2A}^+]$ (1.0 – 20.0 mM) at pH 9.35 using a monomer-dimer saturation reaction model indicates that the dimeric species, probably the hydroxo-bridged $\{\text{EuDO2A}(\text{H}_2\text{O})(\mu\text{-OH})\}_2$, is much more reactive than the monomer. As the EuDO2A^+ equilibration time was increased, the BNPP hydrolysis rates were found to be slower, particularly at high pH. This kinetic effect is attributed to the possible slow formation of less active or inactive polynuclear species such as $\text{L}_4\text{Eu}_4(\mu\text{-OH})_4$.

Introduction

We have been interested in the design, synthesis and characterization of artificial nucleases and ribonucleases employing macrocyclic lanthanide complexes because their high thermodynamic stability, low kinetic lability, high coordination number and charge density (Lewis acidity) allow more design flexibility and stability¹⁻⁴. Due to the complex hydrolytic properties and potential Ln-hydroxide polynuclear cluster formation of cationic lanthanide complexes, the design of efficient agents and the elucidation of possible mechanisms for their promotion of phosphodiester hydrolysis remain to be challenges^{1,4}.

Previously we reported the effects of pH, metal ionic radii, the number of inner-sphere coordinated water molecules, and the charge and concentrations of a number of lanthanide complexes on the promotion of BNPP phosphodiester bond hydrolysis¹. In general, faster promoted BNPP hydrolysis rates were observed for lanthanide complexes with stronger lanthanide ion Lewis acidity, greater number of inner-sphere coordinated water molecules, and greater positive charge on the complex. However, complex formation sometimes alters the expected trends in that it may cause changes of the pK_h values of inner-sphere coordinated water molecules and/or it may result in active or inactive dimer or high order oligomers. This is evident particularly for the heavier lanthanide complexes^{1,5}.

A preliminary study of the effects of concentration of the europium(III) complex of 1,7-bis(carboxymethyl)-1,4,7,10-tetracyclododecane (EuDO2A) on the promotion of BNPP hydrolysis reaction has also been conducted¹. The observed BNPP hydrolysis rate

constant vs. $[\text{EuDO2A}^+]$ data at pH 9.35 were fitted to a monomer-dimer reaction model and the dimer rate constant was 400 times greater than that of the monomer. However, only five data points in the $[\text{EuDO2A}^+]$ concentration range 1.0 mM– 4.75 mM in one solution pH 9.35 were involved. In order to understand more **about** the effects of concentration of lanthanide complexes on BNPP hydrolysis and to elucidate possible mechanisms, we have conducted further studies at two solution pH values (i.e. pH 7.90 and 9.35) and greater concentration ranges. In addition, the equilibration time for the EuDO2A^+ solutions was found to affect the promoted BNPP hydrolysis rates and which required further studies. This paper reports out findings.

Experimental Section

Materials and Standard Solutions were obtained and standardized according to procedures previously reported¹. Europium nitrate solution was standardized by standardized EDTA solution using xylene orange as the indicator. DO2A ligand solution was standardized by pH titrations and complexometric titrations with standardized calcium chloride solution.

Kinetic measurements. All lanthanide complex solutions were freshly prepared by mixing 1.00:1.02 metal salt to ligand molar ratio solutions. The pH of each solution was adjusted to 6.0-6.5 by adding appropriate amount of $(\text{CH}_3)_4\text{NOH}$ solution. To each solution was then added the BNPP solution and the final pH adjusted by adding an appropriate amount of buffer stock solution and used within 30 minutes after preparation, except otherwise specified. MES (2-[N-morpholino]ethanesulfonic acid) ∙ MPS (3-[N-morpholino]propanesulfonic acid) ∙ TAPS (3-[[tris(hydroxymethyl)methyl]-amino]propanesulfonic acid) ∙ CHES (2-[cyclohexylamino]ethane-sulfonic acid) ∙ CAPS (3-[cyclohexylamino]-1-propanesulfonic acid) ∙ CABS (4-[cyclohexylamino]-1-butanethanesulfonic acid) with the respective pK_a values 6.1, 7.2, 8.4, 9.3, 10.4, and 10.7 were used to prepare buffer solutions with the desired pH. The initial rates of the lanthanide complex promoted BNPP hydrolysis were

measured by the initial rates of production of 4-nitrophenolate ion from BNPP hydrolysis by monitoring the absorbance at 400 nm spectrophotometrically. The absorbance at 400 nm was corrected for the degree of formation of 4-nitrophenol at pH 7.9 and which was less than 0.2% in all cases. Corrections for the spontaneous hydrolysis of the BNPP substrate in the buffer solutions were not necessary as they were negligible¹. The concentration of 4-nitrophenolate ion produced was calculated from the extinction coefficient ($18,700 \text{ L mol}^{-1} \text{ cm}^{-1}$, 400 nm). The initial rate of each reaction was obtained directly from the slope of the plot of 4-nitrophenolate ion concentration vs. time, i.e. up to 2000 s for pH 7.90 data and 250 s for pH 9.35 data to ensure less than 5% of the reaction, which was linear with $r^2 \geq 0.98$. All experiments were run at least in duplicates and the reported data represent the average values calculated from the linear regression of each individual data set. Agreement between the calculated initial rates for replicate experiments was within 6% at pH 7.9 and 9.35 for [BNPP]-dependence studies. The data variations were slightly greater for the [EuDO2A⁺]-dependence studies at both pH 7.90 and 9.35 (*vide infra*).

For further lanthanide complex concentration dependence studies, the final BNPP concentration was kept at 0.10 mM and the lanthanide complex concentrations were 1.0-20 mM for EuDO2A⁺ solutions and 10-70 mM for EuHEDTA solutions to fulfill pseudo-first order reaction conditions. The ionic strength was adjusted to 0.10 M with (CH₃)₄NCl. A HP 8453 UV-VIS spectrophotometer was used to measure the absorption increase with time at 400 nm due to the formation of 4-nitrophenolate ion after BNPP hydrolysis¹. Pseudo-first order rate constants were calculated using the integral method after more than three reaction half-lives. The data were fitted to the equation:

$[4\text{-nitrophenolate}] = [\text{BNPP}]_0(1 - e^{-k_{\text{obs}}t})$, where $[\text{BNPP}]_0$ is the initial concentration of BNPP. Microsoft Excel was used for data treatment and Sigma plot was used for curve fitting.

Equilibration time studies. The lanthanide-DO2A complex solutions were prepared in a similar fashion as those for kinetic studies. Different equilibration time was allowed to these solutions as specified in the text. A Model 720 Metrohm Titroprocessor in conjunction with Metrohm Combination Electrode was employed to monitor the solution pH. A HP 8453 UV-VIS spectrophotometer was used to measure the absorption spectra and to monitor the absorbance change with time.

Results and Discussion

Initial rate studies. Solution pH values of 7.90 and 9.35 were selected for the present studies because the pK_h value of EuDO2A^+ was 8.1.⁶ At pH 7.90, only 39% of EuDO2A^+ hydrolyzes and at pH 9.35, 95% of EuDO2A^+ is in the hydrolyzed form. The initial rate studies were performed to determine the order of the reaction. Theoretically the rate can be defined as: $\text{Rate} = k [\text{BNPP}]^x [\text{EuDO2A}^+]^y$. A plot of the logarithmic initial rates vs. $\log [\text{BNPP}]$ would give an intercept $\log (k[\text{EuDO2A}^+]^y)$ and slope x , which is the order of the reaction with respect to $[\text{BNPP}]$. Figure s1 (supporting information) shows some examples of the plots of absorbance vs. time for the EuDO2A^+ promoted BNPP hydrolysis reaction at $[\text{EuDO2A}^+] = 1.0 \text{ mM}$ and various BNPP concentrations (i.e. 0.2-8.0 mM). The initial rate data for $[\text{BNPP}]$ studies are shown in Table 1. The log plots give the respective slope values 0.98 ± 0.03 ($r^2 = 0.999$) and 0.99 ± 0.02 ($r^2 = 0.998$) at pH 7.90 and 9.35, indicating the reaction is first order in $[\text{BNPP}]$. However, similar plots of \log (initial rates) vs. $\log [\text{EuDO2A}^+]$ at $[\text{BNPP}] = 0.10 \text{ mM}$ give the respective slope values 1.31 ± 0.15 and 1.80 ± 0.11 at pH 7.90 and 9.35, indicating that the reaction with respect to $[\text{EuDO2A}^+]$ is complicated, the reaction order is more than one and changes with pH (*vide infra*). Further rate studies on $[\text{EuDO2A}^+]$ were then carried out.

Effects of $[\text{EuDO2A}^+]$ on BNPP hydrolysis rates at pH 7.90 and 9.35. Figure 1 shows the plots of k_{obs} vs. $[\text{EuDO2A}^+]$ at pH 7.90. The data are listed in Table 2 together with those obtained at pH 9.35 and those of EuHEDTA at pH 11. These observed rate constants, k_{obs} , were obtained by monitoring the absorbance at 400 nm due to the formation of 4-nitrophenolate ion from BNPP and fitting the absorbance vs. time data to the equation: $[\text{4-nitrophenolate}] = [\text{BNPP}]_0 (1 - e^{-k_{\text{obs}} t})$, where $[\text{BNPP}]_0$ is the initial concentration of BNPP. A number of such plots and fits are shown in Figure s2 (supporting information). The final absorbance reaches a limiting value of 1.87, indicating that the 0.10 mM BNPP is close to 100% reaction completion. It is noted that the calculated first order BNPP hydrolysis rate constant by NaOH^1 , i.e. k_{OH} , was $2.30 \times 10^{-5} \text{ M}^{-1} \text{ s}^{-1}$. For all studies, controlled BNPP hydrolysis reactions using only the buffer solutions without lanthanide complexes were always studied as references and the rates were all negligible.

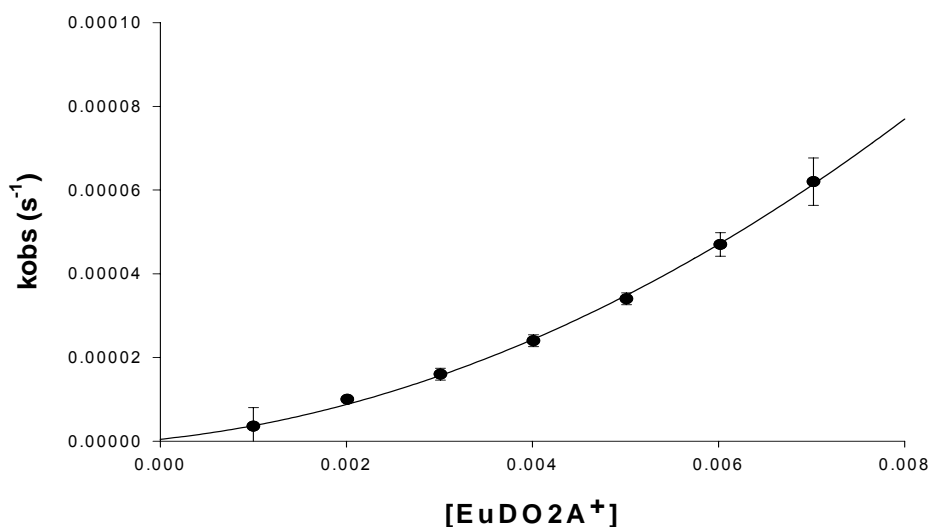
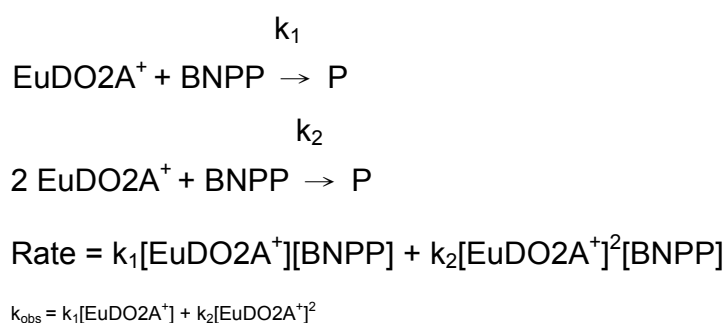


Figure 1. Dependence of pseudo first order rate constant of BNPP hydrolysis on the concentration of EuDO2A^+ at 25°C , pH 7.90, $[\text{MPS}] = 20 \text{ mM}$, $\mu = 0.10 \text{ M}$ $(\text{CH}_3)_4\text{NCl}$, $[\text{BNPP}] = 0.10 \text{ mM}$. The line is calculated based on the best fit to the monomer-dimer reaction model in Scheme 1.

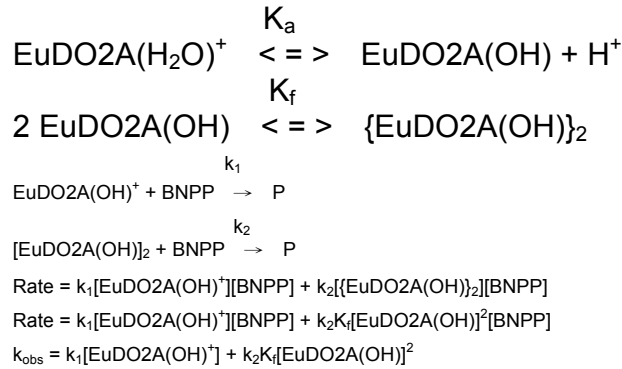
Fitting the data in Figure 1 to a simple monomer reaction model depicted in Scheme 1 gives a second order rate constant $k_1 = (2.3 \pm 0.4) \times 10^{-3} \text{ M}^{-1}\text{s}^{-1}$ and a third order rate constant $k_2 = 0.90 \pm 0.06 \text{ M}^{-2}\text{s}^{-1}$ ($r^2 = 0.999$). These two values are only one eighth and one thirtieth of the respective values obtained earlier at pH 9.35 (i.e. $0.017 \pm 0.016 \text{ M}^{-1}\text{s}^{-1}$ and $26.6 \pm 3.2 \text{ M}^{-2}\text{s}^{-1}$, $r^2 = 0.997$).¹ This is rationalized by the fact that at pH 9.35, the amount of the reactive species, i.e. $\text{EuDO2A}(\text{OH})$, is greater.



Scheme 1. A simple monomer reaction model (pH 7.9).

However, this model is not very desirable because for cationic lanthanide complexes at pH greater than 6.5 the inner-sphere coordinated water molecules could form “hydrate-bridged”, “hydroxo-bridged” or “oxo-bridged” species and alter the reactivities⁷. Scheme 2 shows a monomer-dimer reaction model and the species $\text{EuDO2A}(\text{OH})$ is

assumed to be the reactive one.



Scheme 2. A monomer-dimer reaction model (pH 7.9).

For data treatment, we have followed the method described by Burstyn, et al.^{8,9} Using the following derivations, we can obtain an equation for [EuDO2A(OH)] (equation 1):

$$\begin{aligned} [\text{Eu}^{3+}]_{\text{T}} &= [\text{EuDO2A(H}_2\text{O)}^+] + [\text{EuDO2A(OH)}] + 2\{\text{EuDO2A(OH)}\}_2 \\ K_a &= [\text{EuDO2A(OH)}][\text{H}^+]/[\text{EuDO2A(H}_2\text{O)}^+] \\ K_f &= \{\text{EuDO2A(OH)}\}_2 / [\text{EuDO2A(OH)}]^2 \\ [\text{Eu}^{3+}]_{\text{T}} &= [\text{EuDO2A(OH)}][\text{H}^+]/K_a + [\text{EuDO2A(OH)}] + 2K_f[\text{EuDO2A(OH)}]^2 \\ 2K_f[\text{EuDO2A(OH)}]^2 + ([\text{H}^+]/K_a + 1)[\text{EuDO2A(OH)}] - [\text{Eu}^{3+}]_{\text{T}} &= 0 \\ [\text{EuDO2A(OH)}] &= \{-1.29 + (1.67 + 2K_f[\text{Eu}^{3+}]_{\text{T}})^{1/2}\}/2K_f, \quad K_a = 7.9\text{e-}9 \quad (1) \end{aligned}$$

Substituting equation 1 into the rate law, and follow the method described in a previously reported paper¹, we can obtain $k_1 = 7.4 \times 10^{-3} \text{ M}^{-1}\text{s}^{-1}$, $k_2 = 0.41 \text{ M}^{-1}\text{s}^{-1}$, and $K_f = 15.3 \text{ M}^{-1}$ ($r^2 = 0.998$). Comparing these data with those obtained at pH 9.35 previously with five data points¹ (i.e. $k_1 = 9.1 \times 10^{-3} \text{ M}^{-1}\text{s}^{-1}$, $k_2 = 4.0 \text{ M}^{-1}\text{s}^{-1}$, and $K_f = 8.2$), it is found that both k_1 and K_f values are in the same order of magnitude, and only the k_2 values are different. This indicates that at pH 9.35, other complex and reactive species may be present (*vide infra*).

We have conducted ESI-MS measurement to examine whether EuDO2A⁺ dimer formation is present in the reaction mixture. The preliminary results shown that although

some mass/charge ratio data could be used as evidences, there is still the possibility of gas-phase dimerization which could make the evidences “false-positive”¹⁰. On the other hand, previous potentiometric titration data did not confirm the presence of dimer formation^{6,22}. This was mainly due to the fact that the entire complexation process between trivalent lanthanide ions and DO2A was very slow which makes the determination of stability constants for monomeric lanthanide complexes already difficult¹¹. Indeed, two sets of LnDO2A⁺ complex stability constants have been reported^{6,22}. Before this issue is resolved, complete and reliable speciation studies would be difficult. Nevertheless, it is highly possible that very reactive, but small amount dimers are formed (*vide infra*). We are in the process to obtain single crystals for structural determination as additional support for the above explanations.

For pH 9.35, we have obtained more data by increasing [EuDO2A⁺] to 20 mM, and the results are shown in Figure 2:

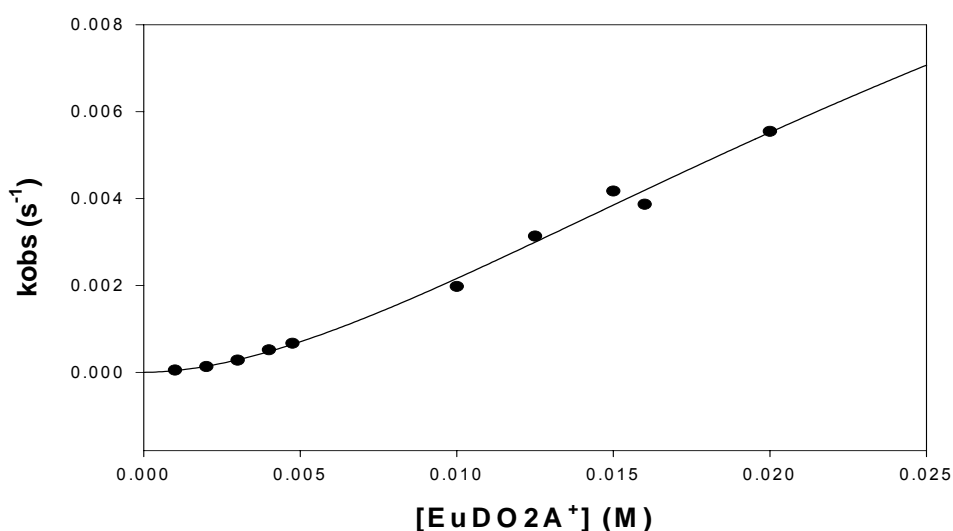
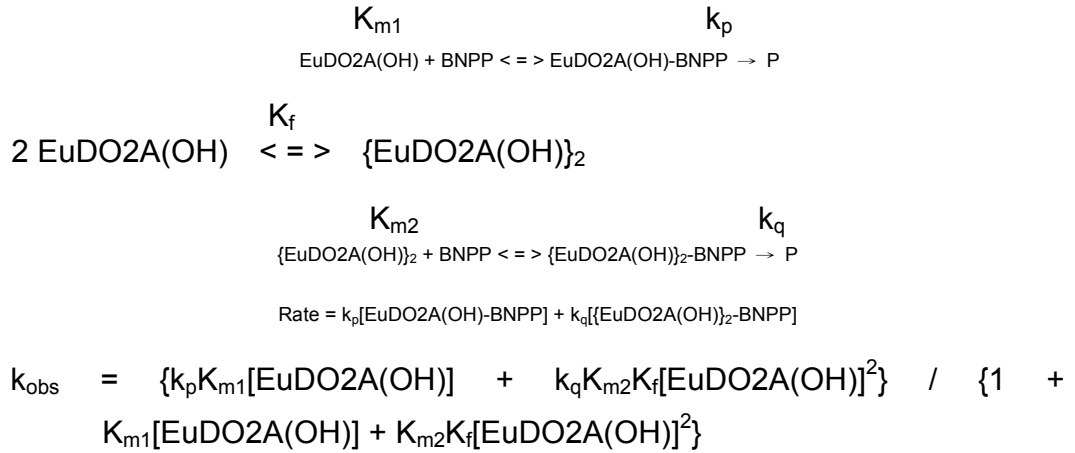


Figure 2. Dependence of pseudo first order rate constant of BNPP hydrolysis on concentration of EuDO2A⁺; 25°C, pH 9.35, [BNPP] = 0.10 mM, μ = 0.10 M (CH₃)₄NCl (Solid line is the best fit to the monomer-dimer saturation reaction model in Scheme 3).

Further increase of [EuDO2A⁺] beyond 20 mM resulted in precipitate formation. The reaction model depicted in Scheme 3 is proposed for data fitting. This scheme ignores the effect of EuDO2A(H₂O)⁺ because at pH 9.35 more than 95% of the EuDO2A⁺ is in the deprotonated form, EuDO2A(OH). Also, Scheme 3 could be considered a more detailed

one than Scheme 2. The product $K_{m1}k_p$ in Scheme 3 could be regarded similar to k_1 of Scheme 2, and the product $K_{m2}k_q$ is similar to k_2 of Scheme 2.



Scheme 3. A monomer-dimer saturation reaction model (pH 9.35).

Substituting $[\text{EuDO2A(OH)}]$ into the rate law, equation 2 is obtained.

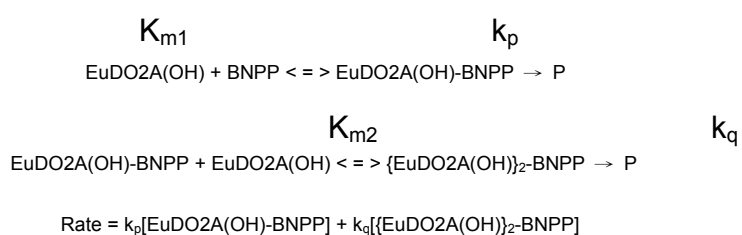
$$\begin{aligned}
 [\text{EuDO2A(OH)}] &= \{-0.5 + (0.25 + 2K_f[\text{Eu}^{3+}]_T)^{1/2}\} / 2K_f \\
 k_{\text{obs}} &= \{k_p K_{m1} \{-0.5 + (0.25 + 2K_f[\text{Eu}^{3+}]_T)^{1/2}\} / 2K_f + k_q K_{m2} K_f \{-0.5 + (0.25 + 2K_f[\text{Eu}^{3+}]_T)^{1/2}\} / 2K_f\}^2 / \{1 + K_{m1} \{-0.5 + (0.25 + 2K_f[\text{Eu}^{3+}]_T)^{1/2}\} / 2K_f + K_{m2} K_f \{-0.5 + (0.25 + 2K_f[\text{Eu}^{3+}]_T)^{1/2}\} / 2K_f\}^2 \quad (2)
 \end{aligned}$$

Fitting the data to equation 2, it gives a dimer formation constant $K_f = 12 \text{ M}^{-1}$, a EuDO2A(OH) monomer-BNPP binding constant $K_{m1} = 2.9 \text{ M}^{-1}$ and a corresponding first order rate constant $k_p = 3.1 \times 10^{-3} \text{ s}^{-1}$, a $\{\text{EuDO2A}(\mu\text{-OH})\}_2$ dimer-BNPP binding constant $K_{m2} = 120 \text{ M}^{-1}$ and a corresponding first order rate constant $k_q = 2.3 \times 10^{-2} \text{ s}^{-1}$ ($r^2 = 0.993$). The $\{\text{EuDO2A(OH)}\}_2$ dimer-BNPP binding constant is 40 times of that of the monomer and its BNPP hydrolysis rate constant is 8 times of that of the monomer. The product, $K_{m2}k_q (2.76 \text{ M}^{-1} \text{ s}^{-1})$ is 307 times of $K_{m1}k_p (8.99 \times 10^{-3} \text{ M}^{-1} \text{ s}^{-1})$, consistent with the fact that dimer has two substrate binding sites, each one of which is more reactive than an isolated monomer.

In three cases and at two different solution pH (i.e. pH 7.90 and 9.35) and with two different reaction models, the dimer formation equilibrium constant K_f values were fitted to be 8.2, 15.3 and 12, which are similar, and the average value is 11.8 M^{-1} . This is about two orders of magnitude smaller than the Cu(II)-N3 macrocyclic dimer complex ($K_f =$

1220 M⁻¹) reported by Burstyn, et al.⁸. In another more relevant study, Yatsimirsky, et al. reported in the lanthanide-BTP (Bis-tris propane) system¹⁰, the potentiometric determined logarithmic dimer formation constant in the form of [2BTP-2Eu-2OH]/[Eu]²[BTP]²[OH]², i.e. log ([2BTP-2Eu-2OH]/[Eu]²[BTP]²[OH]²), is 23.62. To compare the two values, it is necessary to convert the dimer formation expression to be of the same form. Assuming [BTP-Eu]/[BTP][Eu] = 10^{2.44} (that of the Eu^{III}-tris formation constant¹²), [BTP-Eu-OH][H⁺]/[BTP-Eu] = 10^{-8.38} (that of the hydrolysis constant of Eu^{III}), and [H⁺][OH⁻] = 10^{-13.8}, and by substituting these equations to the original definition equation, one can obtain [BTP-2Eu-2OH]/[BTP-Eu-OH]² = 10^{7.90}. This value is more than 6 orders of magnitude greater than that of {EuDO2A(μ-OH)}₂-dimer formation. This discrepancy could be attributed to a possible over-estimation of the BTP-Eu-OH dimer formation constant and an under-estimation of that of the {EuDO2A(μ-OH)}₂ dimer. If the BTP-Eu formation constant is assumed to be similar to that of La-bis-Tris¹³, i.e. 10^{4.70}, then [BTP-2Eu-2OH]/[BTP-Eu-OH]² = 10^{2.82}, which is only about 2 orders of magnitude greater than what we determined, i.e. 11.8 M⁻¹ using the kinetic approach. However, it is entirely possible that the {EuDO2A(μ-OH)}₂-dimer formation constant is lower than that of the BTP-Eu-OH dimer because the EuDO2A(OH) is neutral and BTP-Eu carries three positive charges and the bridging hydroxide ion should prefer the later.

The pH 9.35 data could be treated with another model derived from Morrow, et al.¹⁴ This model assumes that EuDO2A(OH) reacts with BNPP in 1:1 and 2:1 two forms (Scheme 4).



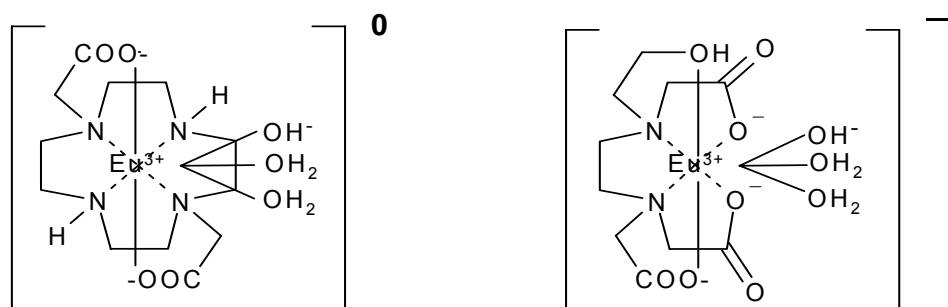
$$k_{\text{obs}} = \frac{\{k_p K_{m1}[\text{EuDO2A(OH)}] + k_q K_{m2} K_{m2} [\text{EuDO2A(OH)}]^2\}}{\{1 + K_{m1}[\text{EuDO2A(OH)}] + K_{m1} K_{m2} [\text{EuDO2A(OH)}]^2\}}$$

Scheme 4. A monomer saturation reaction model (pH 9.35)

Fitting the data to Scheme 4 model, we obtained $K_{m1} = 5.9 \text{ M}^{-1}$, $K_{m2} = 270 \text{ M}^{-1}$, $k_p = 6.3 \times 10^{-3} \text{ s}^{-1}$, and $k_q = 1.4 \times 10^{-2} \text{ s}^{-1}$ ($r^2 = 0.992$). The fitting plot is quite similar to that of Figure 2 and is not shown. The dimeric binding constant K_{m2} is 45 times greater than that

of the monomeric binding constant K_{m1} indicating cooperative binding behavior. This model also predicts that the rate constant of the dinuclear species is about 20 times greater than that of the monomeric species. The product, $K_{m2}k_q$ ($3.78 \text{ M}^{-1}\text{s}^{-1}$) is 102 times of $K_{m1}k_p$ ($3.72 \times 10^{-2} \text{ M}^{-1}\text{s}^{-1}$). However, because it is very likely that $\text{EuDO2A}(\text{OH})$ may form hydroxo-bridged dimer (*vide infra*), this model is less favored than that described in Scheme 3.

Effects of [EuHEDTA] on BNPP hydrolysis rates at pH 11.0. For comparison purpose, the effects of concentration of EuHEDTA on BNPP hydrolysis at pH 11.0 were studied. Both EuDO2A^+ and EuHEDTA have three inner-sphere coordinated water molecules. However, EuDO2A^+ has one positive charge and EuHEDTA has none. The respective pK_h values¹ for EuDO2A^+ and EuHEDTA are 8.1 and 10.1. After hydrolysis, $\text{EuDO2A}(\text{OH})$ carries no net charge but $\text{EuHEDTA}(\text{OH})^-$ is negatively charged (Scheme 5). The negatively charged $\text{EuHEDTA}(\text{OH})^-$ should prevent itself to form dimer or higher order oligomers due to charge repulsion at the specified pH studied.



Scheme 5. Structural formulas of $\text{EuDO2A}(\text{OH})$ and $\text{EuHEDTA}(\text{OH})^-$. The deprotonation site of EuHEDTA could also be that of the hydroxyethyl group of HEDTA.

As expected, in the $[\text{EuHEDTA}] = 10\text{-}70 \text{ mM}$, the k_{obs} vs. $[\text{EuHEDTA}]$ plot shows a saturation kinetic behavior (Figure 3). Fitting the data to the simple saturation kinetic model (Scheme 6) gives a EuHEDTA-BNPP binding constant $K = 8.6(\pm 0.9) \text{ M}^{-1}$ and a first order rate constant $k = 7.3(\pm 0.8) \times 10^{-4} \text{ s}^{-1}$.

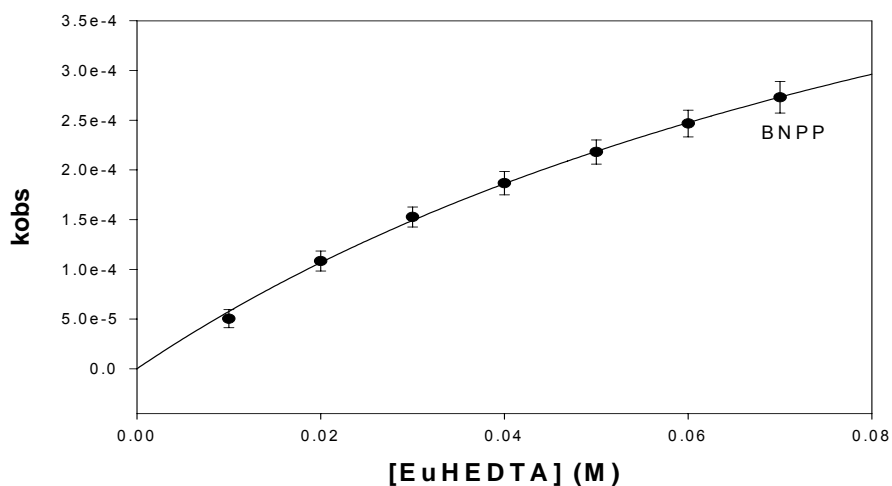
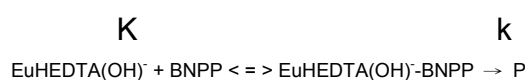


Figure 3. Dependence of pseudo first order rate constant on [EuHEDTA], [BNPP] = 0.10 mM, pH 11.0, 25°C, $\mu = 0.1$ M $(\text{CH}_3)_4\text{NCl}$.



$$k_{\text{obs}} = \frac{k[\text{EuHEDTA}(\text{OH})^-]}{1 + K[\text{EuHEDTA}(\text{OH})^-]}$$

Scheme 6. A saturation kinetic model for EuHEDTA.

The binding constant value 8.6 M^{-1} is on the similar order of that of K_{m1} (2.9 M^{-1}), and the first order rate constant ($k = 7.3 \times 10^{-4} \text{ s}^{-1}$) is smaller than that of EuDO2A(OH) ($k_p = 3.1 \times 10^{-3} \text{ s}^{-1}$), roughly consistent with what is expected.

Comparisons of various EuDO2A-BNPP reaction models and rates and with other systems. The above analyses were achieved by fitting experimental pH 9.35 data to three different models (Schemes 2, 3, and 4). Except the simple monomer reaction model, the other three models seem all to be acceptable if no further information is available. However, the monomer-dimer saturation model (Scheme 3) seems to be the most possible, due to the very possible formation of the hydroxo-bridged dimeric species, $[\text{Eu}(\text{DO2A})(\text{OH})]_2$. Comparing the Scheme 3 fitting data (at pH 9.35) with those reported by others for the BNPP hydrolysis^{5,8-10,15-21}, (Table s1), it is observed that our k_{m1} and k_{m2} values are in the order of 10^{-3} - 10^{-2} s^{-1} , which are about similar or 10 times greater than those reported by others (i.e. 10^{-4} - 10^{-3} s^{-1}). In general, the binding constants of the transition metal complexes with BNPP are greater than those of the lanthanide complexes, e.g. the BNPP binding constant is $\sim 10^2 \text{ M}^{-1}$ for the mononuclear Cu^{II} -bipyridine complex derivatives¹⁵ and $\sim 10^6$ for dimeric Cu^{II} -triaminocyclohexane

species¹⁶. The strong binding may retard the leaving of the reacted substrates and make the catalyst poison. The half-lives of cobalt(III) complex systems for BNPP hydrolysis were found to be less than a couple hundred seconds¹⁹; however, the binding with BNPP was also too strong to be repeatedly used.

On the other hand, EuDO2A(OH)-BNPP binding constant is around 10^1 , and that of the dimer-BNPP is around 10^2 . This is due to the fact that at higher pH, the formation of EuDO2A(OH) results in zero net charge that diminishes the extent of binding with the negatively charged BNPP. The greater coordination number for lanthanide ions also reduces its overall Lewis acidity after ligand complexation.

Worth mentioning is the system studied by Martell, et al¹⁸, the dinuclear Ln-macrocyclic complex is in the ratio of 3:1 to hydrolyze BNPP. At pH 8, the fourth order rate constant was determined to be $k = 4 \times 10^8 \text{ M}^{-3} \text{ s}^{-1}$. The half-life for 1 mM dimer- BNPP reaction was 1.7 second, which is closer to those of natural nucleases (< 1 second). Such a fast rate is attributed to a simultaneous six-metal nuclear reaction. On the other hand, our rate constants (second order rate constants $\sim 0.4 - 4.0 \text{ M}^{-1} \text{ s}^{-1}$) are lower than those of Martell's but similar or slightly greater than those of Yatsimirsky's (second order rate constants $\sim 0.1 - 1.0 \text{ M}^{-1} \text{ s}^{-1}$)¹⁰.

Effects of equilibration time after the preparation of Eu(DO2A)⁺ solutions on the BNPP hydrolysis rates. The data presented before this point were obtained using carefully and freshly prepared Eu(DO2A)⁺ solutions, i.e. within 30 minutes after complex solution preparation. When the mother EuDO2A⁺ solution was prepared at pH 6.0, the solution was allowed enough time (i.e. > 10 hours) for equilibration, and more than 99% of the complexes was predicted to be in the monomeric form using a stability constant $\log K_f = 12.99$.⁶ However, if the Eu(DO2A)⁺ solutions after pH adjustment were allowed to equilibrate for 3 hours and 1 week, the obtained BNPP hydrolysis rate constants were found to be lower as shown in Figure 4, particularly at higher pH. The freshly prepared solutions showed the fastest rates (Figure 4, 30 min. curve). It was also found that the longer the equilibration time for higher pH EuDO2A⁺ solutions, the slower the resulting promoted BNPP hydrolysis rates (Figure 4, 3 hr. and 1 week curves).

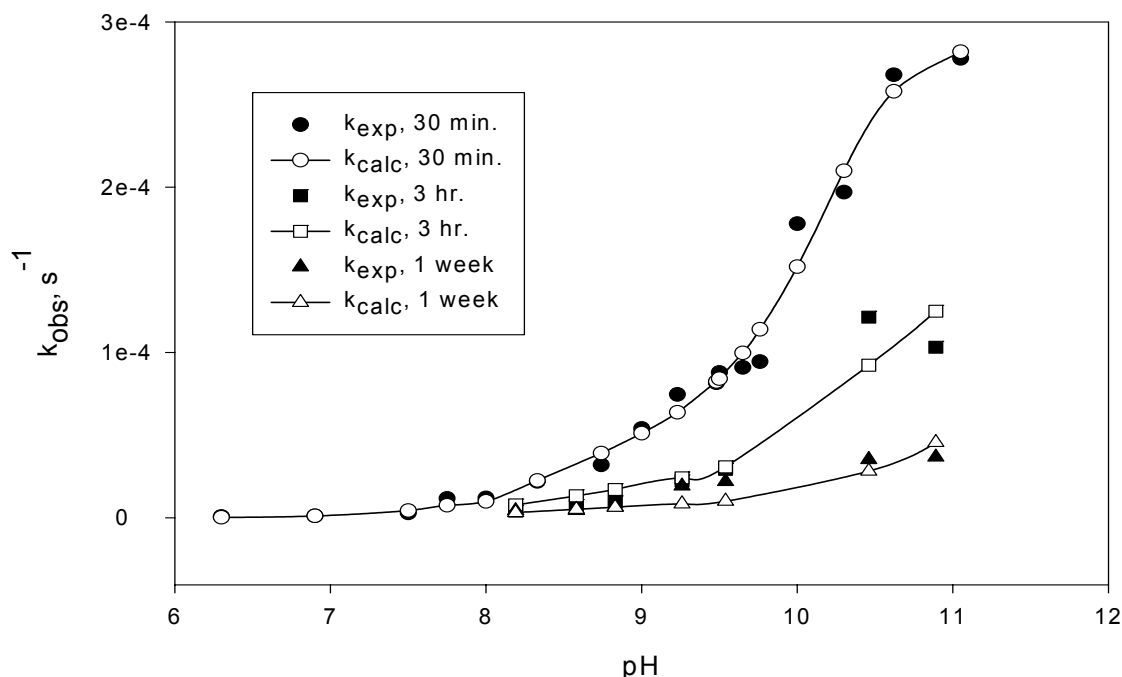


Figure 4. The plots of experimentally observed and calculated BNPP hydrolysis rate constants promoted by EuDO2A^+ after different complex equilibration time vs. pH. The calculated curves were obtained as discussed at the end of this paper (*vide infra*). The experimental and calculated data are listed in Table 3.

In addition, besides the inflection point shown in 30 min. curve at pH 8.1~8.4, all three curves show 2 more common inflection (i.e. rate jump) points at roughly pH 9.0 and pH 10.1. The rate jump beyond pH 8.1~8.4 may indicate that other more reactive, hydroxide-coordinated species are formed. However, the fact that these observed rates decrease with time seems to indicate that these reactive species are transformed into other less reactive and/or inactive lanthanide complex species, particularly at higher pH.

Possible evidence of polynuclear EuDO2A^+ species formation observed during pH titration. The formation of new and/or inactive EuDO2A^+ species corroborates with the pH titration data obtained after various equilibration time (Figure s3, supporting information). Using the data after 30-minute equilibration time, the calculated EuDO2A^+ stability constant is $\log K_f = 13.06$, similar to what we reported previously⁶. The stability constant calculated after 10-hour equilibration time is $\log K_f = 16.78$. If the “out of cell” method is used with an equilibration time of 3 weeks for each data point, the calculated stability constant is $\log K_f = 17.62$, which is still 1.8 log K units lower than that of

GdDO2A⁺ (log K_f = 19.4) reported by Sherry, et al.²² Thus, complex formation between Eu³⁺ and DO2A is a very slow reaction which may last for weeks and affect the determination of stability constants and speciation. This is not necessarily only the formation of monomeric EuDO2A⁺ complex *per se*, but the formations of new species such as dimeric and polynuclear species. It is noted that, this dimer and polynuclear species formation was not considered when the stability constants were determined.)

Thus, the observed results seem to indicate that ***a kinetic effect is present***. During the reaction of BNPP with EuDO2A⁺, the monomeric EuDO2A⁺ complexes form the more reactive dimeric species, which exist in solution with only finite concentrations and continue to form less reactive or inactive polynuclear species, such as the tetrameric species. This might explain why the dimer formation constant is only 11.8 based on the kinetic models (*vide supra*).

Possible evidence of polynuclear CeDO2A⁺ species formation from ultraviolet spectroscopic studies. Because EuDO2A⁺ does not have absorption in the 250-300 nm ultraviolet region, we have studied the CeDO2A⁺ absorption spectral properties in the pH range 6-10.8, in the hope that the data may shed additional lights on what we have observed for EuDO2A⁺ system. As shown in Figure 5, free Ce³⁺ ion at pH 6.0 shows two absorption maxima at 252 nm and 298 nm, and the former peak has much greater intensity. When the Ce³⁺ ion is complexed by DO2A at pH 6.0, the peak intensity at 252 nm is decreased and the peak intensity at 298 nm is increased. The final spectral intensities remain unchanged at pH 6.0 even after 10 hours. However, when the pH of the CeDO2A⁺ solution is adjusted to pH 7, the peak at 252 nm disappears and a peak at 272 nm arises, and the peak at 298 nm is still present. The intensities of the two peaks continue to increase with time. The basic initial spectral profile remains similar but with increased intensity as the pH value is further increased to higher pH, i.e. pH 8 to 10.8 (Figure 5). If the 298 nm peak is chosen and the absorption intensity is monitored with time for the CeDO2A⁺ solutions at various pH (i.e. pH 7.0-10.8), it is observed that the 298 nm absorption intensities continue to grow even up to 3000 second observation time (Figure s4, supporting information). The rate of 298 nm peak intensity growth increases with increasing pH. The absorbances for all solutions grow beyond 3 after 24 hours and still have no sign of reaching equilibrium.

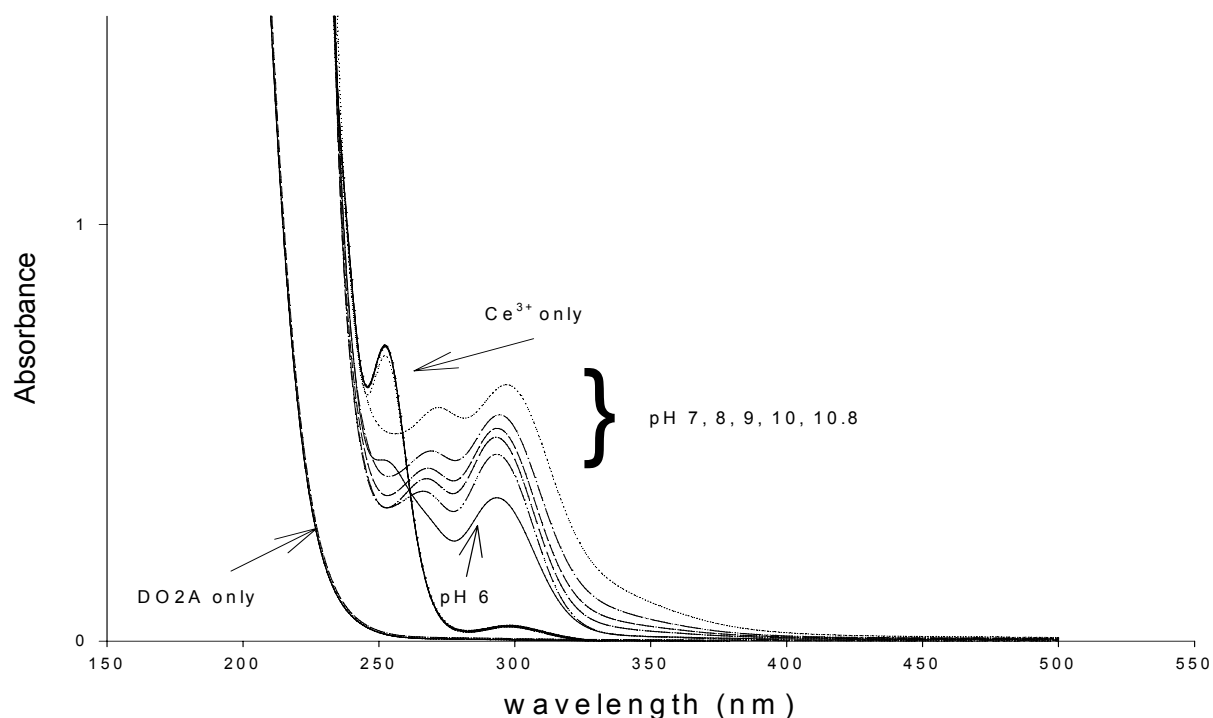
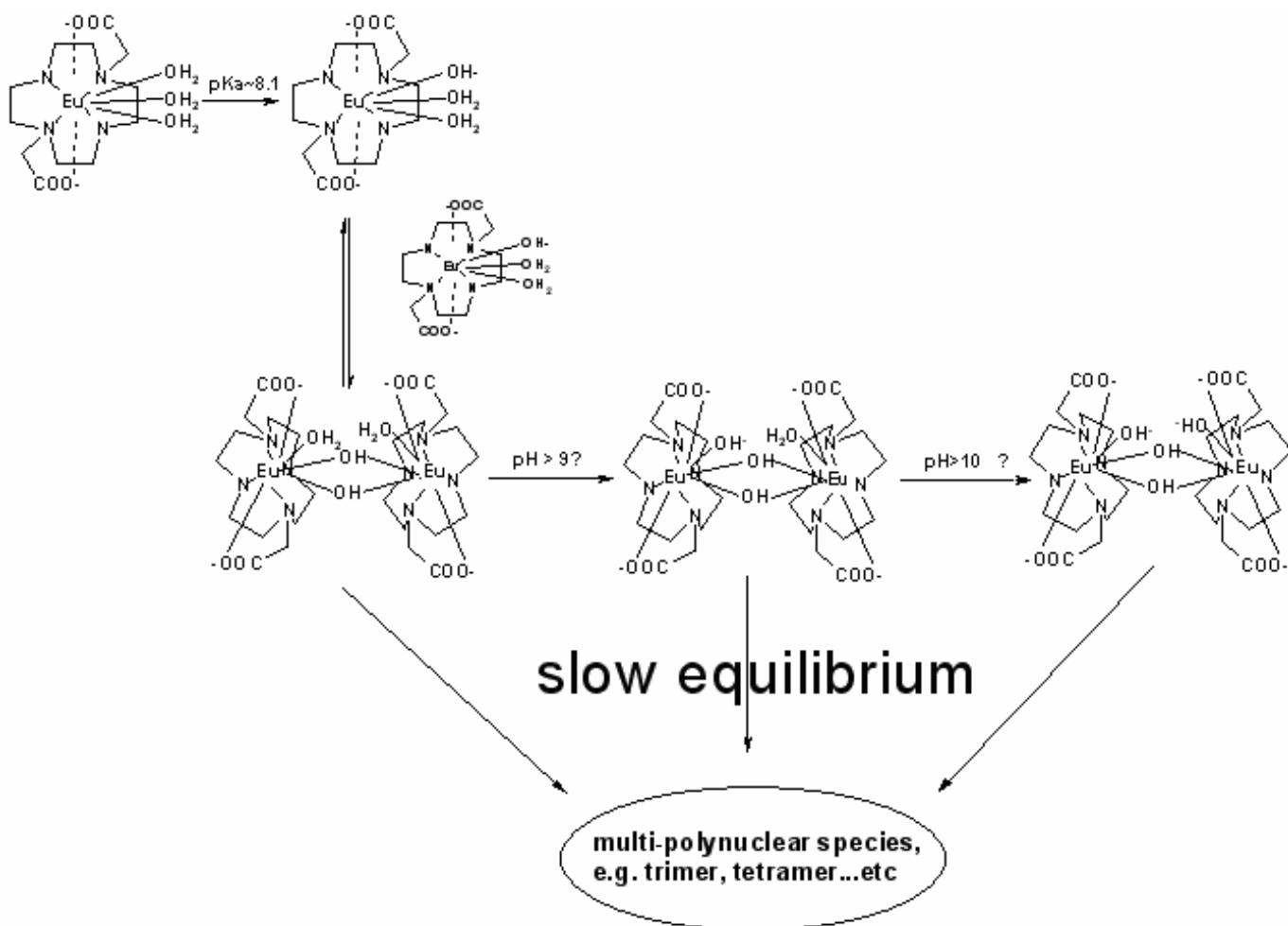


Figure 5. The spectra of 1.0 mM CeDO_2A^+ at 25°C , pH = 6, 7, 8, 9, 10, and 10.8. The Ce^{3+} and DO2A spectra were measured at $[\text{Ce}^{3+}] = 1.0 \text{ mM}$ and $[\text{DO}_2\text{A}] = 1.02 \text{ mM}$, respectively.

The above-mentioned phenomena are quite complicated and require further systematic studies. However, the macrocyclic system reported by Martell¹⁸, et al indicated that their compound disintegrated at $\text{pH} > 10$ and no data was shown after $\text{pH} > 10$. Yatsimirsky, et al also reported that the rate data for the hydrolysis of BNPP by Ln-BTP system were sometimes difficult to reproduce¹⁰. All these seem to indicate that lanthanide ions and complexes could form polynuclear species at high pH, consistent with what have been reported by Yan, Zheng, et al.²³⁻²⁶ The following scheme 7 is therefore proposed as tentative hypothesis for what we have discussed thus far:



Scheme 7. Proposed dimereization, deprotonation, and polynuclear species formations of the EuDO2A⁺ complex.

In Scheme 7, EuDO2A⁺ complex is deprotonated with a pKa ~ 8.1-8.4. The deprotonated EuDO2A(H₂O)₂(OH) may form the hydroxo-bridged dimer, L₂Eu₂(H₂O)₂(μ-OH)₂ where L=DO2A, which could be deprotonated at higher pH to form species such as L₂Eu₂(H₂O)(OH)(μ-OH)₂ and L₂Eu₂(OH)₂(μ-OH)₂ with different BNPP hydrolysis reactivities. All these dimeric species could further form higher order polynuclear species slowly, such as the cubane-shaped tetranuclear species, [EuDO2A(μ-OH)]₄, which may have a [Eu₄(μ-OH)₄] core structure without inner-sphere coordinated water molecule and is inactive for BNPP hydrolysis²³⁻²⁶.

Tentative fitting of k_{obs} vs. pH data as functions of equilibration time. Based on the proposed reaction mechanism for EuDO2A⁺ in Scheme 7, and assuming that the reactive species must contain coordinated hydroxide group(s) as well as coordination unsaturation, and that the formation of inactive species is negligible, the k_{obs} for the

BNPP hydrolysis reaction can be tentatively described as follows (charge of each species is omitted):

$$k_{\text{obs}} = k_1[\text{LEu}(\text{H}_2\text{O})_2(\text{OH})] + k_2[\text{L}_2\text{Eu}_2(\text{H}_2\text{O})_2(\mu\text{-OH})_2] + k_3[\text{L}_2\text{Eu}_2(\text{H}_2\text{O})(\text{OH})(\mu\text{-OH})_2] + k_4[\text{L}_2\text{Eu}_2(\text{OH})_2(\mu\text{-OH})_2] \quad (3)$$

Where k_1 , k_2 , k_3 , k_4 are the respective rate constants for the $\text{LEu}(\text{H}_2\text{O})_2(\text{OH})$, $\text{L}_2\text{Eu}_2(\text{H}_2\text{O})_2(\mu\text{-OH})_2$, $\text{L}_2\text{Eu}_2(\text{H}_2\text{O})(\text{OH})(\mu\text{-OH})_2$, and $\text{L}_2\text{Eu}_2(\text{OH})_2(\mu\text{-OH})_2$ species. Defining K_{h1} , K_{h2} , and K_{h3} as the respective deprotonation (hydrolysis) constants for the $\text{LEu}(\text{H}_2\text{O})_2(\text{OH})$, $\text{L}_2\text{Eu}_2(\text{H}_2\text{O})_2(\mu\text{-OH})_2$, and $\text{L}_2\text{Eu}_2(\text{H}_2\text{O})(\text{OH})(\mu\text{-OH})_2$ species, the total concentration of the EuDO_2A^+ complex, $[\text{LEu}]_t$, is:

$$[\text{LEu}]_t = [\text{LEu}(\text{H}_2\text{O})_3] + [\text{LEu}(\text{H}_2\text{O})_2(\text{OH})] + [\text{L}_2\text{Eu}_2(\text{H}_2\text{O})_2(\mu\text{-OH})_2] + [\text{L}_2\text{Eu}_2(\text{H}_2\text{O})(\text{OH})(\mu\text{-OH})_2] + [\text{L}_2\text{Eu}_2(\text{OH})_2(\mu\text{-OH})_2] \quad (4)$$

Using the K_h relationships and with the dimerization constant, K_f , equation 4 can be written as:

$$[\text{LEu}]_t = [\text{LEu}(\text{H}_2\text{O})_3] + K_{h1}[\text{LEu}(\text{H}_2\text{O})_3]/[\text{H}^+] + K_f K_{h1}^2 [\text{LEu}(\text{H}_2\text{O})_3]^2 / [\text{H}^+]^2 + K_f K_{h1}^2 K_{h2} [\text{LEu}(\text{H}_2\text{O})_3]^2 / [\text{H}^+]^3 + K_f K_{h1}^2 K_{h2} K_{h3} [\text{LEu}(\text{H}_2\text{O})_3]^2 / [\text{H}^+]^4 \quad (5)$$

After rearrangement, equation 5 can be written as:

$$(K_f K_{h1}^2 / [\text{H}^+]^2 + K_f K_{h1}^2 K_{h2} / [\text{H}^+]^3 + K_f K_{h1}^2 K_{h2} K_{h3} / [\text{H}^+]^4) [\text{LEu}(\text{H}_2\text{O})_3]^2 + (1 + K_{h1} / [\text{H}^+]) [\text{LEu}(\text{H}_2\text{O})_3] - [\text{LEu}]_t = 0 \quad (6)$$

Equation 6 is in the form of a quadratic equation, $ax^2 + bx + c = 0$, where x is $[\text{LEu}(\text{H}_2\text{O})_3]$, a is $K_f K_{h1}^2 / [\text{H}^+]^2 + K_f K_{h1}^2 K_{h2} / [\text{H}^+]^3 + K_f K_{h1}^2 K_{h2} K_{h3} / [\text{H}^+]^4$, and b is $1 + K_{h1} / [\text{H}^+]$. Using the values estimated previously, i.e. $K_f = 11.8$, $\text{p}K_{h1} = 8.1$, $\text{p}K_{h2} = 9.0$, and $\text{p}K_{h3} = 10.1$, one can solve for the $[\text{LEu}(\text{H}_2\text{O})_3]$ value at each pH listed in Table 3 for the 30 minutes data

set, and therefore, the $[\text{LEu}(\text{H}_2\text{O})_2(\text{OH})]$, $[\text{L}_2\text{Eu}_2(\text{H}_2\text{O})_2(\mu\text{-OH})_2]$, $[\text{L}_2\text{Eu}_2(\text{H}_2\text{O})(\text{OH})(\mu\text{-OH})_2]$, and $[\text{L}_2\text{Eu}_2(\text{OH})_2(\mu\text{-OH})_2]$ values. Figure 6 shows the “initial” speciation plots of EuDO_2A^+ as functions of pH. The term “initial” is used because as equilibration time is increased, other inactive species are formed and the total effective EuDO_2A^+ concentration will be decreased (*vide infra*).

It is noted that the speciation plots are drawn based on the thermodynamic equilibrium constants, i.e. K_f , K_{h1} , K_{h2} , and K_{h3} , obtained kinetically. Because the overall EuDO_2A^+ system was slow to reach equilibrium, the data collected were subjected to relatively larger uncertainties. Also, all these values are composites of multiple pH-dependent equilibria^{8,9} and are at best, roughly estimated values. However, using these speciation concentration values and a least squares method, one can obtain the best fit k_1 , k_2 , k_3 , and k_4 values and similarly, K_f , K_{h1} , K_{h2} , and K_{h3} values. This can be done by initially estimating the k_1 , k_2 , k_3 , k_4 , K_f , K_{h1} , K_{h2} , and K_{h3} values, calculating the k_{calc} values at several designated pH using equations 6, 5 and 3, and minimizing the sum of $(k_{\text{obs}} - k_{\text{calc}})^2$ at these designated pH by changing the estimated k_1 , k_2 , k_3 , k_4 , K_f , K_{h1} , K_{h2} , and K_{h3} values.

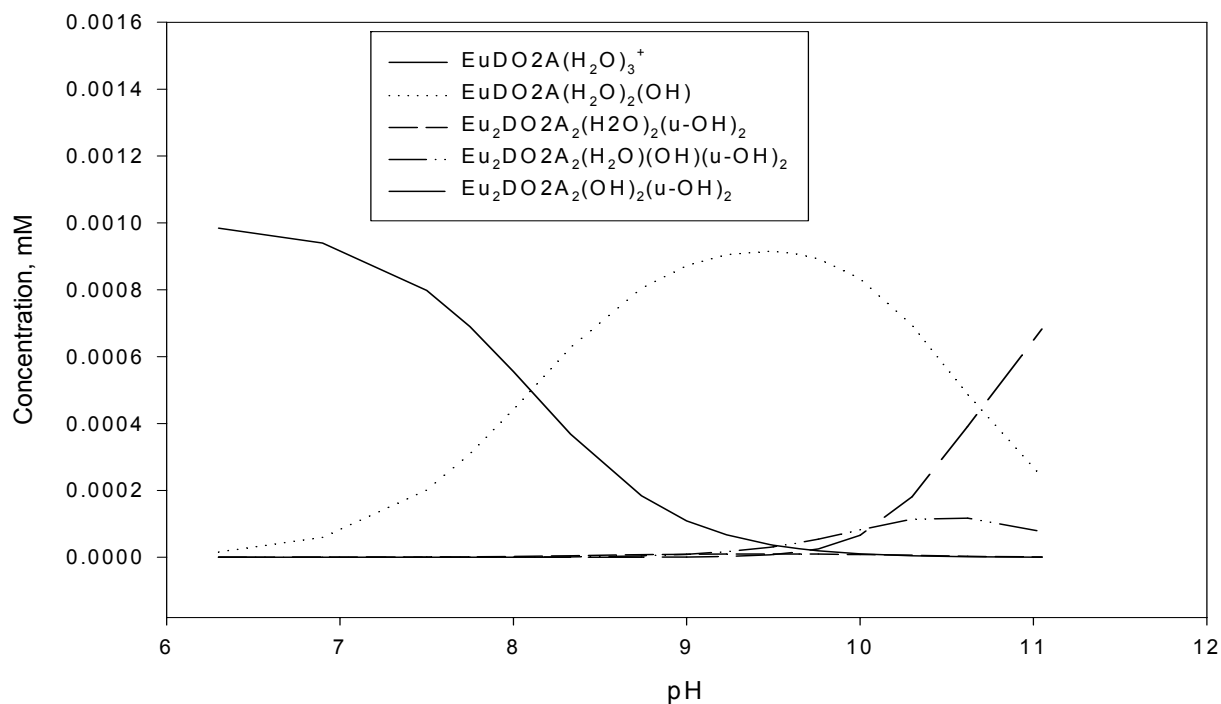


Figure 6. “Initial” speciation plots of EuDO_2A^+ as functions of pH. Total $[\text{EuDO}_2\text{A}^+] =$

1.0 mM. The values were calculated using $K_f = 11.8$, $pK_{h1} = 8.1$, $pK_{h2} = 9.0$, and $pK_{h3} = 10.1$.

The respective best fit k_1 , k_2 , k_3 , and k_4 values thus obtained are $3.08 \times 10^{-2} \text{ M}^{-1}\text{s}^{-1}$, $2.20 \text{ M}^{-1}\text{s}^{-1}$, $1.05 \text{ M}^{-1}\text{s}^{-1}$, and $0.280 \text{ M}^{-1}\text{s}^{-1}$ with a minimized $\sum(k_{\text{obs}} - k_{\text{calc}})^2 = 1.590 \times 10^{-9}$. The relative reactivity is in the decreasing order (L = DO2A): $\text{L}_2\text{Eu}_2(\text{H}_2\text{O})_2(\mu\text{-OH})_2 > \text{L}_2\text{Eu}_2(\text{H}_2\text{O})(\text{OH})(\mu\text{-OH})_2 > \text{L}_2\text{Eu}_2(\text{OH})_2(\mu\text{-OH})_2 > \text{LEu}(\text{H}_2\text{O})_2(\text{OH})$ which is roughly consistent with what expected, i.e. dimers are more reactive and specifically, a dimer with more coordinated water molecules is more reactive. Note that the k_1 and k_2 values, i.e. $3.08 \times 10^{-2} \text{ M}^{-1}\text{s}^{-1}$ and $2.20 \text{ M}^{-1}\text{s}^{-1}$, compare reasonably well with those obtained with Scheme 2 at pH 9.35, i.e. $k_1 = 9.1 \times 10^{-3} \text{ M}^{-1}\text{s}^{-1}$, $k_2 = 4.0 \text{ M}^{-1}\text{s}^{-1}$, and at pH 7.9, i.e. $k_1 = 7.4 \times 10^{-3} \text{ M}^{-1}\text{s}^{-1}$, $k_2 = 0.41 \text{ M}^{-1}\text{s}^{-1}$. If the experimental uncertainties are assumed to be less important, the variations of both k_1 and k_2 values in these three sets of data are therefore due to the consideration of the other two reactive species, i.e. $\text{L}_2\text{Eu}_2(\text{H}_2\text{O})(\text{OH})(\mu\text{-OH})_2$ and $\text{L}_2\text{Eu}_2(\text{OH})_2(\mu\text{-OH})_2$, in the present model but which were not considered previously in the Scheme 2 model.

The respective best fit K_f , K_{h1} , K_{h2} , and K_{h3} values are $K_f = 11.9$, $pK_{h1} = 8.33$, $pK_{h2} = 8.97$, and $pK_{h3} = 10.09$ which are in good agreements with what estimated previously.

As stated previously, the "initial" speciation plots will change with time. The total effective EuDO2A^+ concentration, $[\text{LEu}]_{t,\text{eff}}$, will decrease with time. Using the respective best fit k_1 , k_2 , k_3 , and k_4 values, i.e. $3.08 \times 10^{-2} \text{ M}^{-1}\text{s}^{-1}$, $2.20 \text{ M}^{-1}\text{s}^{-1}$, $1.05 \text{ M}^{-1}\text{s}^{-1}$, and $0.280 \text{ M}^{-1}\text{s}^{-1}$ as well as the K_f (11.9), pK_{h1} (8.33), pK_{h2} (8.97), and pK_{h3} (10.09) values obtained from the data set with 30 minutes equilibration time and by assuming that the conversions of $\text{L}_2\text{Eu}_2(\text{H}_2\text{O})_2(\mu\text{-OH})_2$, $\text{L}_2\text{Eu}_2(\text{H}_2\text{O})(\text{OH})(\mu\text{-OH})_2$, $\text{L}_2\text{Eu}_2(\text{OH})_2(\mu\text{-OH})_2$, and $\text{LEu}(\text{H}_2\text{O})_2(\text{OH})$ to inactive species such as $\text{L}_4\text{Eu}_4(\mu\text{-OH})_4$ take one simplified composite rate, the $[\text{LEu}]_{t,\text{eff}}$ values for the other two data sets (i.e. at 3 hour and 1 week equilibration time, Table 3) can be estimated to be 0.51 mM and 0.23 mM, or 51% and 23% of the initial $[\text{LEu}]_t (=1.0 \text{ mM})$, respectively. This is done also by using a least square method: First, use an initial estimated $[\text{LEu}]_{t,\text{eff}}$ value, calculate the various speciation concentrations using equations 6 and 5. Then, using these speciation concentrations and equation 3, calculate k_{calc} value at each specified pH and minimizing the sum of $(k_{\text{obs}} - k_{\text{calc}})^2$ for all experimental pH by changing the estimated $[\text{LEu}]_{t,\text{eff}}$ values.

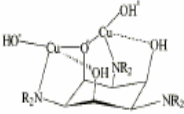
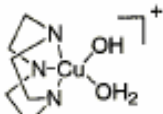
From the $[\text{LEu}]_{\text{t,eff}}$ data, it is seen that the conversions of $\text{L}_2\text{Eu}_2(\text{H}_2\text{O})_2(\mu\text{-OH})_2$, $\text{L}_2\text{Eu}_2(\text{H}_2\text{O})(\text{OH})(\mu\text{-OH})_2$, $\text{L}_2\text{Eu}_2(\text{OH})_2(\mu\text{-OH})_2$, and $\text{LEu}(\text{H}_2\text{O})_2(\text{OH})$ to inactive species are relatively faster initially and gradually slow down but continue even after 1-3 weeks as evidenced by the kinetic and thermodynamic data. The k_{obs} values for the entire processes are estimated (using 30 min. and 3 hr. data points) to be in the order of $\sim 0.22 \text{ hr}^{-1}$ in the beginning (first several hours after sample preparation) and slows down to $\sim 0.11 \text{ d}^{-1}$ or even less after 1 week (using 3 hr. and 1 week data points). This information would be useful for further detailed studies of thermodynamics and kinetics of hydroxide-bridged trivalent lanthanide complex cluster formation.

Conclusions. Trivalent lanthanide ions are good Lewis acids for the promotion of BNPP hydrolysis. However, they need ligands to form complexes to prevent uncontrolled lanthanide hydroxide or oxide formation, i.e. ligand-controlled hydrolysis. The properties of the resulting complexes are modified by the ligands, including charge, steric constraints, the number of inner-sphere coordinated water molecules, etc. In the present study, we found out that the dimeric $\{\text{EuDO}_2\text{A}(\mu\text{-OH})\}_2$ species are more reactive to promote BNPP hydrolysis. But the concentrations of the dimeric species exist in the solution could vary with time, probably reaching limited maximum concentrations and then decrease due to the formation of higher order polynuclear species at high pH. The resulting polynuclear species are inactive or less reactive toward BNPP hydrolysis. In particular, the relatively high rates of $\{\text{EuDO}_2\text{A}(\mu\text{-OH})\}_2$ promoted BNPP hydrolysis reaction are a kinetic event. The freshly prepared solutions show the fastest rates. It is important to apply these discoveries for the design of better macrocyclic lanthanide complex reagents for phosphodiester bond hydrolysis and we are in the process of doing it.

Acknowledgment. The authors wish to thank the National Science Council of the Republic of China (Taiwan) for financial support (grant number NSC-93-2113-M-009-004) of this work. A grant from the Atomic Energy Council is also acknowledged.

Supporting Information Available.:

Table s1. Examples of BNPP cleavage by selected metal complexes.

1.	2.	3.	4.
Cu ^{II} -Bipyridine complex systems	Cu ^{II} -triaminocyclohexane complex systems		
1996, Kramer, et al.	2001, Planalp, et al.	2001, Gajda, et al.	1996, Burstyn, et al.
20°C, pH 6.6, [BNPP]= 0-100mM	50°C, pH 7.2, [BNPP]= 0-6 mM	25°C, pH 8.5, [Cu ₂ L]= 0-4 mM	51°C, pH 7.24 [CuL] _T = 0-10 mM
CuL-BNPP k = 4.4×10 ⁻³ s ⁻¹ K= 0.013 M	CuL-BNPP-CuL k = 4.0×10 ⁻⁴ s ⁻¹ K= 12.3 mM ²	Rate=k[Cu ₂ L][BNPP] k= 0.95 M ⁻¹ s ⁻¹	Rate=k[CuL] _T ^{0.5} [BNPP] k= 8.86×10 ⁻³ M ⁻¹ s ⁻¹
1 mM CuL t _{1/2} = 2.2 × 10 ³ s	1 mM CuL t _{1/2} = 1.8 × 10 ³ s	1 mM Cu ₂ L t _{1/2} = 7.3 × 10 ² s	1 mM CuL t _{1/2} = 2.5 × 10 ³ s

5.	6.	7.
[Co ^{III} (trien)(H ₂ O)(OH)] ²⁺	[Co ^{III} (tren)(H ₂ O)(OH)] ²⁺	[Fe ^{III} Mn ^{II} (BPBPMP) (OAc) ₂]ClO ₄
1997, Schneider, et al.	1989, Chin, et al.	2002, Neves, et al.
50°C, pH 7.0 [CoL]= 0.01 M	50°C, pH 7.0 [CoL]= 0.01 M	25°C, pH 6.7 [BNPP]= 0-4 mM
The quickest k _{obs} = 4.14×10 ⁻³ s ⁻¹	k _{obs} = 4.60×10 ⁻² s ⁻¹	FeMnL-BNPP k = 4.51×10 ⁻⁴ s ⁻¹ K = 2.103 mM
The quickest, 0.01 M CoL t _{1/2} = 167s	0.01 M CoL t _{1/2} = 15.1 s	1 mM FeMnL t _{1/2} = 4.77×10 ³ s

8.	9.	10.
Schiff base macrocycle + 2La ³⁺		Ln ³⁺ only & Eu ³⁺ + ethylenediamine Eu ³⁺ + propylendiamine

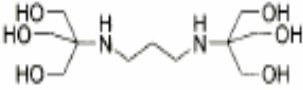
	 <p>Bis-Tris Propane (BTP) + Ln³⁺</p>	<p>Eu³⁺ + Cyclen Eu³⁺ + Trpn</p>
2000, Martell, et al.	2001, Yatsimirsky, et al.	1998, Schneider, et al.
35°C, [La ³⁺]= 0.2-0.8 mM [L]=0.1-0.4 mM,	25°C, 2 mM Ln ³⁺ + 20mM BTP,	50°C, pH 7.0, 0-10 mM [Ln ³⁺] or [LnL]
2La-L-2OH (quickest) R=k[2La-L-2OH] ³ [BNPP] k= 4×10 ⁸ M ⁻³ s ⁻¹	Dy-OH ²⁺ (quickest) R=k[Dy-OH ²⁺][BNPP] k= 0.81 M ⁻¹ s ⁻¹	Er-BNPP(quickest) k = 8.6×10 ⁻⁴ s ⁻¹ K= 3.3×10 ⁻³ M
1 mM L-2La-2OH t _{1/2} = 1.7 s	1 mM Dy-OH ²⁺ t _{1/2} = 855 s	1 mM Er ³⁺ t _{1/2} = 3.5×10 ³ s

Figure s1. Plots of absorbance at 400 nm vs. time (s) for the EuDO2A⁺ promoted BNPP hydrolysis reaction. [EuDO2A⁺] = 1.0 mM, [BNPP] = 0.2-8.0 mM, 25°C, pH 7.90, [MPS] = 20 mM, μ = 0.10 M (CH₃)₄NCl

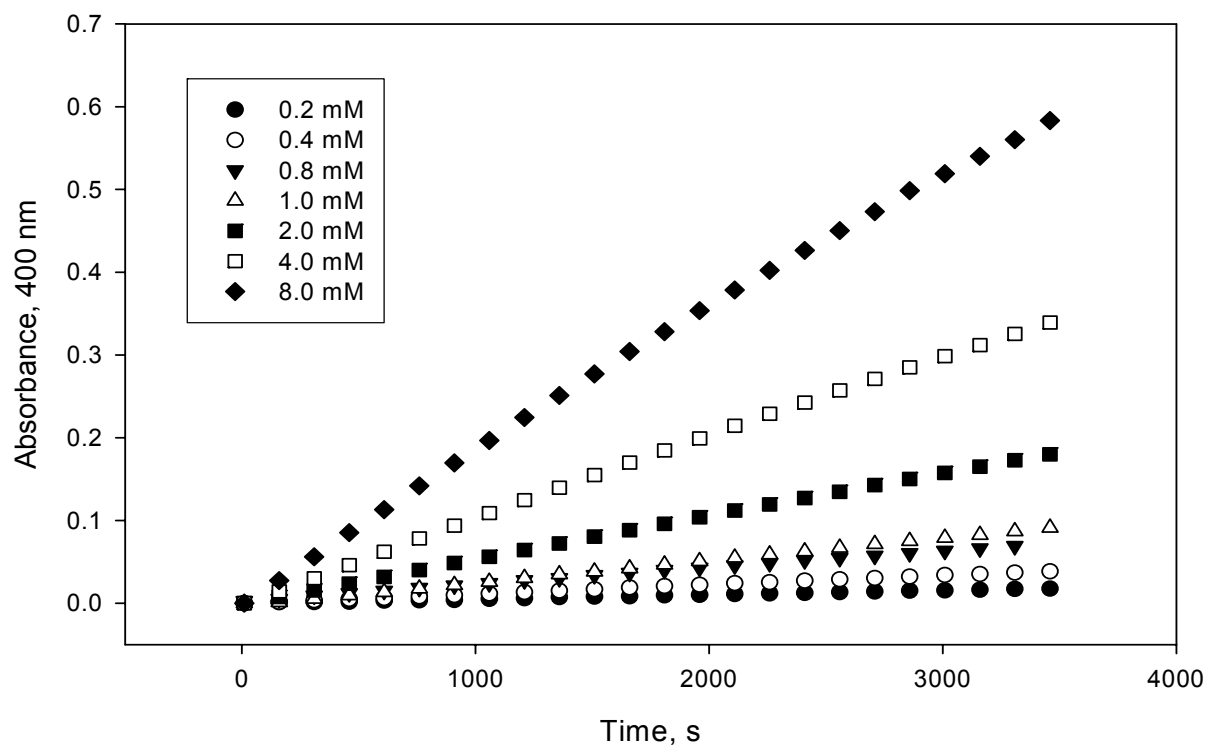


Figure s2. Examples of plots of absorbance change vs. time for the reactions of BNPP with EuDO2A^+ , 5 mM, pH 7.90 (\circ); EuDO2A^+ , 10 mM, pH 9.35 (\blacktriangledown); and EuHEDTA , 20 mM, pH 11.0 (\bullet). $[\text{BNPP}] = 0.10 \text{ mM}$, 25°C , $\mu = 0.10$, $(\text{CH}_3)_4\text{NCl}$. The data were fitted to the equation: $[\text{4-Nitrophenolate}] = [\text{BNPP}]_0(1 - e^{-kt})$. The final absorbances reach a limiting value of 1.87, indicating that the 0.10 mM BNPP is close to 100% reaction completion.

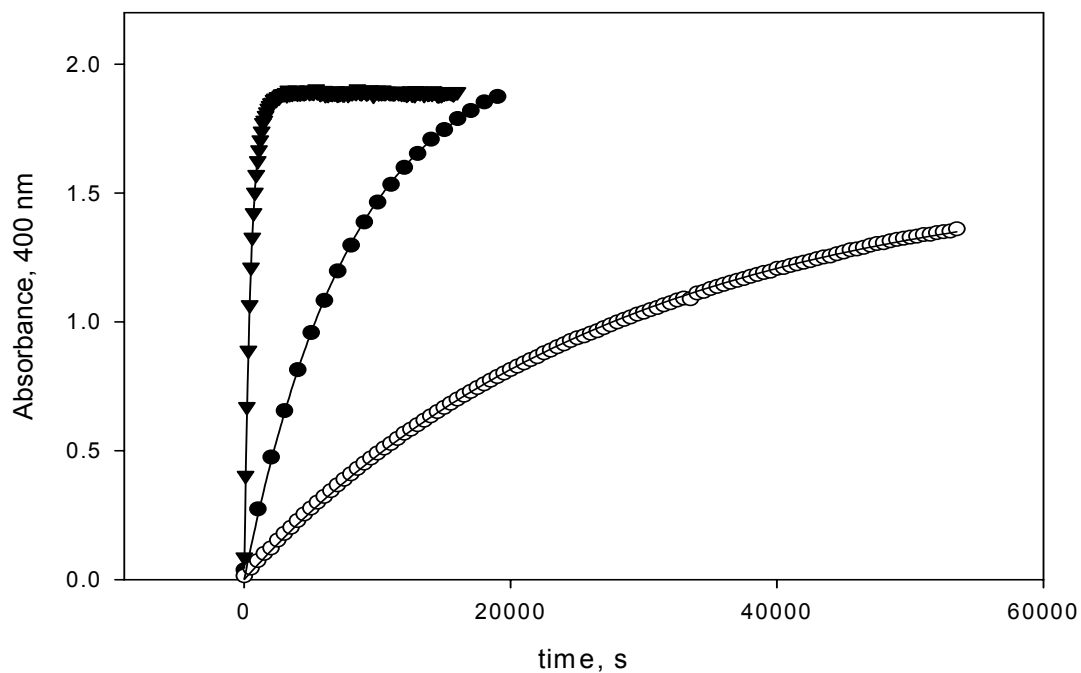


Figure s3. Potentiometric EuDO_2A^+ titration curves with different equilibration time interval (i.e. 30 mins, 10 hrs and 3 weeks) for data acquisition. $[\text{Eu}^{3+}] = 1.0$ mM, $[\text{DO}_2\text{A}] = 1.02$ mM. $\mu = 0.1$, $(\text{CH}_3)_4\text{NCl}$.

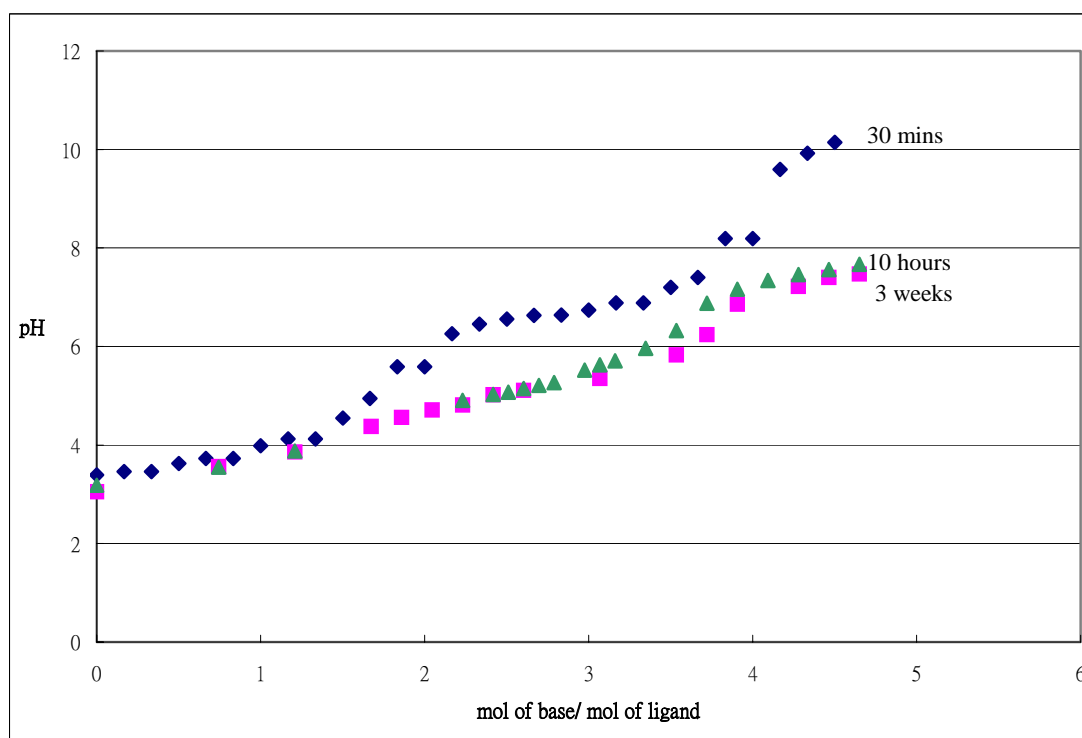


Figure s4. The observed absorbances at 298 nm vs. time for CeDO_2A^+ , 1.0 mM, at various solution pH.

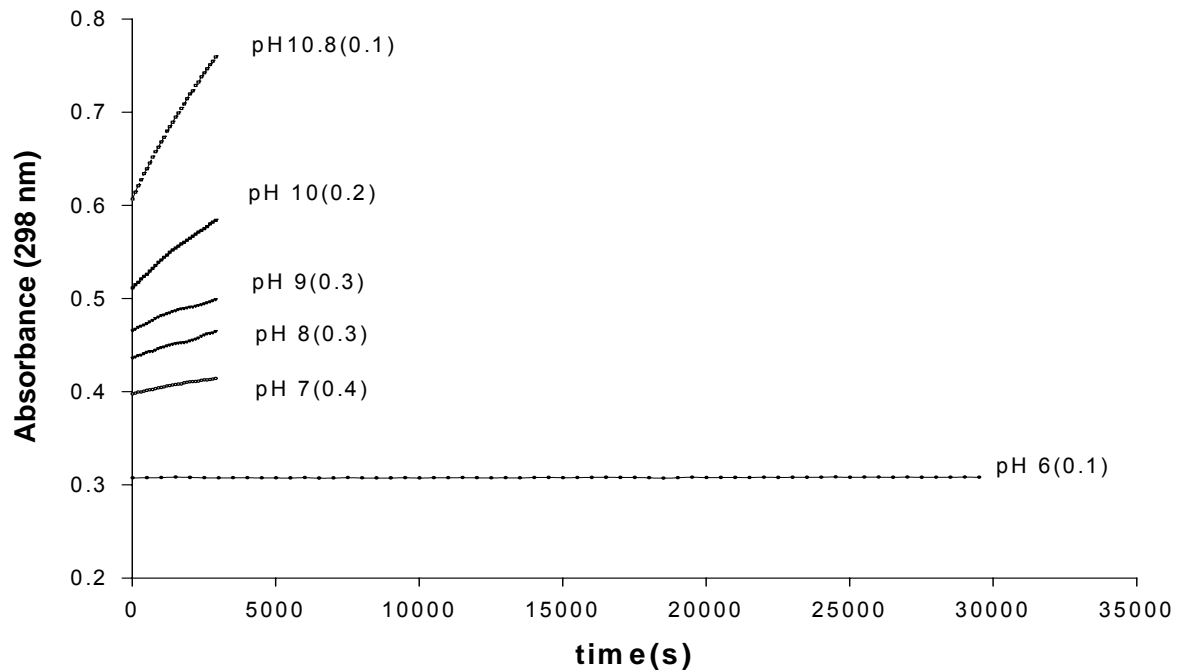


FIGURE CAPTIONS

Figure 1. Dependence of pseudo first order rate constant of BNPP hydrolysis on the concentration of EuDO2A^+ at 25°C , pH 7.90, $[\text{MPS}] = 20 \text{ mM}$, $\mu = 0.10 \text{ M}$ $(\text{CH}_3)_4\text{NCl}$, $[\text{BNPP}] = 0.10 \text{ mM}$. The line is calculated based on the best fit to the monomer-dimer reaction model in Scheme 1.

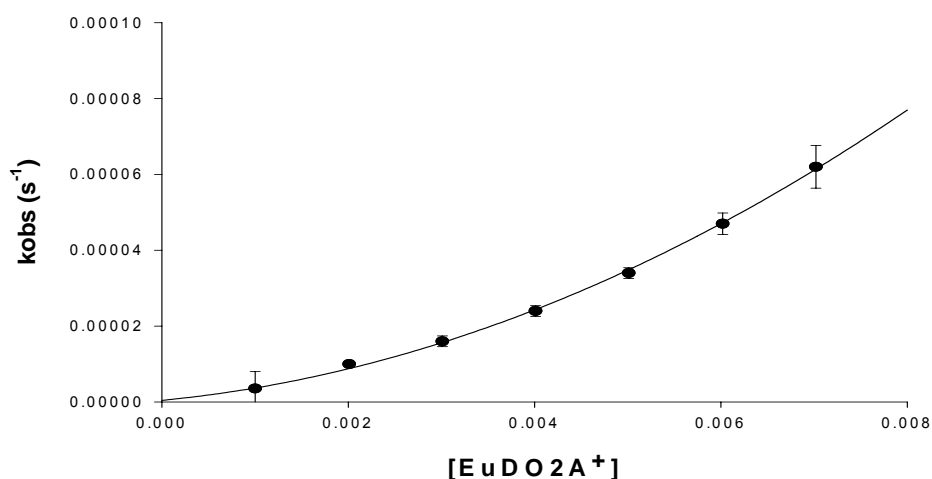


Figure 2. Dependence of pseudo first order rate constant of BNPP hydrolysis on concentration of EuDO2A^+ ; 25°C , pH 9.35, $[\text{BNPP}] = 0.10 \text{ mM}$, $\mu = 0.10 \text{ M}$ $(\text{CH}_3)_4\text{NCl}$. Solid line is the best fit to the monomer-dimer saturation reaction model.

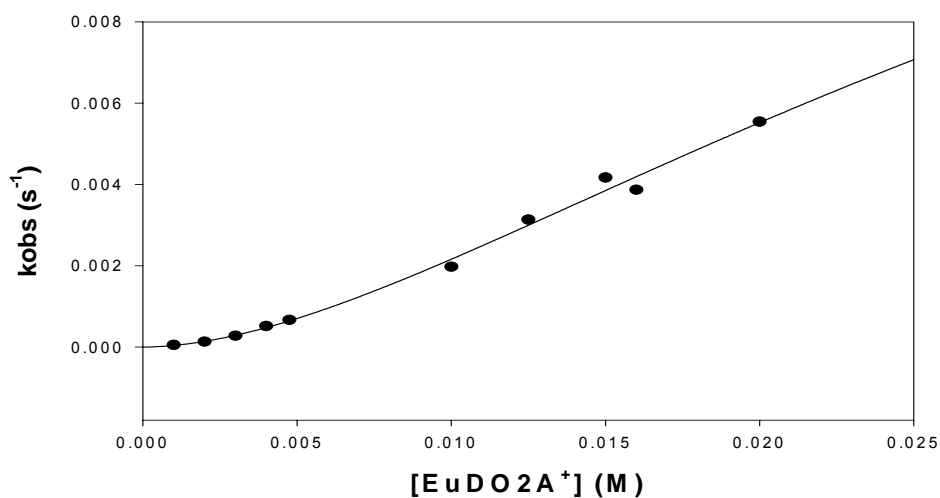


Figure 3. Dependence of pseudo first order rate constant on $[\text{EuHEDTA}]$, $[\text{BNPP}] =$

0.10 mM, pH 11.0, 25°C, $\mu = 0.10 \text{ M } (\text{CH}_3)_4\text{NCl}$.

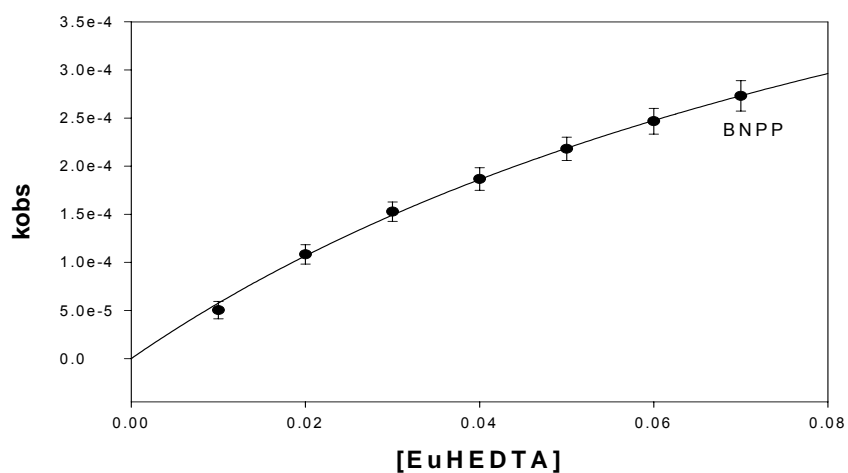


Figure 4. The plots of observed and calculated BNPP hydrolysis rate constants promoted by EuDO_2A^+ after different complex equilibration time vs. pH. The calculated curves were obtained as discussed at the end of this paper (*vide infra*).

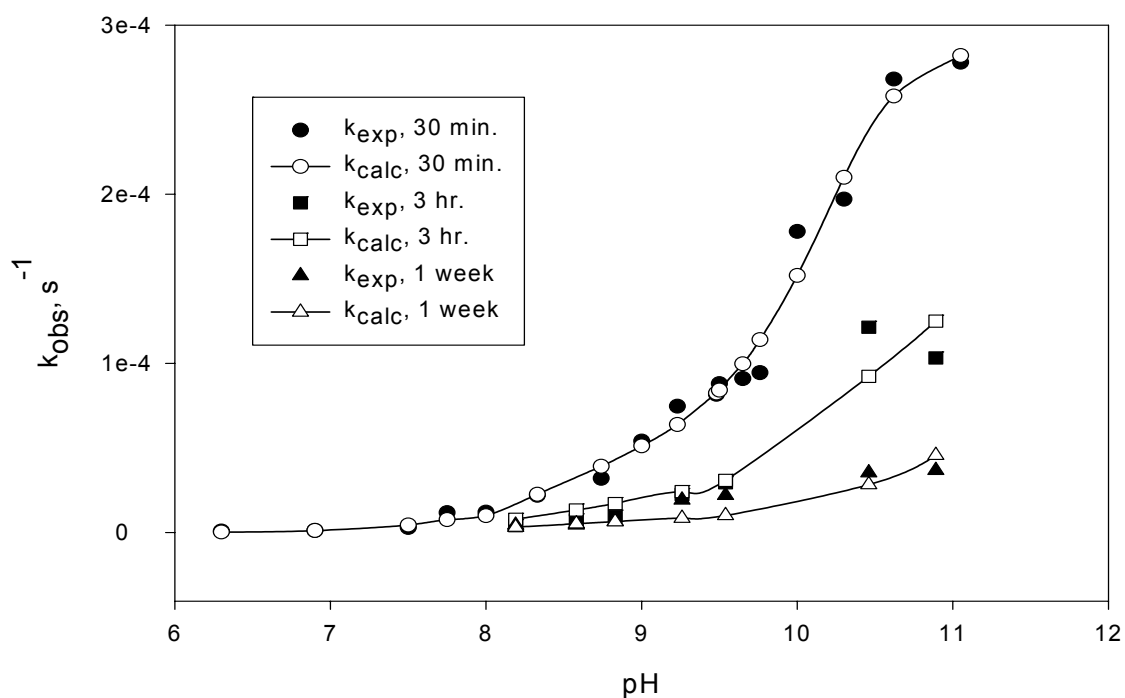
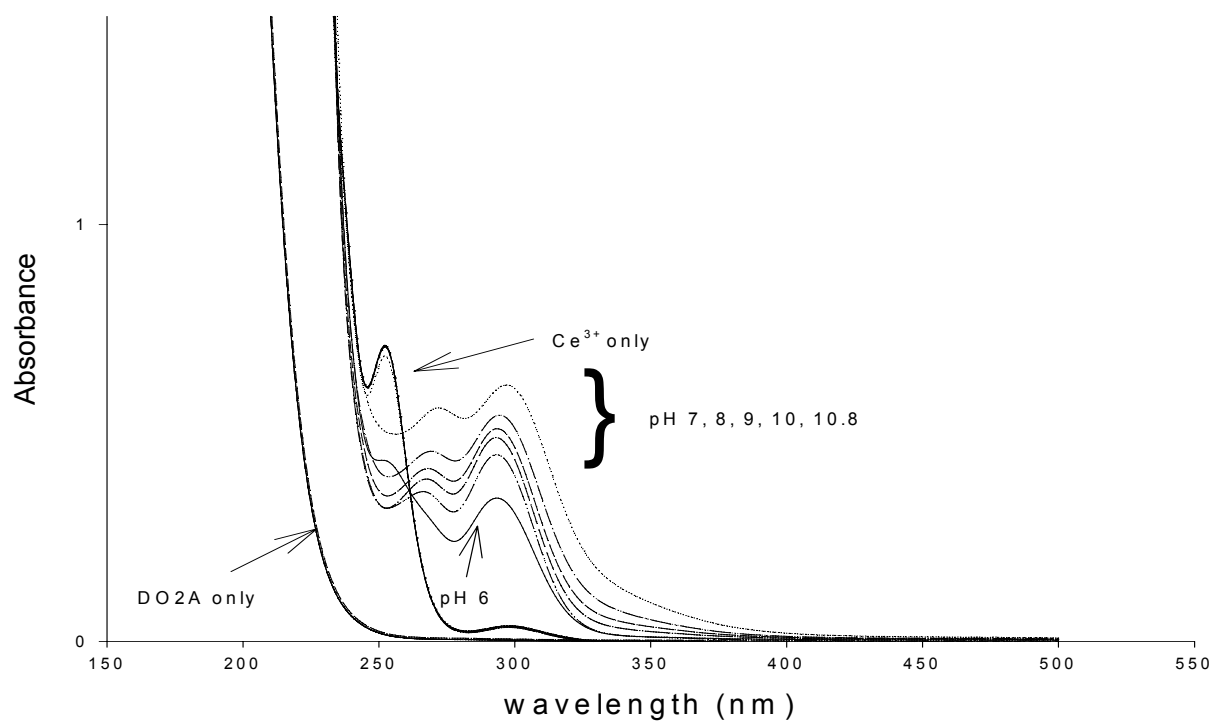


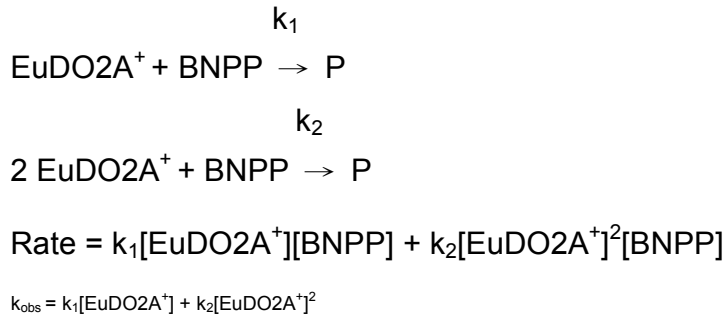
Figure 5. The spectra of $1.0 \text{ mM } \text{CeDO}_2\text{A}^+$ at 25°C, pH = 6, 7, 8, 9, 10, and 10.8. The Ce^{3+} and DO_2A spectra were measured at $[\text{Ce}^{3+}] = 1.0 \text{ mM}$ and $[\text{DO}_2\text{A}]$

=1.02 mM, respectively.

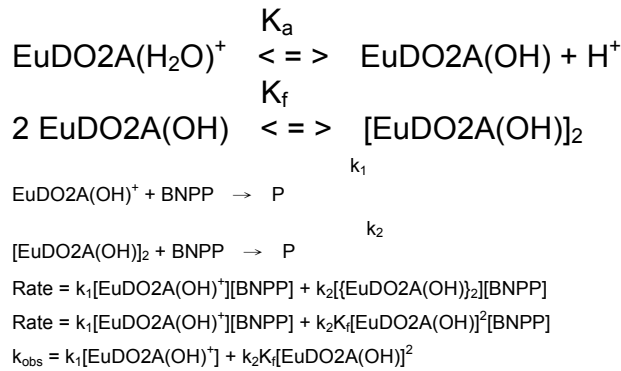


SCHEME TITLES

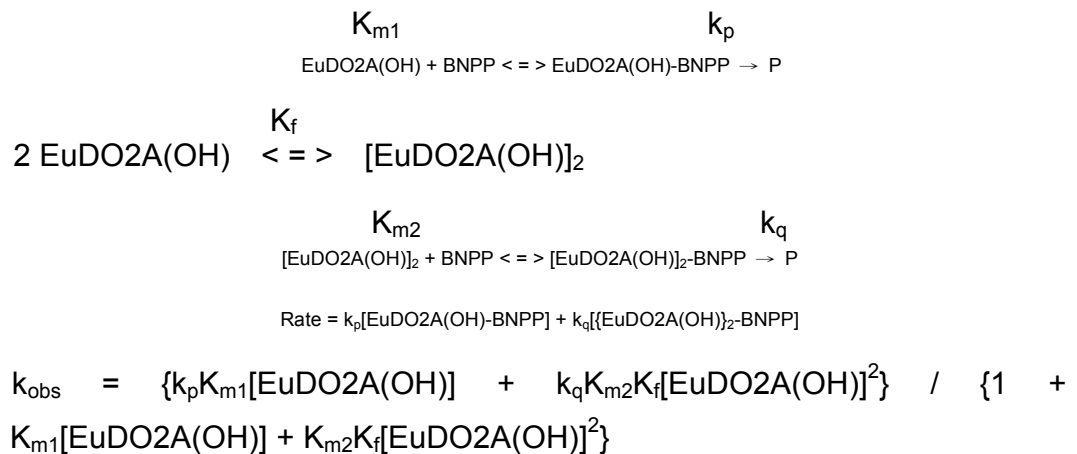
Scheme 1. A simple monomer reaction model (pH 7.9).



Scheme 2. A monomer-dimer reaction model (pH 7.9).

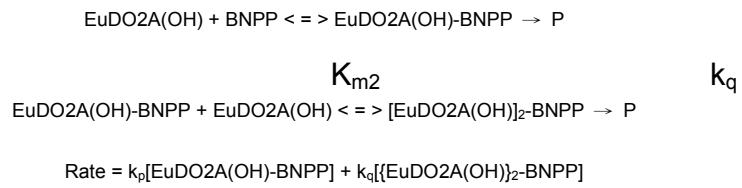


Scheme 3. A monomer-dimer saturation reaction model (pH 9.35).



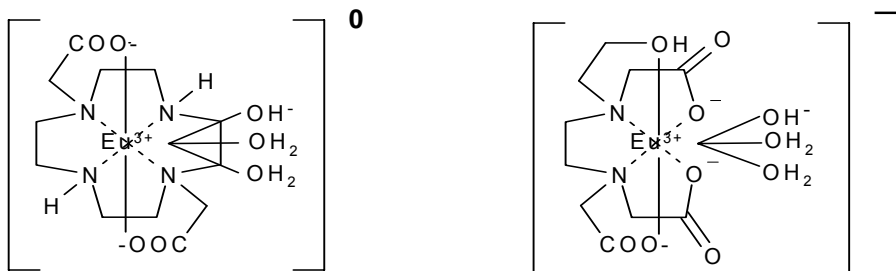
Scheme 4. A monomer saturation reaction model (pH 9.35).



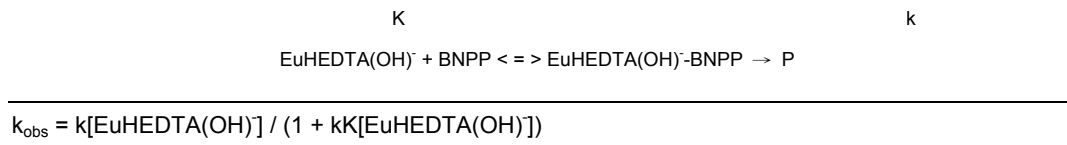


$$k_{\text{obs}} = \frac{\{k_p K_{m1} [\text{EuDO2A(OH)}] + k_q K_{m2} K_{m2} [\text{EuDO2A(OH)}]^2\}}{\{1 + K_{m1} [\text{EuDO2A(OH)}] + K_{m1} K_{m2} [\text{EuDO2A(OH)}]^2\}}$$

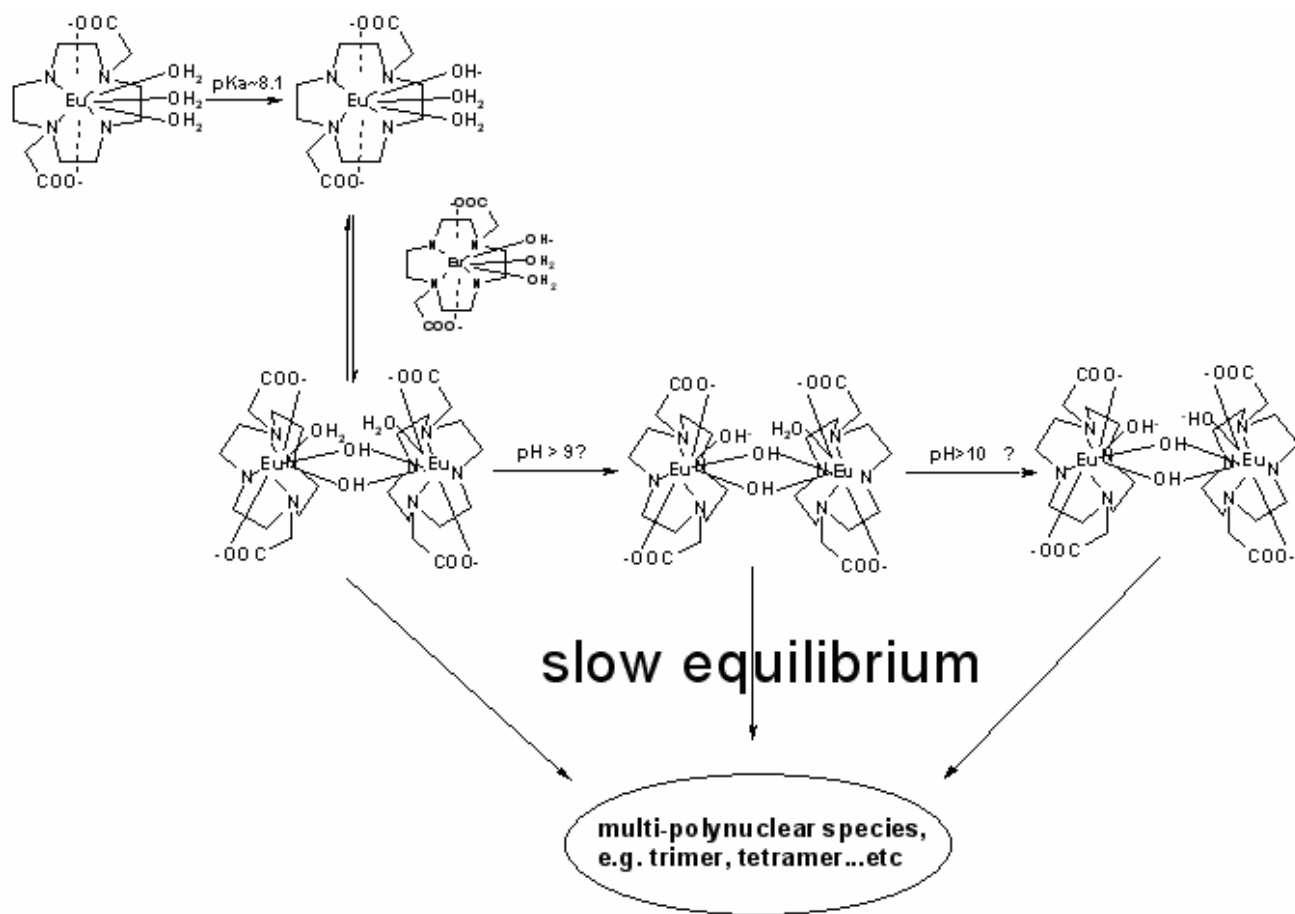
Scheme 5. Structural formulas of EuDO2A(OH) and EuHEDTA(OH)⁻



Scheme 6. A saturation kinetic model.



Scheme 7. Proposed dimerization, deprotonation, and polynuclear species formation of the EuDO2A⁺ complex.



TABLES

Table 1. Initial rates of EuDO2A^+ + BNPP reactions at pH 7.90 and 9.35, 25°C, $\mu = 0.10$, $\text{N}(\text{CH}_3)_4\text{Cl}$. For [BNPP]-dependence initial rates measurements, $[\text{EuDO2A}] = 1.0$ mM. For $[\text{EuDO2A}^+]$ -dependence initial rates measurements, $[\text{BNPP}] = 0.10$ mM.

[BNPP]-dependence studies			[EuDO2A]-dependence studies		
	Initial rates, $\text{M}\cdot\text{s}^{-1}$			Initial rates, $\text{M}\cdot\text{s}^{-1}$	
[BNPP], mM	pH 7.90	pH 9.35	[EuDO2A], mM	pH 7.90	pH 9.35
0.1	-	2.91×10^{-9}	2.0	2.45×10^{-10}	7.48×10^{-9}
0.2	2.32×10^{-10}	5.22×10^{-9}	3.0	5.60×10^{-10}	1.86×10^{-8}
0.4	5.73×10^{-10}	1.12×10^{-8}	4.0	7.11×10^{-10}	3.16×10^{-8}
0.8	1.11×10^{-9}	-	5.0	9.12×10^{-10}	4.82×10^{-8}
1.0	1.36×10^{-9}	2.86×10^{-8}	6.0	1.08×10^{-9}	5.48×10^{-8}
2.0	2.89×10^{-9}	5.79×10^{-8}	7.0	-	7.37×10^{-8}
4.0	5.61×10^{-9}	9.68×10^{-8}	-	-	-
8.0	1.01×10^{-8}	-	-	-	-
20.0	2.21×10^{-8}				

Table 2. The observed BNPP hydrolysis rate constants vs. $[\text{EuDO2A}^+]$ at pH 7.90 and 9.35, and vs. $[\text{EuHEDTA}]$ at pH 11.0. $[\text{BNPP}] = 0.10$ mM, at 25°C, $\mu = 0.10$, $\text{N}(\text{CH}_3)_4\text{Cl}$.

pH 7.90		pH 9.35		pH 11.0	
$[\text{EuDO2A}^+]$, mM	k_{obs} , s^{-1}	$[\text{EuDO2A}^+]$, mM	k_{obs} , s^{-1}	$[\text{EuHEDTA}]$, mM	k_{obs} , s^{-1}
1.00	3.55×10^{-6}	1.00	5.15×10^{-5}	10.0	6.00×10^{-5}
2.00	1.00×10^{-5}	2.00	1.33×10^{-4}	20.0	1.19×10^{-4}
3.00	1.60×10^{-5}	3.00	2.79×10^{-4}	30.0	1.64×10^{-4}
4.00	2.40×10^{-5}	4.00	5.17×10^{-4}	40.0	2.00×10^{-4}

5.00	3.40×10^{-5}	4.75	6.68×10^{-4}	50.0	2.32×10^{-4}
6.00	4.70×10^{-5}	10.0	1.98×10^{-3}	60.0	2.62×10^{-4}
7.00	6.20×10^{-5}	12.5	3.14×10^{-3}	70.0	2.91×10^{-4}
		15.0	4.17×10^{-3}		
		16.0	3.87×10^{-3}		
		20.0	5.55×10^{-3}		

Table 3. The experimentally observed and calculated BNPP hydrolysis rate constants vs. pH by EuDO2A^+ at various equilibration time. $[\text{EuL}] = 1.0 \text{ mM}$, $[\text{BNPP}] = 0.10 \text{ mM}$, 25°C , $\mu = 0.10$, $(\text{CH}_3)_4\text{NCl}$. The calculated values were obtained by using the respective k_1 , k_2 , k_3 , and k_4 values $3.08 \times 10^{-2} \text{ M}^{-1}\text{s}^{-1}$, $2.20 \text{ M}^{-1}\text{s}^{-1}$, $1.05 \text{ M}^{-1}\text{s}^{-1}$, and $0.280 \text{ M}^{-1}\text{s}^{-1}$ and $K_f = 11.9$, $\text{pK}_{h1} = 8.33$, $\text{pK}_{h2} = 8.97$, and $\text{pK}_{h3} = 10.09$, employing equations 6,5 and 3 (see text).

30 minutes			3 hour			1 week		
PH	k_{exp}	k_{calc}	pH	k_{exp}	k_{calc}	pH	k_{exp}	k_{calc}
11.05	2.78×10^{-4}	2.82×10^{-4}	10.89	1.03×10^{-4}	1.25×10^{-4}	10.89	3.68×10^{-5}	4.56×10^{-5}
10.62	2.68×10^{-4}	2.58×10^{-4}	10.46	1.21×10^{-4}	9.23×10^{-5}	10.46	3.53×10^{-5}	2.83×10^{-5}
10.30	1.97×10^{-4}	2.10×10^{-4}	9.54	2.94×10^{-5}	3.09×10^{-5}	9.54	2.20×10^{-5}	1.01×10^{-5}
10.00	1.78×10^{-4}	1.52×10^{-4}	9.26	2.25×10^{-5}	2.42×10^{-5}	9.26	1.93×10^{-5}	8.45×10^{-5}
9.76	9.45×10^{-5}	1.14×10^{-4}	8.83	9.63×10^{-6}	1.71×10^{-5}	8.83	6.68×10^{-6}	6.44×10^{-6}
9.65	9.10×10^{-5}	9.97×10^{-5}	8.58	7.49×10^{-6}	1.33×10^{-5}	8.58	4.49×10^{-6}	5.20×10^{-6}
9.50	8.80×10^{-5}	8.42×10^{-5}	8.19	4.06×10^{-6}	7.88×10^{-6}	8.19	4.39×10^{-6}	3.24×10^{-6}
9.48	8.16×10^{-5}	8.24×10^{-5}						
9.23	7.46×10^{-5}	6.38×10^{-5}						
9.00	5.40×10^{-5}	5.12×10^{-5}						
8.74	3.20×10^{-5}	3.91×10^{-5}						
8.33	2.20×10^{-5}	2.26×10^{-5}						
8.00	1.20×10^{-5}	9.97×10^{-6}						

7.75 1.17×10^{-5} 7.60×10^{-6}

7.50 2.90×10^{-6} 4.42×10^{-6}

6.90 1.20×10^{-6} 1.14×10^{-6}

6.30 8.10×10^{-7} 2.88×10^{-7}

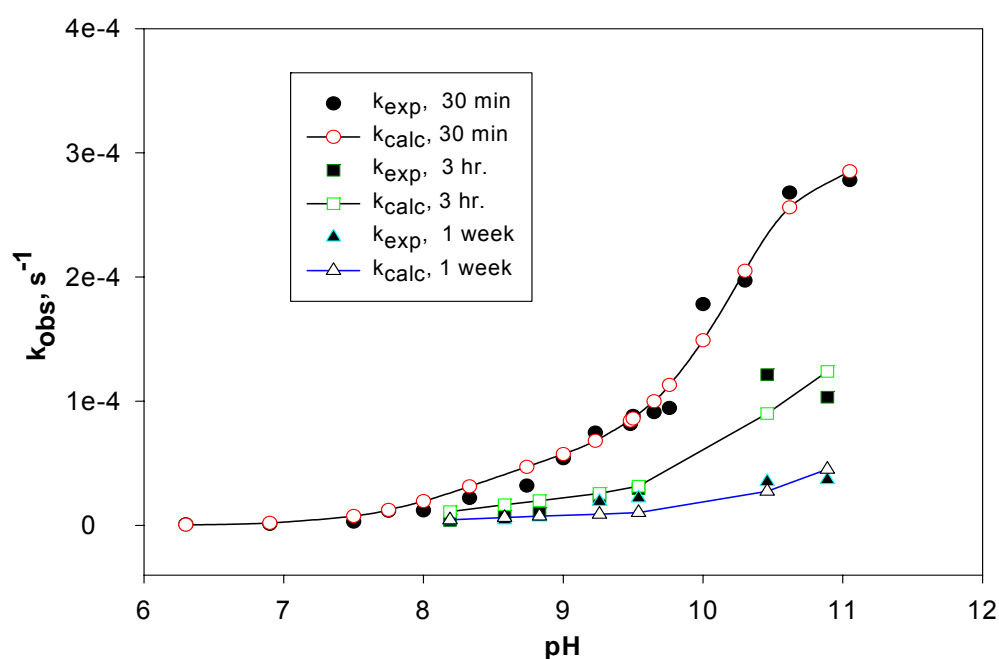
References:

1. This is Part 2 under the general title "Macrocyclic Lanthanide Complexes as Artificial Nucleases and Ribonucleases". Part 1: Chang, C. A.; Wu, B. H.; Kuan, B. Y. *Inorg. Chem.*, **2005**, *44*, 6646-6654.
2. Trawick, B. N.; Daniher, A. T.; Bashkin, J. K. *Chem. Rev.* **1998**, *98*, 939-960.
3. Oivanen, M.; Kuusela, S.; Lönnberg, H. *Chem. Rev.* **1998**, *98*, 961-990.
4. Williams, N. H.; Takasaki, B.; Well, M.; Chin, J. *Acc. Chem. Res.* **1999**, *32*, 485-493.
5. Roigk, A.; Hettich, R.; Schneider, H.-J. *Inorg. Chem.* **1998**, *37*, 751-756.
6. Chang, C. A.; Shieh, F.-K.; Liu, Y.-L.; Chen, Y.-H.; Chen, H.-Y.; Chen, C.-Y. *J. Chem. Soc. Dalton Trans.*, **1998**, 3243-3248.
7. Hurst, P.; Takasaki, B. K.; Chin, J. *J. Am. Chem. Soc.* **1996**, *118*, 9982-9983.
8. Deal, A. K.; Burstyn, J. N. *Inorg. Chem.* **1996**, *35*, 2792-2798.
9. Hegg, E. L.; Mortimore, H. S.; Cheung, C. L.; Huyett, J. E.; Powell, D. L.; Burstyn, J. N. *Inorg. Chem.* **1999**, *38*, 2961-2968.
10. Gómez-Tagle, P.; Yatsimirsky, A. K. *Inorg. Chem.* **2001**, *40*, 3786-3796.
11. Wu, B. H.; Chang, C. A. unpublished results.
12. Pfefferie, J.-M.; Bunzli, J.-C. G. *Helv. Chim. Acta.* **1989**, *72*, 1487-1494.
13. Oh, S. J.; Choi, Y.-S.; Hwangbo, S.; Bae, S.; Ku, J. K.; Park, J. W. *Chem. Commun.* **1998**, 2189-2190.
14. McCue, K. P.; Morrow, J. R. *Inorg. Chem.* **1999**, *38*, 6136-6142.
15. Kovari, E.; Kramer, R. *J. Am. Chem. Soc.* **1996**, *118*, 12704-12709.
16. Deal, K. D.; Park, G.; Shao, J.; Chasteen, N. D.; Brechbiel, M. W.; Planalp, R. P. *Inorg. Chem.* **2001**, *40*, 4176-4182.
17. Gajda, T.; Düpre, Y.; Török, I.; Harmer, J.; Schweiger, A.; Sander, J.; Kuppert, D.; Hegetschweiler, K. *Inorg. Chem.* **2001**, *40*, 4918-4927.
18. Jurek, P. E.; Jurek, A. M.; Martell, A. E. *Inorg. Chem.* **2000**, *39*, 1016-1020.
19. Hettich, R.; Schneider, H. J. *J. Am. Chem. Soc.* **1997**, *119*, 5638-5647.
20. Roigk, A.; Yescheulova, O. V.; Fedorov, Y. V.; Fedorova, O. A.; Gromov, S. P.; Schneider, H. *J. Org. Lett.* **1999**, *1*, 833-835.

21. Karsten, P.; Neves, A.; Bortoluzzi, A. J.; Lanznaster, M.; Drago, V. *Inorg. Chem.* **2002**, *41*, 4624-4626.
22. Huskens, J.; Torres, D.A.; Kovacs, Z.; Andre, J.P.; Geraldes, C.F.G.C.; Sherry, A.D. *Inorg. Chem.* **1997**, *36*, 1495-.
23. Zheng, Z. *J. Chem. Soc. Chem. Commun.* **2001**, 2521-2529.
24. Wang, R.; Carducci, M.D.; Zheng, Z. *Inorg. Chem.* **2000**, *39*, 1836-1837.
25. Zheng, X.-J.; Jin, L.-P.; Gao, S. *Inorg. Chem.* **2004**, *43*, 1600-1602.
26. Wang, R.; Zheng, Z.; Jin, T.; Staples, R. *Angew. Chem. Intl. Ed.* **1999**, *38*, 1813-1815.

SYNOPSIS TOC.

EuDO2A⁺ promoted BNPP hydrolysis k_{obs} vs. pH at various equilibration time



Short text for the table of content:

More detailed analysis of the BNPP phosphodiester bond hydrolysis rate constants data vs. [EuDO2A⁺] (1.0 – 20.0 mM) at pH 9.35 using a monomer-dimer saturation reaction

model indicates that the dimeric species, probably the hydroxo-bridged $[\text{EuDO}_2\text{A}(\text{H}_2\text{O})(\mu\text{-OH})]_2$, is much more reactive than the monomer. As the EuDO_2A^+ equilibration time was increased, the BNPP hydrolysis rates were found to be slower, particularly at high pH. This kinetic effect is attributed to possible slow formation of less active or inactive polynuclear species such as $\text{L}_4\text{Eu}_4(\mu\text{-OH})_4$.

Appendix 2.

**Polysaccharide Composition, Structure, *In Vitro*
Immuno-Modulating and Anti-tumor Activities of Some
Regional Different Strains of *Lentinula edodes***

Key words: α -glucan / immune-modulation / *Lentinula edodes* / polysaccharide/ structure

Chien -Ting Lo¹, Bor-Cheh Wang², C. Allen Chang^{1, #}

¹ Department of Biological Science and Technology, National Chiao Tung University, Hsinchu, Taiwan, ROC.

² Food Industry Research and Development Institute, Hsinchu, Taiwan, ROC.

[#] Corresponding author: C. Allen Chang, Professor, Ph.D., Department of Biological Science and Technology, National Chiao Tung University, 75 Po-Ai Street, Hsinchu, Taiwan, ROC. Phone: 886-3-571-2121 ext. 56903; FAX: 886-3-572-9288.

E-mail: changca@cc.nctu.edu.tw

Running title: α -glucan immune-modulating and anti-tumor activities from *L. edodes*

Abstract

The monosaccharide composition, molecular weight, structural linkage, immuno-modulating and anti-tumor activities were investigated for polysaccharides extracted from different phylogenetic groups of ten regional *Lentinula edodes*. The immuno-modulating properties and anti-tumor activities of these *L. edodes* extracts including crude polysaccharides and hot-water-extracts obtained from culture broth filtrates were tested using several different cell lines. The results showed that the ten isolated *L. edodes* could be classified into three distinct groups using amplified fragment length polymorphism assay. All isolates had similar molecular weight distribution between 1×10^2 and 3×10^3 kDa and the monosaccharide composition analysis revealed the presence of glucose, mannose, xylose, galactose, fucose, rhamnose and arabinose in different ratios. The elucidated structural features of a crude polysaccharide fraction showed a new form of polysaccharide linkage with a backbone of α -(1→4)-glucan and side chains of β -(1→6)-glucan. Most of the culture broth filtrates exhibited significant enhancement in macrophage stimulatory activity. Indirect *in vitro* anti-cancer assay was also positive indicating that the effect is possibly due to a preliminary macrophage stimulatory activity with subsequent release of TNF- α or other biochemicals to inhibit tumor cell growth.

Introduction

Mushrooms such as *rieshi* (*Ganoderma lucidum*), *shiitake* (*Lentinula edodes*.) and others have been cultivated and used for many years (Reshetnikov *et al.*, 2001). More than 140,000 different kinds of species, i.e. roughly 10% of available species on earth have been identified (Wasser, 2002). They have been valued as flavorful and nutritious foods as well as precious medicines, e.g. as immune-modulators, in the Far East. Among them, the shiitake mushroom, *L. edodes* is the most important cultivated mushroom and is easily available from Korea, Russia, Taiwan, China and Japan (Campbell, *et al.*, 1987; Fox, *et al.*, 1994). Of all the mushroom immune-modulators investigated, bioactive polymers from *Lentinula edodes* have been studied the most (Hobbs, *et al.*, 2000).

More than 100 cultivated shiitake strains have been developed. Traditional methods to differentiate various strain typing in shiitake cultivars were usually carried out based on morphological, physiological, and somatic compatibility characteristics (Chiu, *et al.*, 1999). Recently, additional molecular techniques were developed. For example, Vos *et al.* (1995) developed AFLP (amplified fragment length polymorphism) fingerprinting analysis based on selective polymerase chain reaction (PCR) amplification of genomic DNA restriction fragments and demonstrated that AFLP analysis could reproducibly help identify a large number of polymorphic loci to differentiate various strains (Vos, *et al.*, 1995). Applications of AFLP analysis (fingerprinting) for population studies have become quite popular and important, and have been reported frequently (Geornaras, *et al.*, 1999; Jiang, *et al.*, 2000). The technique could successfully differentiate not only the diversity in flowering plants populations but also a wide variety of organisms (Quagliaro, *et al.*, 2001; Savelkoul, *et al.*, 1999; Wang, *et al.*, 2004). For example, AFLP marker techniques have successfully been used to derive the genetic linkage map of *L. edodes* for frozen material and heat dried fruiting bodies (Terashima, *et al.*, 2002; Terashima, *et al.*, 2004).

The basic composition of mushrooms includes vitamins, minerals, phenolic compounds, total carbohydrates, dietary fiber, crude fat, ash, nitrogen, and protein that vary considerably in different strains (Mattila, *et al.*, 2001, 2002). According to Crisan *et al.* and Bano *et al.*, the carbohydrate contents of *L. edodes* varied from 67.5% to 78% on a dry weight basis (Bano, *et al.*, 1988; Crisan, *et al.*, 1978). The carbohydrates in

mushrooms include polysaccharides (PS) such as glucans, mono- and di-saccharides, sugar alcohols, glycogen, and chitin (Kurzman, *et al.*, 1997). Of all, β -glucan has been identified as the major structural component among many polysaccharides with anti-cancer activities (Bohn, *et al.*, 1995). For example, Lentinan (extracted from cell wall of fruiting body), KS-2 (a α -mannan peptide extracted from culture mycelia) and LEM (a β -glucan-protein complex extracted from solid medium) of *L. edodes* are demonstrated to be immuno-potentiators and exhibit anti-cancer activities (Chihara, *et al.*, 1970; Fujii, *et al.*, 1978; Harumi *et al.*, 1989; Suzuki, *et al.*, 1988). Mueller *et al.*, (2000) have reported that binding of glucans to macrophage and neutrophil cell lines resulted in stimulation of the expression of nuclear factor- κ B (NF κ B). The structural elucidations for Lentinan show the presence of only glucose molecules with mostly β -(1 \rightarrow 3)-glucan linkages in the regularly branched backbone and β -(1 \rightarrow 6)-glucan in side chains (Aoki, *et al.*, 1984; Hamuro, *et al.*, 1978). The major active constituent of the KS-2 mycelium extract is reported to be a hetero-glycan protein conjugate containing *ca.* 24.6% protein and 44% monosaccharide in addition to nucleic acid derivatives and vitamins (Breene, *et al.*, 1990). Simultaneously, many other active PS, protein-polysaccharide conjugates and water-soluble lignin's were isolated (Tabata, *et al.*, 1992). However, the reported structures are varied and include α -glucans as well as many hetero-glucans (Mizuno, T., *et al.*, 1995; Mizuno, M., *et al.*, 1998; Tanigami, *et al.*, 1991).

Shida *et al.* reported the extraction of α -(1 \rightarrow 3)-D-glucan from fruiting bodies of *L. edodes* (Shida, *et al.*, 1975, 1978). However, not much attention was paid to the properties of this form of glucan. Rather, modified PS such as those by sulfation, sulfonylation or carboxymethylation that showed high anti-cancer activities gained rapid attention and wide scale applications in recent years (Bao, *et al.*, 2001; Demleitner, *et al.*, 1992, Jiang, *et al.*, 2000, Suzuki, *et al.*, 1991; Willför, *et al.*, 2003). Specifically, α -glucan and modified α -glucan (e.g. as sulfate) of *L. edodes* were demonstrated to show anti-cancer activities against Sarcoma 180 (*in vivo*) and against six tumor cell lines (*in vitro*, Zhang, *et al.*, 2002). In some cases, unmodified α -glucan failed to inhibit *in vitro* tumor growth (Zhang, *et al.*, 2002).

The studies on the structure-activity relationship and diversity of glucans mediated

immuno-pharmacological activities have since gained momentum (Fox, *et al.*, 1994; Nagi, *et al.*, 1993; Ohno, *et al.*, 1995; Suzuki, *et al.*, 1988). The pharmacological activities of mushroom PS against tumors have been thoroughly reviewed (Ooi, *et al.*, 1999). The preliminary anti-cancer mechanisms of whole mushrooms and isolated PS are proposed to involve the intervention of 'T' cells and macrophages (Borchers, *et al.*, 1999). TNF- α (tumor necrosis factor, a pro-inflammatory cytokine) is then released from macrophages or activated 'T' cells in response to microbes or other agents (Zhang, *et al.*, 2004). The detailed mechanisms by which these PS compounds exert their anti-cancer effects remain largely unexplored despite the established vital role of glucans.

In this paper, we have selected ten regional different *L. edodes* and determined the monosaccharide composition, molecular weight distribution, structural linkages and macrophage-stimulating and anti-cancer activities of their PS extracts, hoping to add new and more insights to this important research area.

Results

The step-wise experimental procedures adopted to prepare culture broth filtrate (CBF) and to isolate hot water extract (HWE) of crude PS for composition analysis and anti-cancer activity assays are shown in Fig. 1.

L. edodes culture.

The optimum environmental conditions for culture growth and PS production of mushrooms in liquid cultures are dependent on strains. Initially, the growth conditions of the culture were optimized that showed a stationary phase after 14 days. It was observed that *L. edodes* produced most PS and showed highest immuno-stimulating activity in the stationary phase. The biomass of the CBF extracts of all strains was estimated to be in the range 0.35 to 0.40 g/50 ml and pH between 2.5 and 2.8 for 14 days (Supplementary data, Fig. A and Fig. B). These values would be useful as references for optimization and pilot plant production studies in the future. Recently, the submerged cultivation of mushroom has received much attention in Asian regions as a promising alternative for efficient production of its valuable metabolites, especially PS and ganoderic acids

(Hwang, *et al.*, 2003; Zhang, *et al.*, 2002). It usually takes several months to cultivate the fruiting body of the mushroom, and it is also difficult to control product quality during soil cultivation. There is a great need to supply the market with a large amount of high-quality mushroom products. Therefore, submerged cultivation of mushroom could eventually supplement the need and proves useful over fruiting body cultivation.

Strain typing/phylogenetic mapping.

The ten isolates of *L. edodes* were grouped into three distinct clusters by AFLP: (1) L24 and L25 isolates from China; (2) L1 and L4 isolates from Taiwan; (3) L6, L10, L11, L15, L21 and L23 isolates from Japan. The DNA material and adaptors were digested with restriction enzymes, *Mse* I and *Eco* RI, to prepare the AFLP template for sequence analysis. Two primer sets, *Eco* RI-AC-FAM/*Mse* I-CAA and *Eco* RI-AA-FAM/*Mse* I-CAC, were employed for selective amplification. The band positions of selected primers were used to construct a similarity index and an attempt was made to match the regionally different strains. A dendrogram of the similarity index based on the bands obtained for selected two primer sets was plotted to distinguish the closely related strains (Fig. 2). A very close genetic homogeneity among cultivated strains of Japanese mushrooms, L11, L15 and L10 was seen. Similarly, for the Taiwanese and Chinese mushrooms, the obtained AFLP fingerprints point out close resemblance to the genetic homogeneity. However, L24 and L25 mushrooms from China were quite different from the Japanese and Taiwanese mushrooms. The mushrooms, L1 and L4 were cultivated heterogeneous strains comprising of Japanese strains SL-19 and 271.

The dendrogram obtained using AFLP (fingerprinting) analysis of *L. edodes* provides new insight into the population structure of this mushroom species and proves useful for phylogenetic type studies. The results appear promising and are well supported by results obtained using random amplified polymorphic DNA (RAPD) assay (fingerprinting) for the same species (Huang, *et al.*, 1999). Therefore, application of AFLP fingerprint assay for phylogenetic studies of mushrooms can now be included among other reported species in population studies.

Immuno-modulating and anti-cancer activities.

The molecular weight fractions and chemical compositions of PS produced are strongly dependent on strain variations, extraction methods and culture conditions (Jin, *et al.*, 2003). Therefore, a comparative study of immuno-modulating and anti-cancer properties using CBF deserved further investigation. The CBF of all mushroom strains were used to treat RAW 264.7 cell line to test the immuno-stimulating activity (Fig. 3A). The strains with increasing NBT % reduction follow the order: (L15>L23>L10)> (L21>L6)> (L11>L24)> (L1>L25>L4). Based on the order of highest immuno-stimulating activity exhibits, the CBF of L15 and L23 strains were further tested for its ability to produce TNF- α (Fig. 3B). When lipo-polysaccharide or glucan extracts alone were used, TNF- α release was not impressive. But adding them together resulted in synergistically increased production of TNF- α . Similar behavior was observed among different strains of fungi previously and it was suggested that lipo-polysaccharide triggers a so-called 'priming effect' on PS (Ohno, *et al.*, 1995). Thus, it was necessary to conduct further indirect anti-cancer activity experiments using CBF. Indirect anti-cancer activity tests were conducted on all the selected cancer cell lines with CBF of L15, L23, L10 and L21 strains (Fig. 3C). The cancer cell survival rate was moderate (<60% for AGS and MCF-7) with L15 and very high with L23 (for all selected cancer cell lines). Direct anti-cancer activity experimental results did not show effective inhibition of tumors (Fig. 3D). Among all the cell lines, gastric cancer cell line (AGS) responded to some extent better than others. Normal cell line (MRC-5) responded in a similar range to all other cancer cell lines.

Both CBF and HWE of L15 strain showed better performance in tests for immuno-modulating properties. The HWE of L15 was further fractionated to obtain four different molecular weight fractions (See Supplementary data, Fig. C). The polysaccharide content of the fractions was in the range 0.2-0.7 mg/ml (Fig. 4A). They were further tested for immuno-stimulating activity and roles in the direct anticancer activity. The immunity-enhancing properties of HWE's were similar to those of CBF. The results of immuno-stimulating activity assays of mixtures of all fractions were similar to individual high molecular weight fractions 'B' (Fig. 4B). However, in the direct anti-cancer activity assays, low molecular weight fractions gave better results confirming their vital role in immune-stimulating pathways (Fig. 4C).

Molecular weight and monosaccharide composition.

To deduce the structure-activity relationship, it is important to determine the molecular weight distribution and monosaccharide composition of the various PS isolates. Gel permeation chromatographic studies showed that all isolated PS had up to four similar molecular weight fractions (designated as A, B, C, D) with different distribution in the range 1×10^2 kDa and 3×10^3 kDa (Table I, Supplementary data, Fig. D). A thorough examination revealed that the molecular weight fractions A and D were present in all strains while fractions B and C showed some disparity.

The monosaccharide composition was determined from the standard calibration curves plotted for individual monosaccharide. The data revealed differences in the distribution of glucose, mannose, xylose, galactose, fucose, rhamnose and arabinose in the CBF of all mushrooms (Table II). For example, the L15 PS contained mainly glucose and mannose and the contents of glucose in PS of L1, L4, L6, L10, L11, L21, L23, L24 and L25 were 55.4%, 23.1%, 51%, 56.2%, 47.1%, 47.4%, 56.4%, 88.8% and 55.6%, respectively. The nature of these compositions and differences remain unclear at this moment and would need further investigation when more relevant knowledge and analytical skills are available.

Structures.

The structural features of the crude PS/HWE extracted from strain L15 were elucidated by using the FT-IR, NMR and GC-MS spectroscopic techniques to establish structure-immuno-stimulating and anti-cancer activity relationships. In the FT-IR spectra of the crude PS (all strains), the bands corresponding to the ν (C=O) vibration in the carboxyl group at 1650 cm^{-1} indicate that this carboxyl group was hydrogen bonded (Supplementary data, Fig. E). The absence of carbonyl bands at 1535 cm^{-1} and 1700 cm^{-1} indicates that these strains contain neither proteins nor uronic acids, respectively. In addition to the characteristic bands of glucans in the $1000\text{-}1100 \text{ cm}^{-1}$ range, FT-IR spectra showed a weak band at 850 cm^{-1} (Supplementary data, Fig. E) that revealed the ' α ' configuration of the main glucan linkages (Tsumuraya, *et al.*, 1979).

The chemical shifts of individual proton and carbon peaks are shown in the NMR spectra of L15 HWE (Fig. 5). The two groups of anomeric proton signals centered at δ 5.29 and 4.93 ppm were assigned to (1 \rightarrow 4)-D-Glcp and (1 \rightarrow 6)-D-Glcp, respectively, Fig. 5A (Chakraborty, *et al.*, 2004). The two major carbon peaks at δ 99.68 and 102.43 ppm were assigned to α -(1 \rightarrow 4)-D-Glcp and β -(1 \rightarrow 6)-D-Glcp residues, respectively (Fig. 5B). The anomeric carbon signals at δ 71.55, 71.28, 76.06, 70.09, and 60.86 ppm were assigned, respectively, to C-2, C-3, C-4, C-5, and C-6 of α -(1 \rightarrow 4)-D-Glcp, due to their relatively higher peak intensities. The other carbon signals assigned for β -(1 \rightarrow 6)-D-Glcp are C-2 (73.16), C-3 (76.79), C-4 (69.75), C-5 (73.45) and C6 (66.96). Further confirmation was based on analysis for alditol acetates using GC-MS in crude PS of L15 (Fig. 6, C.T. Lo and Chang, *et al.*, in preparation). The resulting chromatograms demonstrated the presence of α -(1 \rightarrow 4)-linked-D-glucopyranosyl and β -(1 \rightarrow 6)-linked-D-glucopyranosyl moieties in the glucan, i.e. peak a: 1,4,5-tri-O-acetyl-1-deuterio-2,3,6-tri-O-methyl-D-glucitol (m/z: 43, 59, 71, 87, 102, 118, 129, 142, 162, 173, 233; α -(1 \rightarrow 4)) and peak b: 1,5,6-tri-O-acetyl-1-deuterio-2,3,4-tri-O-methyl-D-glucitol (m/z: 43, 59, 71, 87, 102, 118, 129, 143, 162, 173, 189, 233; β -(1 \rightarrow 6)). The 1,4,5,6-tetra-O-acetyl-1-deuterio-2,3-di-O-methyl-glucitol (peak c, m/z: 43, 59, 74, 85, 102, 118, 127, 142, 162, 201, 261) indicates (1 \rightarrow 4) and (1 \rightarrow 6) linkage (Chakraborty, *et al.*, 2004).

Linkage assignment was further confirmed by the ^1H - ^{13}C HSQC 2D-NMR spectrum that shows the cross relationships of the proton and carbon peaks that define glycosidic linkages (Chakraborty *et al.*, 2004; Ahrazem *et al.*, 2003, Supplementary data, Fig. F). Note that the chemical shifts of C-4 and C'6 typify (1 \rightarrow 4)-linked and (1 \rightarrow 6)-linked glucose residues, respectively (Grün *et al.*, 2005). Also note that the relative positions of the anomeric signals for both constituents (denoted H-1 and H'-1) are typical for an α -anomeric and a β -anomeric configuration. Although this linkage has been found for other mushrooms, it is new for the HWE from *L. edodes*.

Analysis of the L15 HWE monosaccharide composition revealed that the one with

the highest content is glucose (68.9%), the next is mannose (20%), and the remaining five constitute a total of 11%. This composition is rare, particularly for the presence of a total of seven different monosaccharides, and has not been reported in the literature. The tentative ¹³C NMR peak assignments for the mannopyranosyl residual are: C1 (96.02), C2 (69.65), C3 (70.35), C4 (78.5), C5 (74.25), C6 (61.2) (Willför *et al.*, 2003; Chow *et al.*, 2005).

Discussion

Structural features and the Immuno-modulating and anti-cancer activities.

The procedures adopted to test the immuno-modulating and anti-cancer activities were similar to the experiments described by several authors (Shida, *et al.*, 1978; Tada, *et al.*, 1986). The common protocol adopted is the use of fruiting bodies, extractions using aqueous or non-aqueous phases and structural characterization of the isolated products. Some experimental modifications were introduced including the method of isolation of the PS and the experimental steps involving treatment of cancer cell lines with PS. An important result of this study was the ability of the PS to stimulate immune cells irrespective of method of isolation, i.e. either using CBF or HWE or fractionated HWE. The PS from both HWE and crude polysaccharide seem to contain similar backbone structures.

Strains L15 and L4 showed the respective higher and lower immuno-stimulating activity (macrophage stimulating activity). An attempt was made to correlate the molecular weight and monosaccharide composition with immuno-stimulating activity. It was found that a great difference exists in the distribution ratio of low molecular weight D (mw 11.7 kDa, L4>L15). Among the other molecular mass fractions of L4 and L15, fraction C (mw 534 kDa) was absent in both the strains, fractions B were in similar ratios (mw 2700 kDa, L15~L4), and the ratio of high molecular weight fraction A was L15>L4 (mw >2750 kDa). It is likely that low molecular weight fraction may be related for the reduced immuno-stimulating activity. On a separate paper, we have found a good correlation between the monosaccharide composition and the immuno-stimulating activity (C-T Lo and C.A. Chang *et al.*, in preparation). For example for strains L15 and L4 that showed higher and lower immuno-stimulating activity, the differences in the amount of

glucose (L15>L4), mannose (L4>L15), xylose (L4>L15) and arabinose (L4>L15) are characteristic. For L4, the mannose content is 49.2% and glucose content is only 23.1%.

Comparing the strains L15 and L24 (immuno-stimulating activity: L15>L24), the amount of glucose is high in L24 (L24>L15) while mannose, xylose and arabinose are high in L15 (L15>L24). The glucose content in L24 is 88.8%. Similar trends can be observed among other strains. It seems that the glucose content must maintain at an adequate level to achieve a better immuno-stimulating activity; too high or too low a glucose content level is not appropriate for high immuno-stimulating activity. It is not certain how other monosaccharides affect the immuno-stimulating activity. However, it is possible these monosaccharides together with glucose may affect the three dimensional structures of the polysaccharides and hence, immuno-stimulating activity. The correlation of monosaccharide composition and high molecular mass fractions with the anti-cancer properties of mushrooms was also reported from other studies (Jin, *et al.*, 2003; Kim, *et al.*, 2000).

Ohno *et al.* reported that the release of TNF- α by macrophages could be induced by β -glucans with specific molecular weights and lower branching ratios. The mechanisms for the recognition of β -glucans by macrophage were proposed to be fairly complex and the β -glucans were assumed to be broken down to lower molecular weight fragments through various cellular functions (Ohno, *et al.*, 1995; Okazaki, *et al.*, 1995). Also, the addition of lipo-polysaccharide resulted in a "priming effect" and increased the TNF- α production by various β -glucans (Ohno, *et al.*, 1995; Okazaki, *et al.*, 1995) Our results showed that structurally different α -glucans extracted from different mushroom strains could also stimulate RAW 264.7 cells to secrete TNF- α . A synergistic effect on the TNF- α release by adding lipo-polysaccharide was also observed in the *in vitro* studies. It would be of interest to see if the same effect is observed in the *in vivo* studies.

In the indirect anti-cancer activity, the cytotoxic response of peritoneal macrophages and enhanced release of TNF- α are accounted for increased immuno-stimulating activity. Among the regional strains classified, the mushroom isolates from Japan showed the highest immuno-stimulating activity, followed by isolates from China and Taiwan,

respectively. PS in different strains of mushroom have anti-cancer activities that differ greatly in their chemical compositions and configurations. Although it is difficult to correlate the structure and anti-cancer activity, particularly due to the difficulty in determining the three dimensional structures, some correlations can be inferred.

Earlier investigations revealed that the enhanced immuno-stimulating activity of the mushrooms might be due to the presence of α -glucans (Stuelp-Campelo, *et al.*, 2002). Not only mushrooms, α -glucan in the PS was also identified in several medicinal plant extracts (Nair, *et al.*, 2004; Stuelp-Campelo, *et al.*, 2002; Wang, *et al.*, 2003). All of these active PS, regardless of their origin, were obtained by different extraction methods and collected at different fractions and were found to vary in polymer structures. In some of the studies, extracted glucans with varying substituted monosaccharides in the side chain have shown enhanced immuno-modulating activity (Capek, *et al.*, 2004), e.g. Bao *et al.* using hot water extracted PS from *Ganoderma lucidum*. (Bao, *et al.*, 2002). Ukawa *et al.* found out that the neutral monosaccharide composition, i.e. fucose, xylose., mannose., galactose, and glucose, in the PS from isolates of fruiting bodies of *Lyophyllum decastes* Sing. was different from other species and this along with various protein content exerted increased anti-cancer activity (Ukawa, *et al.*, 2000). Tomati *et al.* discovered that among the monosaccharides present in the hot water extract of CBF of *L. edodes*, glucose content was the highest and xylose second, with a 7:1 ratio. Other monosaccharides were ribose, arabinose and mannose and the total content was less than 1% (Tomati, *et al.*, 2004). Similar phenomena were observed for some medicinal plant extracts, used as anti-cancer compounds (Shin, *et al.*, 1997).

Conclusions and future studies

Natural polysaccharides with various monosaccharide composition are difficult to synthesize in the laboratory, yet they are quite efficacious in many biological events and pharmacological treatment. We have established an experimental platform by adopting several classical and modern chemical and molecular biological protocols to prepare these materials and to use them for further studies and biotechnological applications. These include submerged liquid phase culture, separation by extraction, precipitation and

chromatographic purification, molecular weight and structural characterization by various chromatographic and spectroscopic techniques such as FT-IR, NMR and GC-MS, and various biological activity assays. This report reveals that the polysaccharide fractions in the molecular weight range 1×10^2 and 3×10^3 kDa of the culture broth filtrate (CBF) and hot water extract (HWE) from *L. edodes* mycelia are able to show macrophage-stimulating and indirect anti-cancer activities. A new form of polysaccharide linkage with a backbone of α -(1 \rightarrow 4)-glucan and side chains of β -(1 \rightarrow 6)-glucan has been identified. It is important to further identify the key structural features at lower molecular weight fractions necessary to maintain similar or better biological activities to establish a clearer structure-activity relationship and for more convenient handling of future pharmacological and nutraceutical applications. The detailed mechanisms as well as related signal transductions involved with the biological activity such as macrophage-stimulation and subsequent release of TNF- α and/or other biochemicals to inhibit tumor growth need further clarification. The effects of these polysaccharides on other biological events such as cell-cell interactions are also worth exploring. We are currently in the process to do so.

Materials And Methods

Strains, media, and growth conditions.

The ten strains of *L. edodes* are: No.135 (L24) and No.939 (L25) from China, Tainung No. 1 “white cap” (L1) and “red cap” (L4) from Taiwan, Japanese 271 (L11, L15), Jongxing 5 (L6), Jongxing 8 (L10), Hey-King-Gang (L21) and Jong-Wen 600 (L23) from Japan.

The culture growth conditions were optimized by first incubating the mushroom (L11) for 3, 5, 7, 12, 14, 17, 19, 21, 24, 26, 28 and 31 days at 26°C. The culture broth of *L. edodes* was obtained from medium (pH 4.5) containing 2% oat, 0.5% yeast extract, 0.1% KH₂PO₄, 0.05% MgSO₄, 0.15% CaCO₃, at 26°C and reciprocating shaking (150 rpm/min) and fermented for 14 days. The cultivation developed in the flasks was transferred to static incubation. The liquid was filtered (*Membrane filter pore size >0.45 μ m*), to collect the culture broth filtrate (CBF) and then passed through the autoclave. The mycelia

pellets were collected and washed with distilled water. The mycelia pellet dry weight was determined by drying in an oven for 7 days at 60°C.

Polysaccharide isolation.

The CBF was added to three volumes of 95% ethanol and stored at 4°C overnight. The precipitate was collected by centrifugation, followed by washing with 75% ethanol, and then freeze-dried to obtain a culture precipitate. One gram of crude polysaccharide is treated with boiling water (120°C) to prepare a HWE that was filtered (Milli-pore, 0.22 µm) for immunoassay and freeze-dried for further analyses.

Amplified fragment length polymorphism analysis (AFLP).

Mycelia were harvested onto filter paper, rinsed with distilled water, and freeze-dried. Genomic DNA for each progeny was extracted by use of the DNeasyTH Plant Mini Kit (*Qiagen, Hilden*) and DNAs were eluted twice from the DNA binding column with 100 µl AE (50 mM NaAcetate pH 5.2, 10mM EDTA) solution. AFLP analysis was carried out adopting modification of the procedure described by Vos et al., (Vos, *et al.*, 1995), Terashima et al., (Terashima, *et al.*, 2002), the instruction manual of the AFLP core Reagent Kit (*Invitrogen*), and the AFLP Microbial Fingerprinting Kit (*Applied Biosystems*). Electrophoresis and detection of amplified fragments were performed using the 373 DNA Genetic Analyzer (*Perkin Elmer*). Each gel track ranged from the size-marker 50 bp band to the 500 bp band. Patterns were normalized with reference to molecular mass of the internal ROX-labeled size standard that was added to each sample. After normalization, the levels of genetic similarity between the AFLP patterns were calculated with Pearson correlation. For cluster analysis of AFLP banding patterns, the un-weighted pair group method using arithmetic averages (UPGMA) was used (Vauterin, *et al.*, 1992). Internal standards of *L. edodes* strains used are BCRC 36024 (CBS 454.69, IFO 8340) and 36482 (MUCL 28773). Phylogenetic grouping was performed using Bio Numerics software.

Molecular weight determination.

The molecular weight fractions of CBF extract was determined using a gel-chromatographic technique with H₂O (0.3 ml/min) as a mobile phase (Waters Hsp-Gel AQ5.0, Waters 1515 isocratic pump, 717 plus injector and 2410 RI detector). The calibration curve was constructed with standard dextrans (Polymer Standards Service) within the range of molecular weight from 180 to 2,100,000 Da. Four distinct fractions were identified and labeled as A, B, C, and D, accordingly. L15 HWE was injected into the gel-permeation chromatograph column (Mix D column, PL Aqua-gel-OH), mobile phase being H₂O, and collected five different fractions- A, B, C, D, and E, using the same fraction collector as described for CBF extraction.

Monosaccharide composition.

Monosaccharide analysis was performed using the method of Blakeney and Hoebler (Blakeney, et al., 1983; Hoebler, et al., 1989). PS from CBF (2 mg) was completely hydrolyzed in a sealed tube with 0.3 ml of 2M trifluoroacetic acid (TFA) at 120°C for 90 min to convert the monosaccharides into alditol acetates. The amounts of neutral monosaccharides in the PS were analyzed as alditol acetates by gas chromatography (GC, Varian 3800). Myo-inositol (1 mg) was added as an internal standard. The amounts of neutral monosaccharides (PS contents) were determined using the phenol-sulfuric acid method (Chakraborty, et al., 2004; Kiho, et al., 1989; Terashima, et al., 2004).

Structure analysis.

In order to determine the functional group of the most immunological active strain, crude polysaccharide or HWE was further characterized using FTIR (all strains) and NMR (L15) spectroscopic techniques. The glycosyl linkage composition was analyzed using gas chromatography (all strains). The FTIR spectra were obtained from 1mg of crude polysaccharide in 100 mg of KBr. Twelve scans were accumulated with a resolution of 2 cm⁻¹ in the range 500-1800 cm⁻¹ (Jasco 8900) (Bao, et al., 2002; Capek, et al., 2004; Kim, et al., 2000). Glycosyl linkage composition analysis was carried out by taking 1.0 mg of crude polysaccharide that was methylated using the modified NaOH-DMSO (dimethyl sulfoxide) method (Bao, et al., 2002; Capek, et al., 2004; Komaniecka, et al., 2003; Terashima, et al., 2002). The per-methylated product was hydrolyzed, reduced,

acetylated and then analyzed by GC-MS (*HP 6890/MSD 5973*) at 25°C.

The ¹H, ¹³C NMR and DEPT (Distortionless Enhancement by Polarization Transfer) experiments were recorded at 600 and 150 MHz respectively, on a Bruker DMX-600 spectrometer (Bao, et al., 2002; Chakraborty, et al., 2004; Tomati, et al., 2004). The exchangeable proton in HWE residue was exchanged with deuterium by adding sufficient D₂O (99.96% atom²H, Aldrich). The ¹H and ¹³C NMR spectra were recorded at 25°C. Methanol was used as an internal standard (δ 49 ppm) for the ¹³C spectrum. The ¹H NMR spectrum was recorded by adjusting the HOD signal at δ 4.68 ppm. 2D-NMR experiments (COSY and HSQC) were performed by using the standard XWIN-NMR 3.5 software.

Macrophage stimulating activity assay.

The O₂-production of macrophage cell line (Mouse BALB/C macrophage, RAW 264.7) was measured by a modified nitroblue tetrazolium (NBT, Sigma) reduction assay. The RAW 264.7 was cultured in Dulbecco's modified Eagle's medium (DMEM, Gibco) containing 10% fetal bovine serum (FBS, Hyclone). Macrophage cell lines were placed into wells of a 96-well microtiter plate (2.5 x 10⁵ per well) and were treated with 20 µl of CBF or HWE for 48 h at 37°C. After removal of the supernatant, the macrophage cell line monolayer was covered with 100 µl of 2 mg ml⁻¹ of NBT. The plates with stimulated cells were incubated for 4 h at 37°C. The reduced formazan within macrophage cell line was solubilized in DMSO (Merck). Optical density was measured using an ELISA reader at 570 nm (Rodriguez, et al., 1996; Tsumuraya, et al., 1979). *L. edodes* culture medium was used for control experiments and PBS (phosphate-buffer saline) as blank solution for optical density experiments. The % NBT reduced is estimated using the equation: $\frac{[(\text{Sample Average}) - (\text{Blank Average})]}{[(\text{Control Average}) - (\text{Blank Average})]} \times 100$.

Preparation of 'T' cell.

T-cell line (J45.01, Human acute 'T' cell) was placed into wells of a 96-well microtiter plate (9 x 10³ per well) and was treated with 20 µl of CBF for 72 h. The determination of

3-(4,5-dimethylthiazol-2-yl)-2,5-diphenyltetrazolium bromide (MTT) was performed by a colorimetric assay as described in Tada *et al.*, 1986.

TNF- α release activity.

The ability of CBF of *L. edodes* strains L15 and L23 to stimulate production of tumor necrosis factor- α (TNF- α) by mouse BALB/C macrophage cell line (RAW 264.7) was investigated. The RAW 264.7 cells were cultured in DMEM containing 10% FBS. Macrophage cell lines were placed into wells of a 24-well microtiter plate (2.5×10^5 per well) and stimulated with or without CBF (negative control) or lipo-polysaccharide (*Sigma*, 10 $\mu\text{g/ml}$) for 5 to 24 h in a humidified 5% CO₂, 37°C incubator. After incubation, culture supernatant was collected by centrifugation and measured using a TNF- α Kit (Entogen) in ELISA system (MRX, Dynex). The control experiments were conducted using PBS (Dulbeccos, Ca²⁺/Mg²⁺ free, D-PBS, GibcoBRL 21600-010). The positive control assay was conducted using lipo-polysaccharide.

Direct anti-cancer activity assay.

Normal cell line (MRC-5) of human embryonal lung cell-density of 3×10^3 , human cervical carcinoma cancer cell line (Hela), cell density of 1.5×10^3 , human gastric cancer cell line (AGS), cell density of 3×10^3 per well, human hepatocellular carcinoma cell line (Hep G2), cell density of 3×10^3 per well, human breast cancer cell line (MCF-7), cell density of 3×10^3 per well were placed into wells of a 96-well microtiter plate and were treated with 20 μl of CBF (all strains) or HWE (L15 only). The plates with stimulated cells were incubated for 72 h at 37°C. MTT solution was prepared in PBS at 5mg/ml concentration. This MTT solution (20 μl) was added to each well. It was further incubated for 4 h. Thereafter, the supernatant was aspirated carefully from each well, and the formazan crystals were dissolved in DMSO (Merck). Optical density was measured using ELISA reader at 540 nm. Then the % viability was calculated in comparison to control, taking control (culture *L. edodes* medium) as 100% viable.

Indirect anti-cancer activity assay.

Macrophage cell lines (RAW 264.7) were placed into wells of a 96-well microtiter plate (2.5×10^5 per well) and were treated with 20 μ l of CBF (L15, L10, L21 and L23) for 48 h. After incubation, culture supernatant was collected by centrifugation and then added (20 μ l/well) to MRC-5, Hela, AGS, Hep G2 and MCF-7 contained in 96-well microtiter plates. The entry with 0 μ l/well was used as control that contained only the cells. The plates with stimulated cells were incubated for 72 h at 37°C. The MTT solution prepared in PBS at 5mg/ml concentration was added (20 μ l) to each well. Culture macrophage medium is the control. Further analysis was carried out as described in anti-cancer activity for MTT colorimetric assay.

The resulting data of all the above experiments are presented as a mean (S.D. from triplicates).

Acknowledgements

We wish to express our thanks to Prof. Anne Lien-Ju Chao (NTHU) for help on statistical analysis and Mr. Ming-Wei Kang for providing the GS-MS data. This study was supported by the Bioresources collection & Research Center, Food Industry Research and Development Institute, Hsinchu, Taiwan ROC. A grant from the National Science Council of the Republic of China (Taiwan) for partial support (grant number NSC-93-2113-M-009-004) of this work is also acknowledged.

Abbreviations

PS, polysaccharides; HWE, hot-water-extract; CBF, culture broth filtrates; AFLP, amplified fragment length polymorphism; PCR, polymerase chain reaction; TNF- α , tumor necrosis factor, a pro-inflammatory cytokine; UPGMA, un-weighted pair group method using arithmetic averages; TFA, trifluoroacetic acid; DEPT, Distortionless Enhancement by Polarization Transfer; NBT, nitroblue tetrazolium; FBS, fetal bovine serum; MTT, 3-(4,5-dimethylthiazol-2-yl)-2,5-diphenyltetrazolium bromide; TNF- α , tumor necrosis factor- α ; RAPD, random amplified polymorphic DNA.

References

- Aoki, T. (1984) "Lentinan" Immunology studies: Immune modulation agents and their mechanisms. *Femchel, R.L., and Chirgis, M.A.*, (Eds) 25, 62-77.
- Ahrazem, O., Prieto, A., San-Blas, G., Leal, J.A., Jimenez-Barbero, J., Bernabe M. (2003) Structural differences between the alkali-extracted water-soluble cell wall polysaccharides from mycelial and yeast phases of the pathogenic dimorphic fungus *Paracoccidioides brasiliensis*. *Glycobiology*, 13, 743-747.
- Bano, Z., Rajarathnam, S. (1988) Pleurotus mushrooms. Part II. Chemical composition, nutritional value, post-harvest physiology, preservation, and role as human food. *CRC Crit. Rev. Food Sci. Nutr.* 27, 87-158.
- Bao, X., Duan, J., Fang, X., Fang, J. (2001) Chemical modifications of the (1→3)-β-D-glucan from spores of *Ganoderma lucidum* and investigation of their physicochemical properties and immunological activity. *Carbohydr. Res.* 336, 127-140.
- Bao, X.F., Wang, X.S., Dong, Q., Fand, J.N., Xiao, Y.L. (2002) Structural features of immunologically active polysaccharides from *Ganoderma lucidum*. *Phytochem.* 59, 175-181.
- Blakeney, A.B., Harris, P.J., Henry, R.J., Stone, B.A. (1983) A simple and rapid preparation of alditol acetates for monosaccharide analysis. *Carbohydr. Res.* 113, 291-299.
- Bohn, J. A., BeMiller, J. N. (1995) (1→3)-β-D-glucans as biological response modifiers: A review of structure-functional activity relationships. *Carbohydr. Polymers.* 28, 3-14.
- Borchers, A.T., Stern, J.S., Hackman, R.M., Keen, C.L., Gershwin, M.E. (1999) Mushrooms, tumors and immunity. *Proc. Soc. Experimen. Biol. and Med.* 221, 281-293.
- Breene, W.M. (1990) Nutritional and medicinal value of specialty mushrooms. *J. Food Protec.* 53, 883-94, 899.
- Campbell, A.C., Slee, R.W. (1987) Commercial cultivation of Shiitake in Taiwan and Japan. *Mush. J.* 170, 45-53.
- Capek, P., Hribalova, V. (2004) Water-soluble polysaccharides from *Salvia officinalis* L. possessing immunomodulatory activity. *Phytochem.* 65, 1983-1992.

- Chakraborty, I., Mondal, S., Pramanik, M., Rout, D., Islam, S.S. (2004) Structural investigation of a water-soluble glucan from an edible mushroom, *Astraeus hygrometricus*. *Carbohydr. Res.* 339, 2249-2254.
- Chihara, G., Himuri, J., Maeda, Y.Y., Arai, Y. and Fukuoka, F. (1970) Fractionation and purification of the polysaccharides with marked antitumor activity, especially, lentinan, from *L. edodes* (Berk) SING. *Cancer Research.* 30, 2776-2781.
- Chiu, S.W., Wang, Z.M., Chiu, W.T., Lin, F.C., Moore, D. (1999) An integrated study of individual *Lentinula edodes* in nature and its implication for cultivation strategy. *Mycol. Res.* 103, 651-660.
- Chow, J.T-N., Williamson, D.A., Yates, K.M., Goux, W.J. (2005) Chemical characterization of the immunomodulating polysaccharide of *Aloe vera* L. *Carbohydr. Res.* 340, 1131-1142.
- Crisan, E. V., Sands, A. (1978) Nutritional value. In *The Biology and Cultivation of Edible Mushrooms*; Chang, S. T., Hayes, W. A., Eds.; Academic Press: New York.
- Demleitner, S., Kraus, J., Franz, G. (1992) Synthesis and anti-tumor-activity of sulfoalkyl derivatives of curdlan and lichenan. *Carbohydr. Res.* 226, 247-252.
- Fox, H.M., Burden, J., Chang, S.T., Peberdy, J.F. (1994) Mating Type incompatibility between commercial strains of *Lentinula edodes*. *Exp. Mycology.* 18, 95-102.
- Fujii, T., et al. (1978) Isolation and Characterization of a New Antitumor Polysaccharide, KS-2, Extracted from Culture Mycelia of *Lentinus Edodes*, *The Journal of Antibiotics.* 31, 1079-1090.
- Geornaras, I., Kunene, N.F., Holy, A. von, Hastings, J.W. (1999) Amplified Fragment Length Polymorphism Fingerprinting of *Pseudomonas* Strains from a Poultry Processing Plant. *Appl. Environ. Microbiol.* 65, 3828-3833.
- Grün, C. H., Hochstenbach, F., Humbel, B. M., Verkeij, A. J., Sietsma, J. H., Klis, F. M., Kamerling, J. P., Vliegthart, J. F.G. (2005) The structure of cell wall α -glucan from fission yeast. *Glycobiology.* 15, 245-257.
- Hamuro, J., Wagner, H., Rollinghoff, M. (1978) Beta (1-3) glucans as a probe for T cell specific immune adjuvants. II. Enhanced in vitro generation of cytotoxic T lymphocytes. *Cell Immunol.* 38, 328-35.
- Harumi S., Akira, O., Sunao, Y., Kenzo, S., Hiroaki, S. Toda. S. (1989) Inhibition of the infectivity and cytopathic effect of human immunodeficiency virus by water-soluble

- lignin in an extract of the culture medium of mycelia (LEM). *Biochemical and Biophysical Research Communications*. 160, 367-373.
- Hobbs, Ch. (2000) Medicinal values of *Lentinus edodes* (berk.) Sing. (*Agaricomycetideae*). A literature review. *Int. J. Med. Mushrooms*. 2, 287-302.
- Hoebler, C., Barry, J.L., David, A., Delort-Laval, J. (1989) Rapid acid hydrolysis of plant cell wall polysaccharides and simplified quantitative determination of their neutral monosaccharides by gas-liquid chromatography. *J. Agric. Food Chem.* 37, 360-367.
- Huang, R.C., Hung, M.L., Wang, B.C. (1999) Phylogenetic study and grouping of commercial shiitake isolates in Taiwan. *J. Chinese Agric. Chem. Soc.* 37, 431-441.
- Hwang, H.J., Kim, S.W., Choi, J.W., Yun, J.W. (2003) Production and characterization of exopolysaccharides from submerged culture of *Phellinus linteus* KCTC 6190. *Enzyme and Microbial tech.* 33, 309-319.
- Jiang, S.C., Louis, V., Choopun, N., Sharma, A., Huq, A., Colwell, R.R. (2000) Genetic Diversity of *Vibrio cholerae* in Chesapeake Bay Determined by Amplified Fragment Length Polymorphism Fingerprinting. *Appl. Environ. Microbiol.* 66,140-147.
- Jin, Y., Zhang, L., Zhang, M., Chen, L., Cheung, P.C.K., Oi, V. E. C., Lin, Y. (2003) Anti-tumor activities of heteropolysaccharides of *Poria cocos* mycelia from different strains and culture media. *Carbohydr. Res.* 338, 1517-1521.
- Kiho, T., Yoshida, I., Nagai, K., Ukai, S., Hara, C. (1989) Polysaccharides in fungi α -(1 \rightarrow 3)-D-glucan from an alkaline extract of *Agrocybe cylindracea*, and anti-tumor-activity of its O-(carboxymethyl)ated derivatives. *Carbohydr. Res.* 189, 273-279.
- Kim, S.U., Jung, I.C., Kwon, Y.I., Dim, S.Y., Lee, J.S., Lee, H.W., et al. (2000) Characteristics and purification of proteoglycan from *Phellinus igniarius*. *J. Korean Soc. Agri. Chem. Biotechnol.* 43, 57-62.
- Komaniecka, I., Choma, A. (2003) Isolation and characterization of periplasmic cyclic β -glucans of *Azorhizobium caulinodans*. *FEMS Microbiol. Lettr.* 227, 263-269.
- Kurzman, R. H., Jr. (1997) Nutrition from mushrooms, understanding and reconciling available data. *Mycoscience*. 38, 247-253.
- Mattila, P., Konko, K., Eurola, M., Pihlava, J.M., Astola, J., Vahteristo, L., Hietaniemi, V., Kumpulainen, J., Valtonen, M., Piironen, V. (2001) Contents of vitamins, mineral elements, and some phenolic compounds in cultivated mushrooms. *J. Agric. Food Chem.* 49, 2343-2348.

- Mattila, P., Salo-vaananen, P., Konko, K., Aro, H., Jalava, T. (2002) Basic Composition and Amino Acid Contents of Mushrooms Cultivated in Finland. *J. Agric. Food Chem.* 50, 6419-6422.
- Mizuno, T., Saito, H., Nishitoba, T., Kawagishi, H. (1995) Anti-tumor-active substances from mushrooms. *Food Rev. Int.* 11, 23-61.
- Mizuno, M., Morimoto, M., Minato, K., Tsuchida, H. (1998) Polysaccharides from *Agaricus blazei* stimulate lymphocyte T-cell subsets in mice. *Biosci. Biotechnol. Biochem.* 62, 434-437.
- Mueller, A., Raptis, J., Rice, P.J., Kalbfleisch, J.H., Stout, R.D., Ensley, H.E., Browder, W., Williams D.L. (2000) The influence of glucan polymer structure and solution conformation on binding to (1→3)-β -D-glucan receptors in a human monocyte-like cell line. *Glycobiology*, 10, 339-346.
- Nagi, N., Ohno, N., Adachi, Y., Aketagawa, J., Tamura, H., Shibata, Y., Tanaka, S., Yadomae, T. (1993) Application of limulus test (G pathway) for the detection of different conformers of (1→3)-beta-D-glucans. *Biol Pharm Bull.* 16, 822-828.
- Nair, P.K.R., Rodriguez, S., Ramachandran, R., Alamo, A., Melnick, S.J., Escalona, E., Garcia Jr., P.R., Wnuk, S.F., Ramachandran, C. (2004) Immune stimulating properties of a novel polysaccharide from the medicinal plant *Tinospora cordifolia*. *Int. J. Immunopharmacology.* 4, 1645–1659.
- Ohno, N., Asada, N., Adachi, Y., Yadomae, T. (1995) Enhancement of LPS triggered TNF-alpha (tumor necrosis factor-alpha) production by (1→3)-beta-D-glucans in mice. *Biol Pharm Bull.* 18, 126-33.
- Okazaki, M., Adachi, Y., Ohno, N., Yadomae, T. (1995) Structure activity relationship of (1→3)-beta-D-glucans in the induction of cytokine production from macrophages, *in vitro*. *Biol. Pharm. Bull.* 18, 1320-1327.
- Ooi, E.C.V., Liu, F. (1999) A review of pharmacological activities of mushroom polysaccharides. *Int. J. Med. Mushrooms.* 1, 195-206.
- Quagliaro, G., Vischi, M., Tyrka, M., Olivieri, A.M. (2001) Identification of Wild and Cultivated Sunflower for Breeding Purposes by AFLP Markers. *The Journal of Heredity.* 92, 38-42.
- Reshetnikov, S.V., Wasser, S.P., Tan, K.K. (2001) Higher Basidiomycota as a source of anti-tumor and immunostimulating polysaccharides. *Int. J. Med. Mushrooms.* 3,

361-394.

- Rodriguez, A.B., Barriga, C., Lea, R.W. (1996) Effect of prolactin, *in vivo* and *in vitro*, upon heterophil phagocytotic function in the ring dove (*Streptopelia risoria*). *Dev. Comp. Immuno.* 20, 451-457.
- Savelkoul, P.H.M., Aarts, H.J.M., De Haas, J., Dijkshoorn, L., Duim, B., Otsen, M., Rademaker, J.L.W., Schouls, L., Lenstra, J.A. (1999) Amplified-Fragment Length Polymorphism Analysis: the State of an Art. *J. Clinical Microbiol.* 37, 3083–3091.
- Shida, M., Hargu, K., Matsuda, K. (1975) On the water-soluble heterogalactan from the fruit bodies of *Lentinus edodes*. *Carbohydr. Res.* 41, 211-218.
- Shida, M., Uchida, T., Matsuda, K. (1978) A (1→3)- α -D-glucan isolated from the fruit bodies of *Lentinus edodes*. *Carbohydr. Res.* 60, 117-127.
- Shin, K.S., Kiyohara, H., Matsumoto, T., Yamada, H. (1997) Rhamnogalacturonan II from the leaves of *Panax ginseng* C.A. Meyer as a macrophage Fc receptor expression-enhancing polysaccharide. *Carbohydr. Res.* 300, 239-249.
- Stuelp-Campelo, P.M., Benign, M., De Oliveira, M., Lea, A.M.C., Carbonero, E.R., Gorin, P.A.J., Iacomini, M. (2002) Effect of a soluble α -D-glucan from the lichenized fungus *Ramalina celastri* on macrophage activity. *Int. Immunopharmacology.* 2, 691–698.
- Suzuki, I, Hashimoto, K, Yadomae, T. (1988) The effects of a highly branched beta-1,3-glucan, SSG, obtained from *Sclerotinia sclerotiorum* IFO 9395 on the growth of syngeneic tumors in mice. *J. Pharmacobiodyn.* 11, 527-532.
- Suzuki, T., Ohno, N., Adachi, Y., Cirelli, A. F., Covian, J. A., Yadomae, T. (1991) Preparation and biological-activities of sulfated derivatives of (1→3)- β -D-glucans. *J. Pharmacobio-Dyn.* 14, 256-266.
- Tabata, T., Watanabe, W., Horita, K., Kamegai, J., Moriyama, S., Hibino, Y., Ohashi, Y., Sugano, N. (1992) Mitogenic activities of heteroglycan and heteroglycan—protein fractions from culture medium of *Lentinus edodes* mycelia. *Immunopharmacology.* 24, 57-63.
- Tada, H., Shiho, O., Kuroshima, K., Koyama, M., Tsukamoto, K. (1986) An improved colorimetric assay for interleukin-2. *J. Immunol. Methods.* 93, 157.
- Tanigami, Y., Kusumoto, S., Nagao, S., Koikeguchi, S., Kato, K., Kotani, S. and Shiba, T. (1991) Partial degradation and biological activities of an anti-tumor polysaccharide from rice bran. *Chem. Pharm. Bull.* 39, 1782-1787.
- Terashima, K., Matsumoto, T., Hayashi, E., Fukumasa-Nakai, Y. (2002) A genetic

- linkage map of *Lentinula edodes* (shiitake) based on AFLP markers. *Mycol. Res.* 106, 911-917.
- Terashima, K., Matsumoto, T. (2004) Strain typing of shiitake (*Lentinula edodes*) cultivars by AFLP analysis, focusing on a heat-dried fruiting body. *Mycoscience.* 45, 79–82.
- Tomati, U., Belardinelli, M., Galli, E., Iori, V., Capitani, D., Mannina, L., Viel, S., Segre, A. (2004) NMR characterization of the polysaccharidic fraction from *L. edodes* grown on olive mill wastewaters. *Carbohydr. Res.* 339, 1129-1134.
- Tsumuraya, Y., Misaki, A. (1979) Structure of the water insoluble α -D-glucan of *Streptococcus salivarius* HHT. *Carbohydr. Res.* 74, 217-225.
- Ukawa, Y., Ito, H., Hisamatsu, M. (2000) Anti-tumor effects of (1→3)- β -D-Glucan and (1→6)- β -D-Glucan purified from newly cultivated mushroom, Hatakeshimeji (*Lyophyllum decastes* Sing.). *J. Biosci. Bioengg.* 90, 98-104.
- Vauterin L.A., Vauterin P. (1992) Computer-aided objective comparison of electrophoresis patterns for grouping and identification of microorganisms. *Eur. Microbiol.* 1, 37-41.
- Vos, P., Hogers, R., Bleeker, M., Reijans, M., Lee, T., Hornes, M., Frieters, A., Pot, J., Peleman, J., Kuiper, M., Zabeau, M. (1995) AFLP: a new technique for DNA fingerprinting. *Nucleic Acids Res.* 23, 4407–4414.
- Wang, X.S., Dong, Q., Zuo, J.P., Fang, J.N. (2003) Structure and potential immunological activity of a pectin from *Centella asiatica* (L.) Urban. *Carbohydr. Res.* 338, 2393–2402.
- Wang, Z.Y., Tsoi, K.H., Chu, K.H. (2004) Applications of AFLP technology in genetic and phylogenetic analysis of penaeid shrimp. *Biochem. Systematics and Ecol.* 32, 399–407.
- Wasser, S.P. (2002) Medicinal mushrooms as a source of anti-tumor and immunomodulating polysaccharides. *Appl. Microbiol. Biotechnol.* 60, 258–274.
- Willför, S., Sjöholm, R., Laine, C., Roslund, M., Hemming, J., Holmbom, B. (2003) Characterisation of water-soluble galactoglucomannans from Norway spruce wood and thermomechanical pulp. *Carbohydr. Pol.* 52, 175-187.
- Williams, D. L., Pretus, H. A., McNamee, R. B., Jones, E. L., Ensley, H. E., and Browder I. W. (1992) Development of a water-soluble, sulfated (1→3)- β -glucan biological response modifier derived from *Saccharomyces-cerevisiae*. *Carbohydr. Res.* 235,

247-257.

- Zhang, P., Zhang, L., Cheng, S. (2002) Solution properties of an α -(1,3)-D-glucan from *L. edodes* and its sulfated derivatives. *Carbohydr. Res.* 337, 155-160.
- Zhang, L., Chen, L., Xu, X., Lin, Y., Cheung, P.C.K., Kennedy, J.F. (2004) Comparison on chain stiffness of a water-insoluble (1 \rightarrow 3)- α -D-glucan isolated from *Poria cocos* mycelia and its sulfated derivative. *Carbohydr. Polym. In Press.*
- Zhong, J.J., Tang, Y.J. (2004) Submerged cultivation of medicinal mushrooms for production of valuable bioactive metabolites. *Adv./Biochem. Engin./Biotechnol.* 87, 25-59.

Table I. Molecular weight ratio of CBF extracted from different strains

Strain/M.W.	L1	L4	L6	L10	L11	L15	L21	L23	L24	L25
Fraction A >2,754,000	0.5	2.5	2.1	3.4	1.7	3.4	2.1	2.5	1.8	3.2
Fraction B 2,754,000	-	0.4	0.4	0.8	-	0.4	0.4	-	0.6	0.7
Fraction C 534,000	1.3	-	-	-	1.8	-	-	0.6	-	-
Fraction D 11,700	1.7	5	1.9	2.2	0.3	0.9	0.7	0.7	5.5	2.8

Table II. Monosaccharide composition of fractionated polysaccharide from different strains of *L. edodes*

<i>Lentinula edodes</i>	L1	L4	L6	L10	L11	L15	L21	L23	L24	L25
Arabinose %	6.03	11.19	8.25	7.77	6.76	5.41	8.42	7.73	2.22	6.45
Xylose %	4.82	10.65	5.89	5.58	5.21	3.83	5.88	5.49	1.13	4.55
Mannose %	32.28	49.22	31.83	26.89	36.24	20.02	33.5	26.72	7.23	30.91
Galactose %	1.44	5.09	2.59	3.56	4.3	1.42	3.73	3.19	0.03	1.87
Glucose %	55.44	23.1	50.95	56.2	47.12	68.93	47.36	56.36	88.82	55.58
Rhamnose %	0	0.22	0.24	0	0.14	0.28	0.56	0.32	0.45	0.4
Fucose %	0	0.52	0.24	0	0.24	0.11	0.56	0.19	0.12	0.24
Exopolysaccharide Content (mg/ml)	0.58	0.61	0.53	0.31	0.48	0.44	0.2	0.15	0.59	0.59

FIGURE CAPTIONS

- Fig. 1:** Step-wise experimental protocol adopted to isolate CBF and crude polysaccharide from *L. edodes* mycelia.
- Fig. 2:** Dendrogram of *L. edodes* constructed using AFLP assay
- Fig. 3:** (A) Macrophage stimulatory activity assay (% NBT reduction) using CBF of all strains. (B) TNF- α release activity using CBF of L15 and L23. (C) Indirect anti-cancer assay (% MTT reduction) using CBF of 4 different strains. (D) Direct anti-cancer assay using CBF of all strains. The CBF was first treated with immune cell lines-RAW 264.7 (% NBT reduction) and J45.01 (% MTT reduction) and then added to other different cancer cell lines (% MTT reduction)
- Fig. 4:** (A) Polysaccharide content of different molecular weight fractions (A, B, C, D and E) extracted from L15 HWE, (B) Macrophage stimulatory activity (%NBT reduction) of obtained weight fractions, and, (C) Direct anti-cancer assay (% MTT reduction) of obtained weight fractions
- Fig. 5:** NMR spectra of crude PS hot water extracted from L15. (A) The two anomeric proton signals are at δ 5.29 and 4.93 ppm that were assigned as (1 \rightarrow 4)-D-Glcp and (1 \rightarrow 6)-D-Glcp (600 MHz), (B) The anomeric carbon signals for the (1 \rightarrow 4)-D-Glcp and (1 \rightarrow 6)-D-Glcp residues were assigned at δ 99.68 and 102.43 ppm, respectively, from ^{13}C (150 MHz). The carbon signals at δ 71.55, 71.28, 70.09, and 60.86 ppm correspond, respectively, to C-2, C-3, C-5, and C-6 of (1 \rightarrow 4)-D-Glcp. The other signals for (1 \rightarrow 6)-D-Glcp are C-2 (73.16), C-3 (76.79), C-4 (69.75), and C-5 (73.45),
- Fig. 6:** GC-MS data for the alditol acetates derived from the methylated polysaccharide HWE isolated from *Lentinula edodes*. The presence of (a) 1,4,5-tri-O acetyl-1-deuterio-2, 3, 6-tri-O-methyl-D-glucitol and, (b) 1,5,6- tri-O acetyl-1-deuterio-2, 3, 4-tri-O-methyl-D-glucitol were detected. (c) The 1,4,5,6-tetra-O-acetyl-1-deuterio-2,3-di-O- methyl-glucitol indicates (1 \rightarrow 4) and (1 \rightarrow 6) linkage.

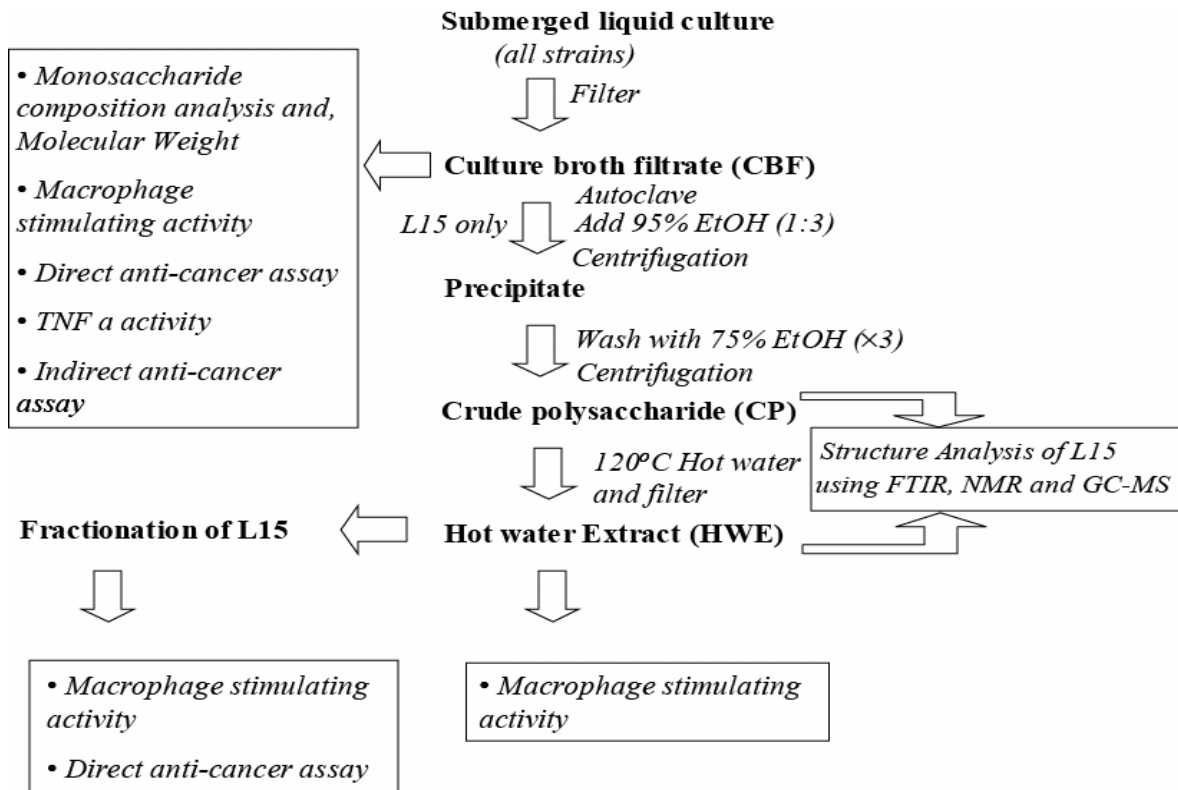


Fig. 1

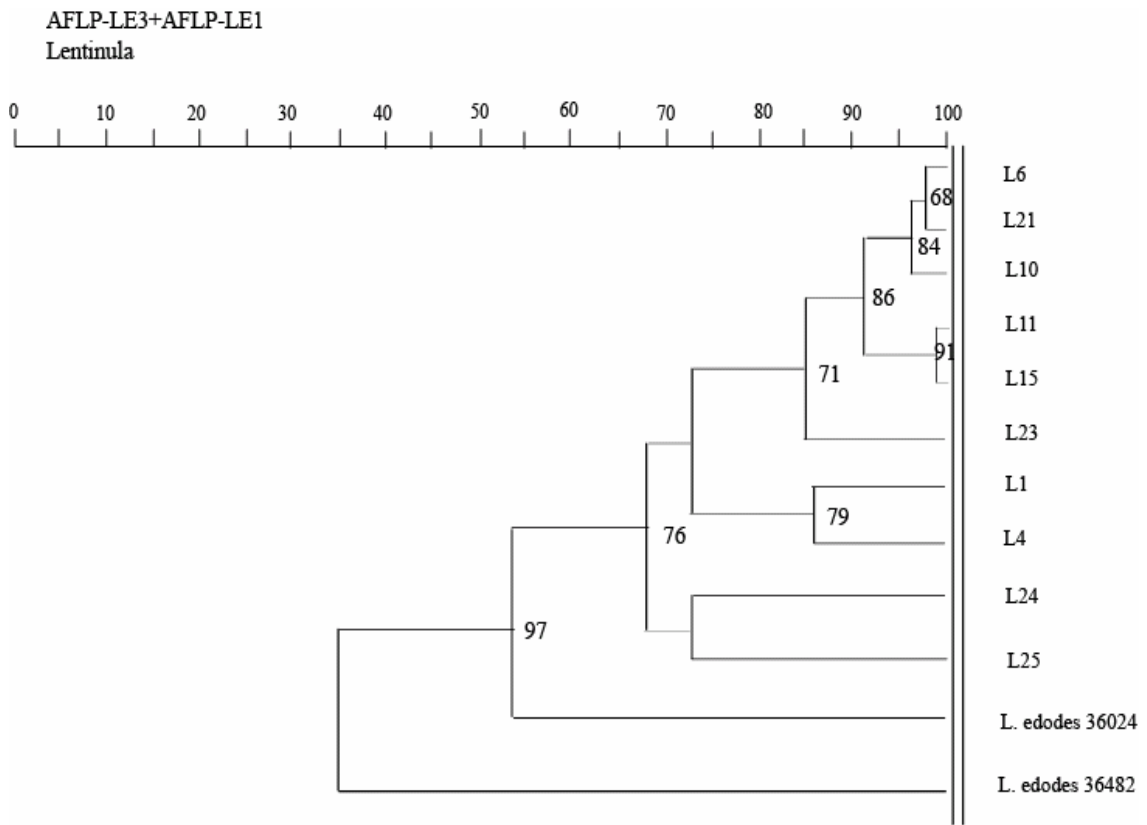
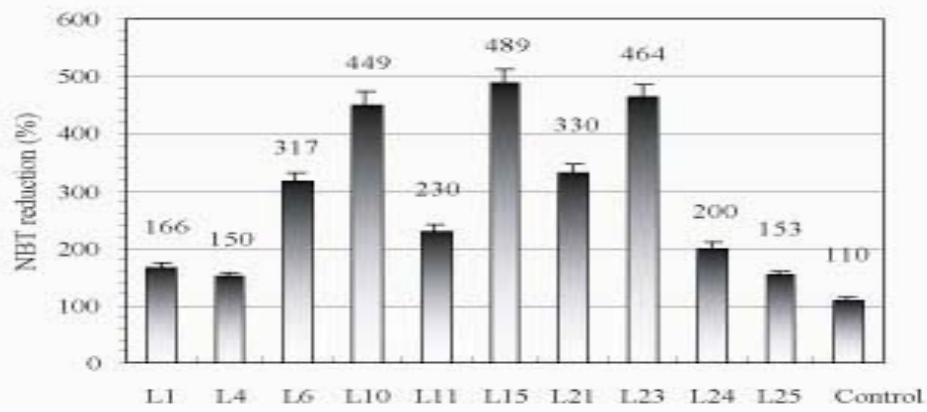
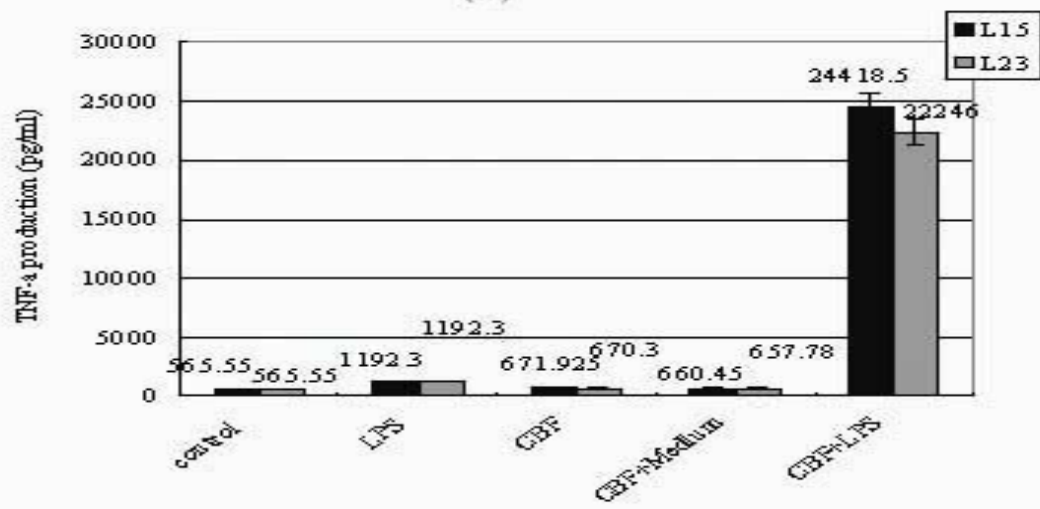


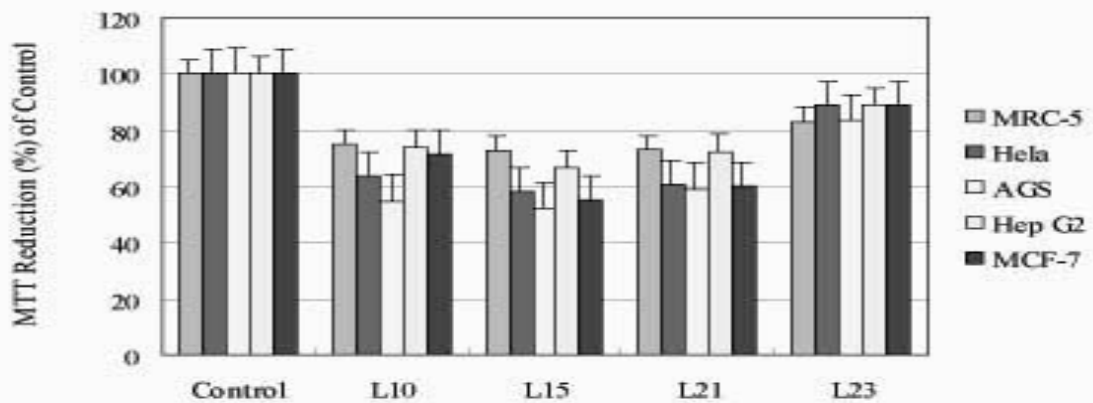
Fig. 2



(A)



(B)



(C)

Fig. 3

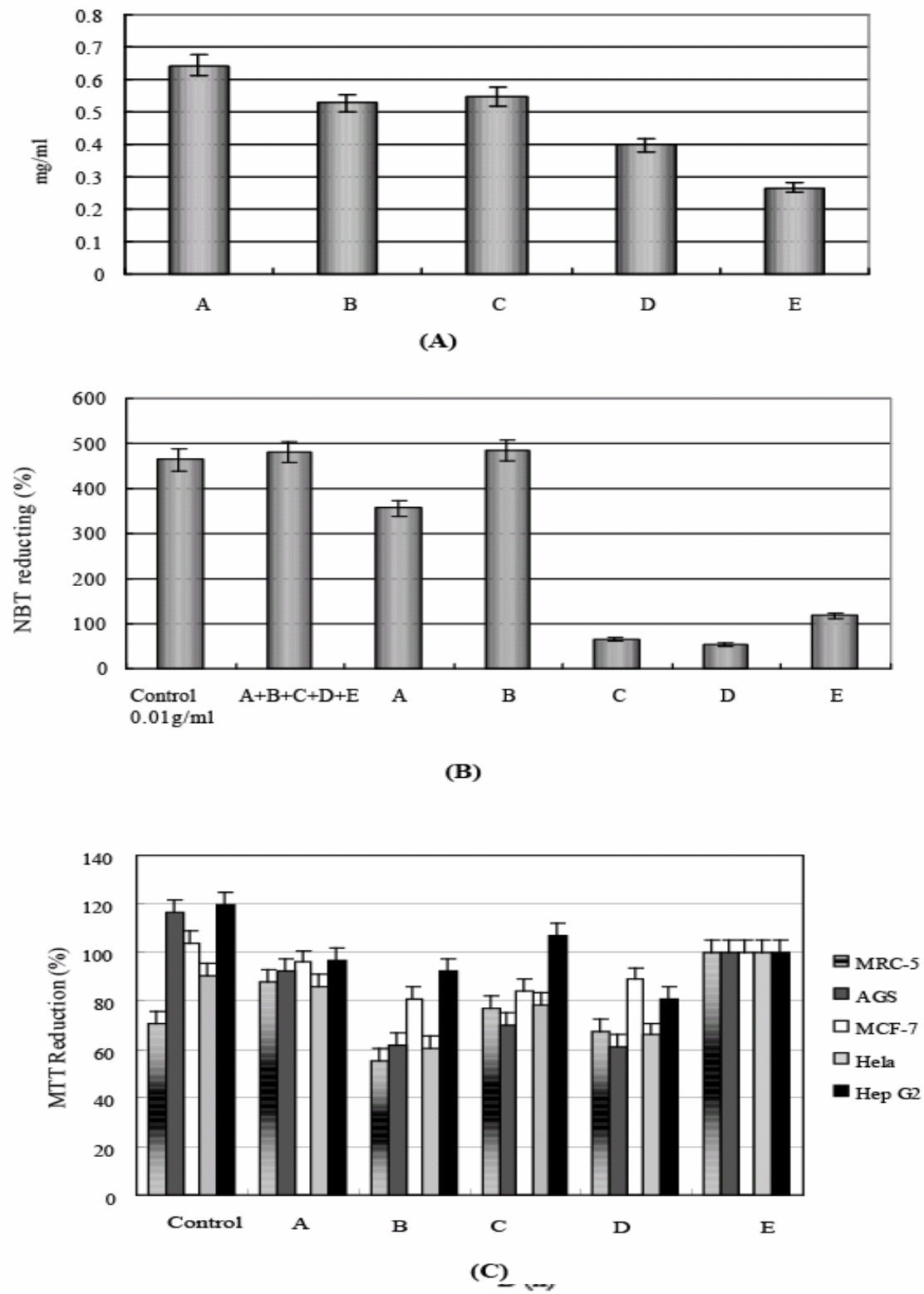
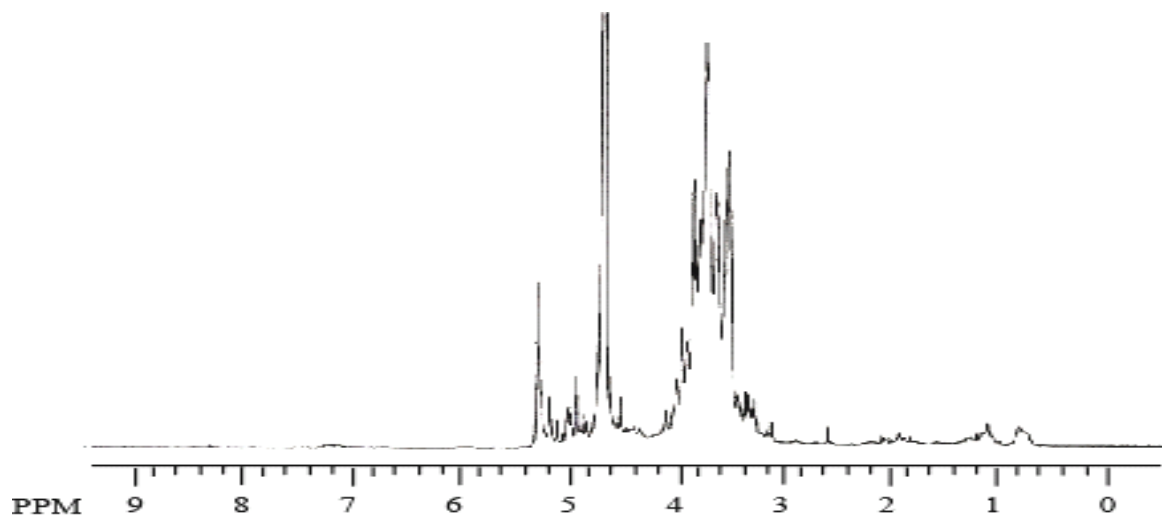
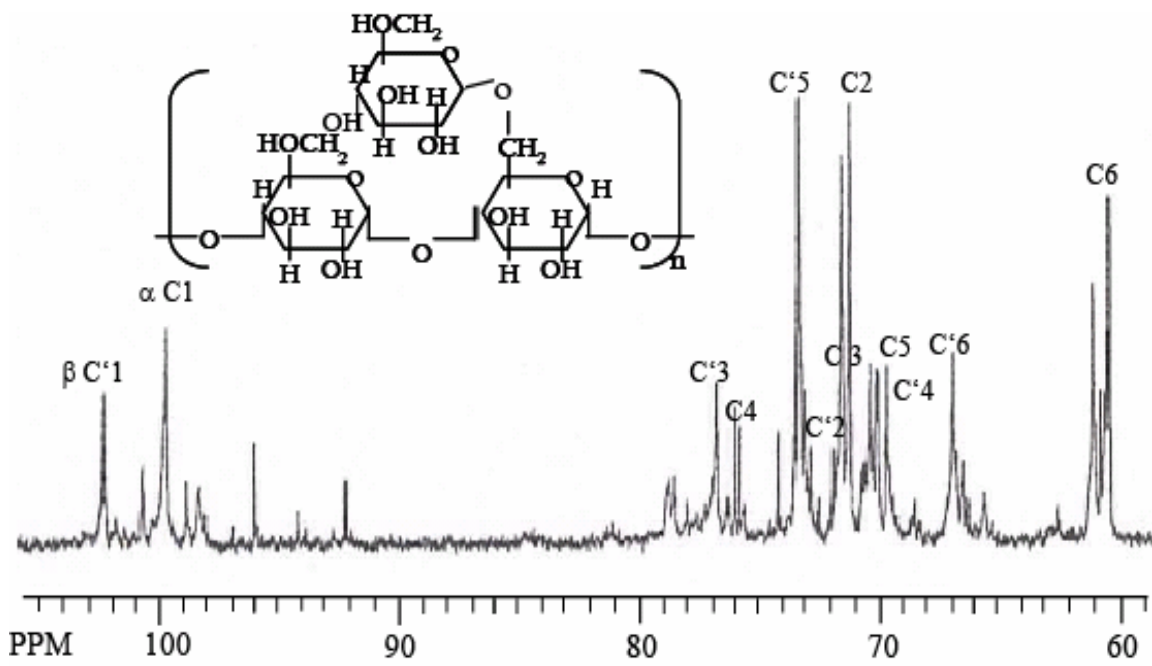


Fig. 4



(A)



(B)

Fig. 5

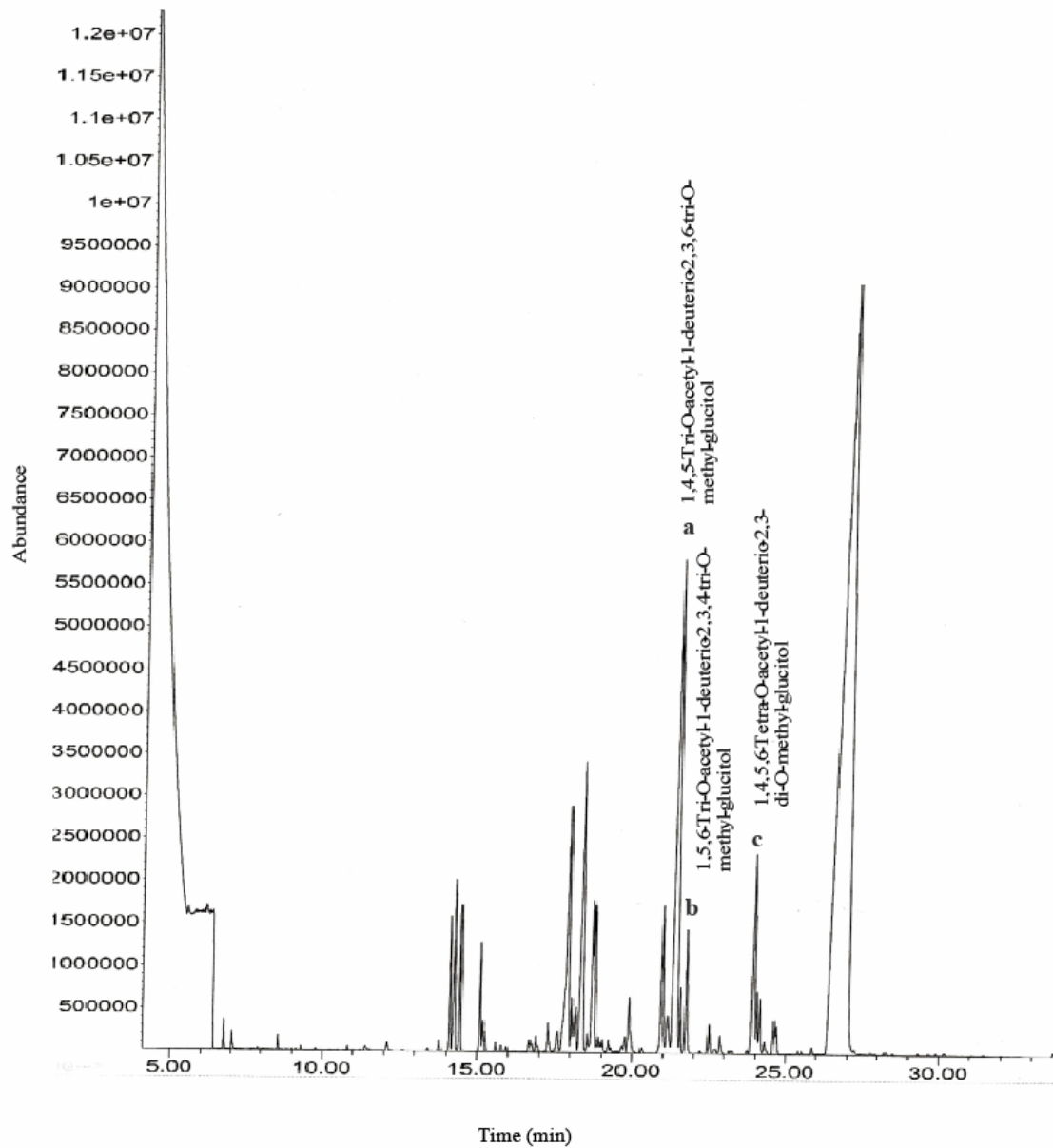


Fig. 6

Supplementary Data

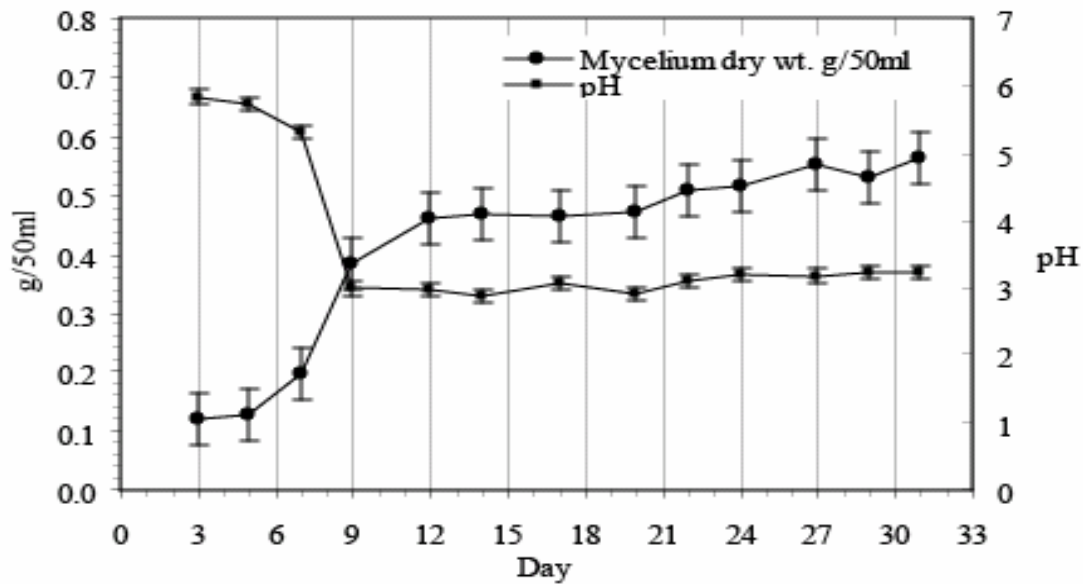


Fig. A: Time course of the mycelium growth of *L. edodes* 'L11' strain flask culture at 25°C, initial pH 4.5 and 150 rpm.

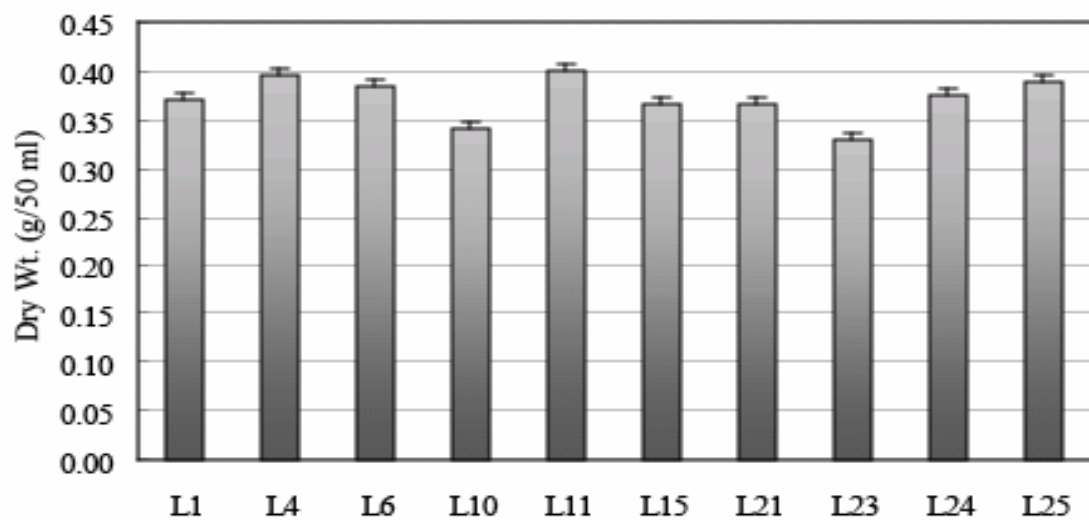


Fig. B: Dry cell weight of mushroom strains

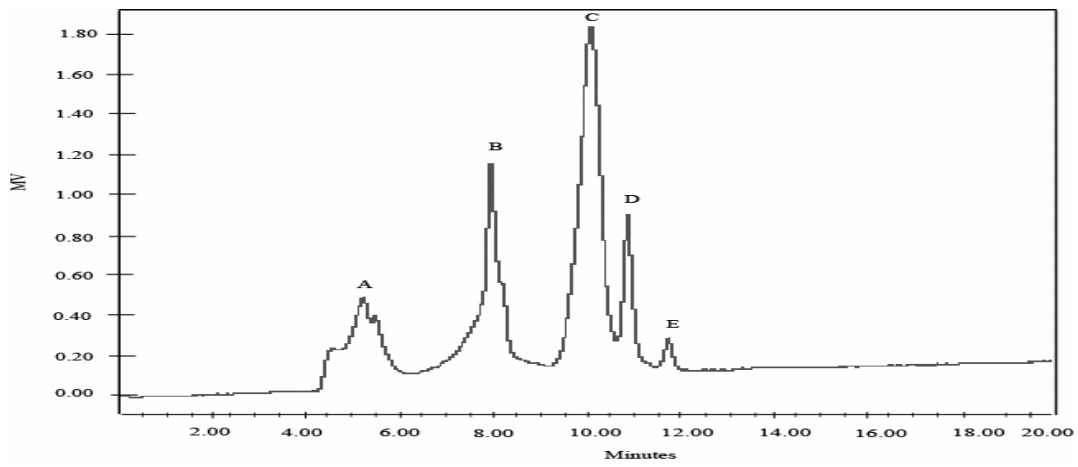


Fig. C: Molecular weight fractions of L15 HWE. (A) 1,702,000, (B) 12,600, (C) 1,470, (D) and (E) <1,470.

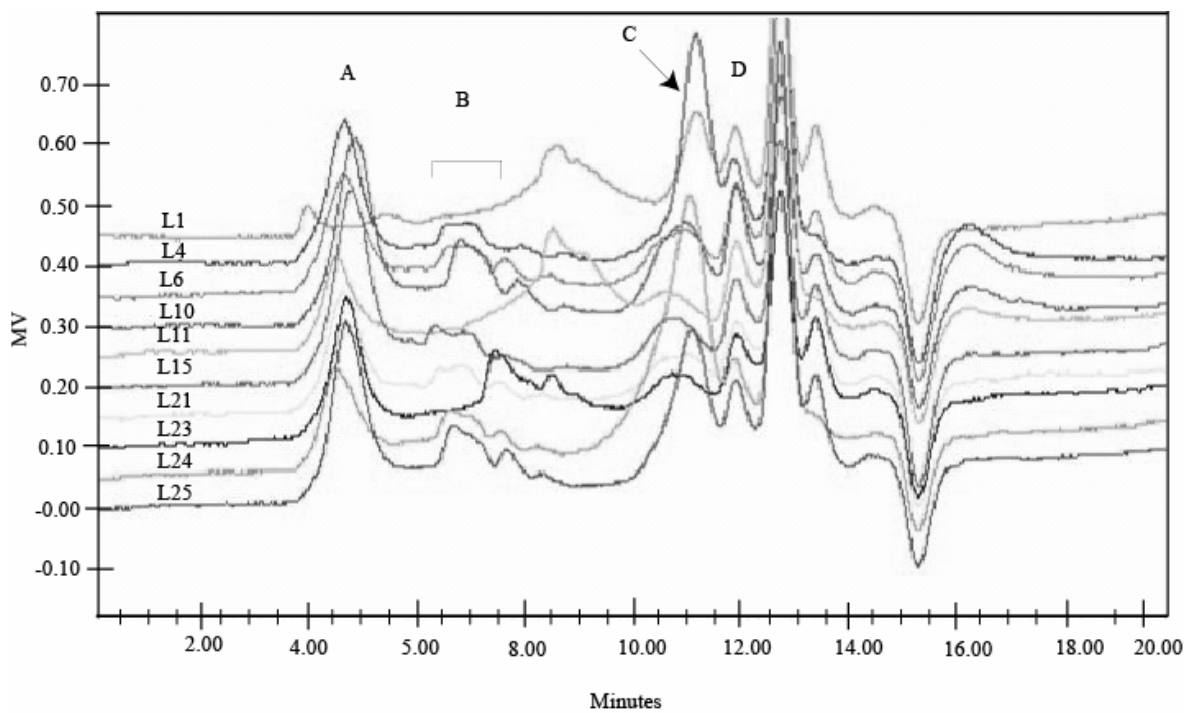


Fig. D: GP chromatogram obtained from CBF of mushroom strains. Molecular weight fractions are indicated.

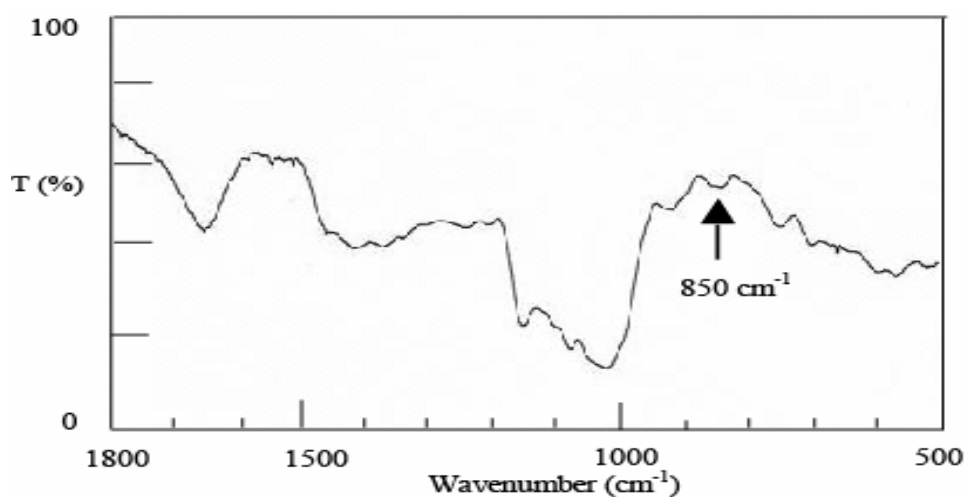


Fig. E: A typical FTIR spectrum recorded from crude PS of 'L15'

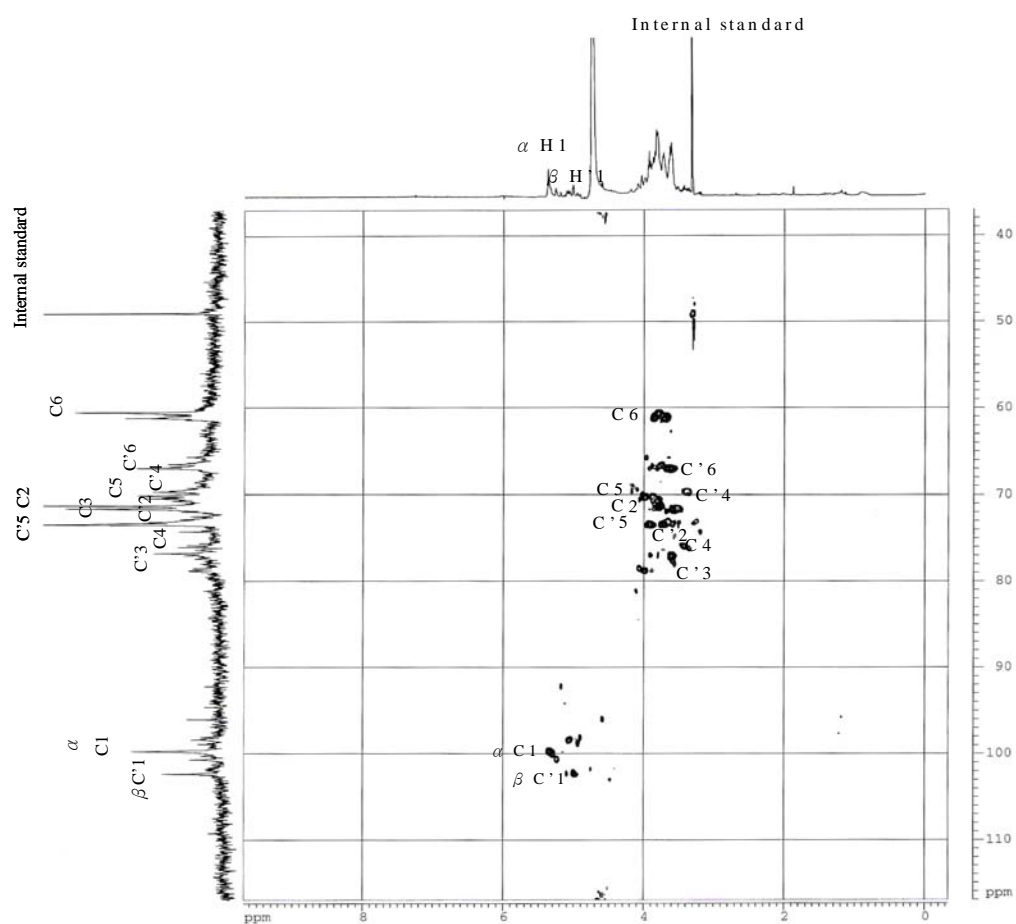


Fig. F. The 2D (HSQC) NMR spectrum of the L15 HWE in D₂O.